

INFORMATION TO USERS

This manuscript has been reproduced from the microfilm master. UMI films the text directly from the original or copy submitted. Thus, some thesis and dissertation copies are in typewriter face, while others may be from any type of computer printer.

The quality of this reproduction is dependent upon the quality of the copy submitted. Broken or indistinct print, colored or poor quality illustrations and photographs, print bleedthrough, substandard margins, and improper alignment can adversely affect reproduction.

In the unlikely event that the author did not send UMI a complete manuscript and there are missing pages, these will be noted. Also, if unauthorized copyright material had to be removed, a note will indicate the deletion.

Oversize materials (e.g., maps, drawings, charts) are reproduced by sectioning the original, beginning at the upper left-hand corner and continuing from left to right in equal sections with small overlaps.

Photographs included in the original manuscript have been reproduced xerographically in this copy. Higher quality 6" x 9" black and white photographic prints are available for any photographs or illustrations appearing in this copy for an additional charge. Contact UMI directly to order.

Bell & Howell Information and Learning
300 North Zeeb Road, Ann Arbor, MI 48106-1346 USA
800-521-0600

UMI[®]

Behavior of the atomic oxygen 5577 Ångström emission intensity at
mid-latitudes: a climatological view

Kerry Ann Deutsch

A dissertation submitted in partial fulfillment
of the requirements for the degree of

Doctor of Philosophy

University of Washington

2000

Program Authorized to Offer Degree: Geophysics Program

UMI Number: 9995362

UMI[®]

UMI Microform 9995362

Copyright 2001 by Bell & Howell Information and Learning Company.

All rights reserved. This microform edition is protected against
unauthorized copying under Title 17, United States Code.

Bell & Howell Information and Learning Company
300 North Zeeb Road
P.O. Box 1346
Ann Arbor, MI 48106-1346

In presenting this dissertation in partial fulfillment of the requirements for the Doctoral degree at the University of Washington, I agree that the Library shall make its copies freely available for inspection. I further agree that extensive copying of this dissertation is allowable only for scholarly purposes, consistent with "fair use" as prescribed in the U.S. Copyright Law. Requests for copying or reproduction of this dissertation may be referred to Bell and Howell Information and Learning, 300 North Zeeb Road, Ann Arbor, MI 48106-1346, to whom the author has granted "the right to reproduce and sell (a) copies of the manuscript in microform and/or (b) printed copies of the manuscript made from microform."

Signature *Kung Inn Deutsch*

Date *5 December 2000*


University of Washington
Graduate School

This is to certify that I have examined this copy of a doctoral dissertation by

Kerry Ann Deutsch

and have found that it is complete and satisfactory in all respects,
and that any and all revisions required by the final
examining committee have been made.

Chair of Supervisory Committee:

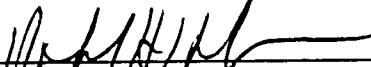


G. Hernandez

Reading Committee:

Kenneth C. Clark

Ken C. Clark



Robert Holzworth

Date:

DEC. 5, 2000

University of Washington

Abstract

Behavior of the atomic oxygen 5577 Ångström emission intensity at mid-latitudes: a climatological view

by Kerry Ann Deutsch

Chair of Supervisory Committee:

Professor G. Hernandez
Geophysics Program

A global mid-latitude study of the atomic oxygen green line emission intensity at 5577 Å has been undertaken with the goal of developing a climatological understanding of the emission behavior and its usefulness as a tracer for the atmosphere near 97 km. Long-term observations have been analysed at nine stations covering periods of ~8 – 12 years, for a total of over 90 years of measurements. The results of this investigation show that the emission typically exhibits a maximum near the summer solstice and again near the fall equinox, before falling to a low winter-time level that persists into the middle of spring. Importantly, the oft-reported maximum at the spring equinox is not a statistically significant feature on the climatological time scale. This finding has implications on our understanding of the dominant processes operating in the region. Specifically, the role of seasonally varying vertical diffusion caused by breaking gravity waves must be readdressed in light of the absence of a strong maximum at the spring equinox.

This work also addresses the relationship between the green line emission intensity and geomagnetic and solar activity. Results show that failing to exclude observations taken under high geomagnetic activity conditions leads to increased springtime emission levels and may be one explanation for this feature as has been reported by others. The influence of solar activity on the green line emission over the long term is shown to exhibit a hysteresis effect within a given solar cycle, confirming that there is not a simple linear relationship between the two processes.

Finally, a critical examination is made of how long of a data series is necessary to fully achieve a climatological understanding of this emission and how this understanding may reasonably be used to advance our

understanding of the upper middle atmosphere region. After ~ 10 years, features with periods less than one year become stable (or achieve climatology), but the data examined here show unresolved power at periods approaching the series length which need longer data coverage to fully characterize.

TABLE OF CONTENTS

List of Figures	iii
List of Tables	v
Chapter 1: Introduction	1
1.1 Seminal works in the study of O(¹ S) emission	2
1.1.1 Geographic and temporal variations	2
1.2 Chemistry	5
1.2.1 Oxygen chemistry and the green line generating mechanism	5
1.2.2 Green line chemistry	7
1.2.3 Calculated emission rate	10
1.3 Focus of this work	10
Chapter 2: Instrumentation	11
2.1 Visual Photometers	11
2.2 Electronic Photometers	16
2.2.1 Turret Photometer	16
2.2.2 Mobile Automatic Scanning Photometer (MASP)	17
2.2.3 Tilting Photometer	18
2.3 Birefringent Photometer	21
2.4 Fabry–Perot Spectrometers	24
Chapter 3: Data and Analysis	29
3.1 Long term data sets	29
3.1.1 Lord Rayleigh’s data	29
3.1.2 Sacramento Peak	31
3.1.3 Fritz Peak spectrometer	31

3.1.4	Mobile Automatic Scanning Photometers (MASP)	32
3.1.5	Kiso	33
3.1.6	Mt. John	35
3.2	Supplemental short term data sets	35
3.3	Analysis	38
3.3.1	Statistical analysis	38
3.3.2	Superposed epoch analysis	42
3.3.3	Variations of the analysis routine for special cases	44
3.3.4	Geomagnetic Activity	46
Chapter 4:	Results and Discussion	51
4.1	Implications of the missing springtime emission maximum	57
4.2	An additional effect of gravity waves in the upper mesosphere/lower thermosphere region	64
4.3	Variations of the green line emission with solar and geomagnetic activity	67
4.3.1	Solar activity	67
4.3.2	Geomagnetic activity	68
4.4	Variations in hemispheric behavior	74
4.5	Departures from the climatological behavior	77
4.5.1	Is this truly a climatological scale work?	79
Chapter 5:	Conclusion	82
Bibliography		86

LIST OF FIGURES

1.1 Altitude distribution of atomic oxygen	6
2.1 Rayleigh’s visual auroral filter	12
2.2 Night sky spectrum from 5000–7000 Å.	14
2.3 High resolution night sky spectra from 5430–5615 Å.	15
2.4 Lord Rayleigh’s visual photometer	15
2.5 Optical assembly of the turret photometer	17
2.6 Optics of the MASP photometer	19
2.7 Optics of the tilting photometer	20
2.8 Transmission curves for normal (line) and tilted (continuum) incidence angles	22
2.9 Optical components of the birefringent photometer.	23
2.10 Ray diagram for a Fabry–Perot etalon	25
2.11 Fringes from a Fabry–Perot etalon	25
2.12 Mechanical setup of a Fabry–Perot etalon	27
2.13 Emission profile measured by a Fabry–Perot spectrometer	28
3.1 Map of datasets	30
3.2 Raw nightly brightness averages for Kiso and Fritz Peak	34
3.3 Comparison of Fritz Peak and Kiso data sets	35
3.4 Example of two green line brightness time series	40
3.5 Periodogram for Kiso (KIS) and Mt. John (MJO) data sets	41
3.6 Comparison between statistical analysis and superposed epoch for Kiso and Mt. John	43
3.7 Examination of the effect of ignoring the long term power on the resultant seasonal variation at Kiso.	44
3.8 Negligible effect of hourly binning	45
3.9 Investigation of the use of measurement uncertainties	46

3.10	Power spectra of the A_p time series between 1979–1991.	49
4.1	Seasonal behavior of the green line brightness at nine long term stations.	52
4.2	Effects on the seasonal behavior at Sacramento Peak from varying the length of each night's observation period.	54
4.3	Effects of using only the 2300 LT hour measurements to form nightly averages.	55
4.4	Seasonal behavior of the green line brightness at ten short term stations.	56
4.5	Long term comparisons of the seasonal behavior of the green line emission at five pairs of closely spaced geographic stations.	58
4.6	Altitude variation of vertical eddy diffusion.	61
4.7	Seasonal variation of the green line as calculated by the Garcia and Solomon's GWB model.	62
4.8	Variation of atomic oxygen concentration caused by changes in the eddy diffusion coefficient.	63
4.9	Gravity wave vertical propagation variations at the solstices.	66
4.10	Gravity wave vertical propagation variations at the equinoxes.	67
4.11	Relationship between green line intensity and solar 10.7 cm flux.	69
4.12	Phase differences between green line intensity and solar 10.7 cm flux.	70
4.13	Power spectra of the Kiso time series.	71
4.14	Reconstructed time series from the significant 1 and 2 yr ⁻¹ oscillations found in the Kiso data, for both A_p filtered and non-filtered conditions.	72
4.15	Raw Kiso data, for both A_p filtered and non-filtered conditions.	73
4.16	Relationship between the mid-spring and fall peak amplitudes with solar F10.7 cm flux for both A_p filtered and non-filtered conditions.	75
4.17	Artificial noise (top) and reconstructed (bottom) data series for Kiso.	77
4.18	Seasonal behavior at Fritz Peak for 1979, 1980, 1981, and 1982.	78
4.19	Periodogram for various subsets of the Kiso data series.	80

LIST OF TABLES

3.1	Summary of long-term airglow datasets	36
3.2	Summary of supplemental airglow datasets	39

ACKNOWLEDGMENTS

The work presented in this dissertation is not the result of an isolated effort, and I would be remiss if I failed to reflect my appreciation for all those who have aided me along the way. Thanks especially to my advisor, Gonzalo Hernandez, for letting me find my own path and for keeping years and years worth of data in hopes that someone might find use for it one day. I would also like to thank the Ken Clark, Robert Holzworth, and Michael McCarthy for their helpful comments and suggestions.

This work would have been impossible without the kindness of many people who provided data to me. The early Christchurch measurements were made available from Don Neff, who generously mailed off his original notebooks, providing not only the observations but also the weather records for the data series. Don Slater of Battelle Pacific Northwest Laboratories provided all of the MASP data and exhibited limitless patience in answering endless emails about the observations. Contemporary measurements from l'Observatoire de Haute-Provence were obtained through the generosity of Gerard Thuillier. Craig Tepley provided the data from Sutherland, rescuing them from almost certain doom in an observatory cleaning. Helen Coffey of the National Geophysical Data Center oversaw the digitization of many of the old IGY and IQSY airglow data sets, even when it seemed like I was the only person interested in such things. Finally, the Kiso data was obtained from the World Data Center C2 in Japan. I am deeply indebted to these people for making this work possible.

I would also like to thank the members of the Space Physics group for their friendship and support, even if I did largely ignore the charged particles. Special thanks to Ben Barnum, Kirsten Lorentzen, Andrew Meadows, Ruth Skoug, and John Williams, who made life in JHN 342 enjoyable over the years.

To my parents, who infused all their kids with encouragement, I am grateful for your support and love, and I will do my best to pass it along when my turn comes. And, most importantly of all, I owe an immense amount to my husband, Eric, for somehow helping me see this thing through to the end and for years of enduring Seattle winters while I escaped to drier parts. Thanks for your faith in me.

even when my own wasn't so strong. Up for a hike or two?

Financial support of this investigation by National Science Foundation grants ATM-9300274, ATM-9610200, and OPP-9615157 is gratefully acknowledged.

Chapter 1

INTRODUCTION

Aeronomy combines the disciplines of physics and chemistry to investigate the properties and behavior of planetary atmospheres. More precisely, as specified in *Brasseur and Solomon* [1986], aeronomy is the 'branch of science dealing with the atmosphere of the Earth and the other planets with reference to their chemical composition, physical properties, relative motion, and reactions to radiation from outer space'. An important part of aeronomy involves the so-called airglow emissions, which directly result from physical and chemical processes in the upper atmosphere. By using the properties of these emissions (i.e. intensity, line width, and Doppler-shifted wavelength) as tracers, one can gain considerable insight about the basic environment (density, temperature, composition, etc.) of the middle and upper atmospheric regions in which they occur. Examining the geographical and temporal variations of airglow emissions at various heights in the 80 to 300 km range also allows the investigation of the role of dynamical processes at work there. The question of whether chemistry or dynamics dominates the behavior of the middle and upper atmosphere is one of the open issues in aeronomy today. This is a complex question to address, largely because of the strong interactions between these mechanisms.

While many airglow emissions exist throughout the upper atmosphere, the work presented here focuses on the atomic oxygen transition $O(^1S) \rightarrow O(^1D)$ leading to emission at 5577 \AA , commonly referred to as the 'green line'. Studies of the usually sub-visual green line emission are ubiquitous throughout aeronomy and have been undertaken over almost eighty years. With such a broad base of observations of the emission itself, the question now becomes what this information can tell us about the workings of the middle and upper atmosphere.

This first chapter provides the framework for the remainder of this dissertation. First a review of the major historical developments in green line studies is given. Next we discuss the presently understood generation mechanism for the emission and the importance of the green line in the context of its significance to the upper atmosphere. Finally, the specific topics that are addressed by this work are presented. Our results will be discussed in the context of how the development of a climatological understanding of the green line emission

can advance our understanding of the upper middle atmosphere.

1.1 Seminal works in the study of $O(^1S)$ emission

As recounted in the review article by *Greer* [1988], the green line was first noted as an annoyance to astronomers by *Campbell* [1895], who found that this emission, previously associated only with aurora, was in fact present all over the sky. The wavelength of the line was first measured by *Slipher* [1919] (auroral) and *Babcock* [1923] (airglow), but the identity of the line remained a mystery until *McLennan and Shrum* [1924] identified it as a forbidden transition of atomic oxygen. Given this long history, it is not surprising that nearly every aspect of the emission has been already examined: the generation mechanism, emission height, geographic and temporal (diurnal, seasonal, and long term) variations, and correlations with other physical phenomena. A complete accounting of all green line intensity studies is not intended in the scope of this work. The aim of this present short review is to highlight, in approximate chronological order within each section, the main advances that have served to characterize, explain, and utilize this emission.

1.1.1 Geographic and temporal variations

The first multi-station studies of the green line brightness behavior were undertaken by *Rayleigh* [1924] and *Rayleigh and Spencer Jones* [1935]. In the former, Lord Rayleigh concluded that there was no significant variation in green line intensity measured near-concurrently in England, Italy, and South Africa. The latter results included claims of both an annual and a semi-annual variation at England, South Africa, and Australia. While the semi-annual variation was reported to have roughly the same amplitude at the three stations, there was a difference in the amplitude of the annual variation, which was found to be stronger in England than in South Africa. It must be noted, however, that Rayleigh made these claims of semi-annual variation in England even though he had a significant gap during his observations during summertime (due to the high latitude of the station).

Studies of geographic variation of the green line on a much smaller local scale have also been reported. It was found that the emission is not from a uniform layer, and that the structure was variable even on a time scale of less than one night [*Barbier et al.*, 1951; *Roach et al.*, 1953; *Roach*, 1955]. These early contributors noted that the motion of such airglow patches might shed light on the dynamical processes working near the emission layer. These ideas have been confirmed more recently with airglow imager observations (i.e., [*Colerico et al.*, 1996]) of bright structures of emission which move through a fixed field of view.

Shipboard studies by *Nakamura* [1958] and *Davis and Smith* [1965] found a minimum in airglow intensity near the equator, but *Nakamura* [1958] found a second minimum near 40° geographic latitude, and *Davis and Smith* [1965] placed the maxima near 30 – 40°N and 40°S. Satellite data from Ogo 6 [*Donahue et al.*, 1973], ISIS-2 [*Cogger et al.*, 1981], and WINDII [*Shepherd et al.*, 1999b] have since confirmed the existence of a low-latitude minimum and mid-latitude maximum. *Fukuyama* [1977] examined measurements at 13 low and middle latitudes and found that the emission intensity increased with increasing latitude. This variation was tied to a similar latitudinal variation in the effects of solar activity, as will be discussed later.

Many researchers have investigated the daily variation of the emission. *Dufay and Tcheng* [1946]; *Roach and Pettit* [1951]; *Christophe-Glaume* [1965]; *Petitdidier* [1978]; and *Fukuyama* [1976] all found that the general behavior at mid-latitudes exhibited a maximum of intensity near local midnight. Other studies have questioned this result, either deeming the variation insignificant [*Smith and Owen*, 1966] or noting that prior results may be due to the extended observing hours in winter, for which the early evening and late morning levels are low [*Smith and Steiger*, 1968]. *Brenton and Silverman* [1970] investigated the latitudinal dependence of the diurnal behavior of the emission, and found that it could best be described by grouping the stations into three latitude bands. North of ~ 44°N, they found little variation in brightness throughout the night. From 44°N to 22°N, a maximum occurred during the night, and from 19°N to 34°S there was large variability along with a significant minimum during the night. *Burnside and Tepley* [1990] found large temporal variations of the diurnal behavior at Arecibo, Puerto Rico and Sutherland, South Africa: some months exhibited almost no nightly variation, while others showed a clear maximum at some time during the night.

Semi-annual seasonal behavior of the green line emission has also received much attention. *Roach* [1955] found similar seasonal behavior in California (6 years of data) and France (4 years), with intensity minima in the spring and winter and a maximum in the fall. While *Christophe-Glaume* [1965] also reported this general behavior (along with a maximum in the summer) based on an eleven year study at Haute-Provence Observatory (OHP) and shorter term studies at other locations, she also noted substantial variations in the sizes of the maxima from station to station, and mentioned that the springtime maximum at OHP was very weak (which agreed with *Barbier* [1959]'s assessment at the same station), although it did occur in nearly every year of observation that she had. The seasonal variation described by *Fukuyama* [1977] included definite maxima in summer and fall and a smaller peak in late winter/early spring at many mid-latitude stations over observation periods from 2 – 12 years, which agreed with earlier studies by *Barbier* [1959], *Neff* [1965] (2 years of observations in Christchurch, New Zealand) and *Yano* [1967] (6 years in Japan). *Cogger et al.* [1981] reported maxima in mid-April and mid-October at all mid-latitudes from two years of ISIS-2 satellite observations.

Long term studies have also been conducted, oftentimes with the aim of searching for correlations between airglow intensity and solar and/or geophysical phenomena. *Rayleigh and Spencer Jones* [1935] used almost ten years of data at three stations to note strong correlation between the green line yearly mean brightnesses with yearly mean sunspot areas, but they found no correlation between brightness and magnetic activity. The correlation with sunspot area (or later, sunspot number) was confirmed by others, including *Barbier* [1959]; *Hernandez and Silverman* [1964]; and *Christophe-Glaume* [1965]. *Fukuyama* [1977] also came to the same conclusion, but noted that there may be a latitudinal variation in the solar activity dependence.

Other correlations have been investigated as well. *Dandekar and Silverman* [1964] found evidence that the intensity of the green line increased on the night after a large solar flare. In another study of the relationship between solar phenomena and airglow brightness, *Rosenberg and Zimmerman* [1967] chose to examine the correlation between monthly and nightly solar 10.7 cm flux and 5577 Å intensity. They concluded that the brightness was correlated slightly more with 10.7 cm than with sunspot number, and also that the level of correlation depended upon the phase of the solar cycle.

The historical review just given describes the studies of the nighttime green line emission. It should be noted that the emission is present during daylight and twilight hours as well, although the source mechanism differs from the nighttime emission, as will be described later. Due to the high sky background level during the daytime, however, these measurements are much more difficult to discern. Ground based green line studies were undertaken during both twilight [*Dufay and Dufay*, 1948; *Megill*, 1960] and daytime [*Noxon*, 1963], while rocket and satellite (Atmospheric Explorer C, UARS) observations have been made of the daytime emission [*Schaeffer and Fastie*, 1972; *Schaeffer et al.*, 1972; *Frederick et al.*, 1976; *Singh et al.*, 1996]. The data presented in this dissertation are all taken under nighttime conditions.

In recent years, emphasis has shifted away from trying to understand the mechanisms which affect and control the green line emission to learning how this emission can be used to improve our understanding of the atmosphere at the height it occurs. One of the most important ways that airglow research has been used towards this end is through its use to provide observational constraints on atmospheric models [*Garcia and Solomon*, 1985]. The green line emission has proven particularly useful in this regard, in large part due to its height. At ~ 95 km (i.e., *O'Brien et al.* [1965]), the emission layer is quite near the mesopause, the boundary between the mesosphere and thermosphere located at ~ 85 km. The processes which occur at and near this region reflect the transition between the well-mixed and the stratified regions of the atmosphere. Because of its height of origin, the green line emission is likely to be sensitive to these processes.

In order to examine these results and their implications for the middle atmosphere, it is first necessary to understand exactly how a specialized measurement of this one emission line can lead to much broader

understanding of this atmospheric region as a whole. The next section will begin with a discussion of how the basic chemistry of the green line relates to the broader atmospheric chemistry, and then follow with an examination of the dynamical processes that may be reflected in measurements such as those presented in this work.

1.2 Chemistry

1.2.1 Oxygen chemistry and the green line generating mechanism

It is interesting to note that although many efforts have been undertaken to explain the behavior of this emission process, the details are not yet fully clear, over eighty years since its discovery. One of the earliest challenges facing airglow researchers was determining whether the source of the emission was atmospheric or extra-terrestrial. As outlined by *Chamberlain* [1995], the first proof that the emission was of atmospheric origin was provided by *Yntema* [1909], who concluded that the scattering of starlight could not explain the variations of airglow intensity with zenith angle.

The first attempts at determining an emitting height for auroral green line emission came from photographic observations of *Störmer* [1910, 1911], who placed the source above 100 km. Non-auroral green line emission height determinations were made *Van Rhijn* [1921]. By assuming a constant thin emitting layer in a spherical atmosphere, he developed a relationship between the zenith angle and observed intensity which led to a crude geometric determination of the layer height from ground observations.

Later ground-based attempts to determine the height of the nighttime green line emission produced a wide range of estimates, placing the source from ~ 60 km up to above 400 km [*Barbier*, 1952; *Chamberlain*, 1995]. Rocket measurements in the late 1950s [*Heppner and Meredith*, 1958; *Tousey*, 1958] found that the emission occurred between ~ 80 and 120 km, peaking between 94 and 100 km. Later rocket, radar, and satellite measurements have further refined this value to a peak emission at 95 km in a layer approximately 7 km thick [*O'Brien et al.*, 1965; *Dandekar and Silverman*, 1964; *Witt et al.*, 1979; *Ogawa et al.*, 1987; *Hernandez and Killeen*, 1988; *Swensen et al.*, 1989; *Hernandez et al.*, 1995b; *Plagmann et al.*, 1998].

The emission's identification as a forbidden atomic oxygen transition, combined with the early height measurements indicating a high altitude source, suggested that a pool of atomic oxygen must exist near 100 km. Figure 1.1 shows the measured altitude distribution of atomic oxygen concentration reported by the CIRA 1972 reference atmosphere [*COSPAR*, 1972]. This profile is an annual mean for the 30° latitude region. While the profile does not reflect seasonal or other variations in the atomic oxygen density, it does

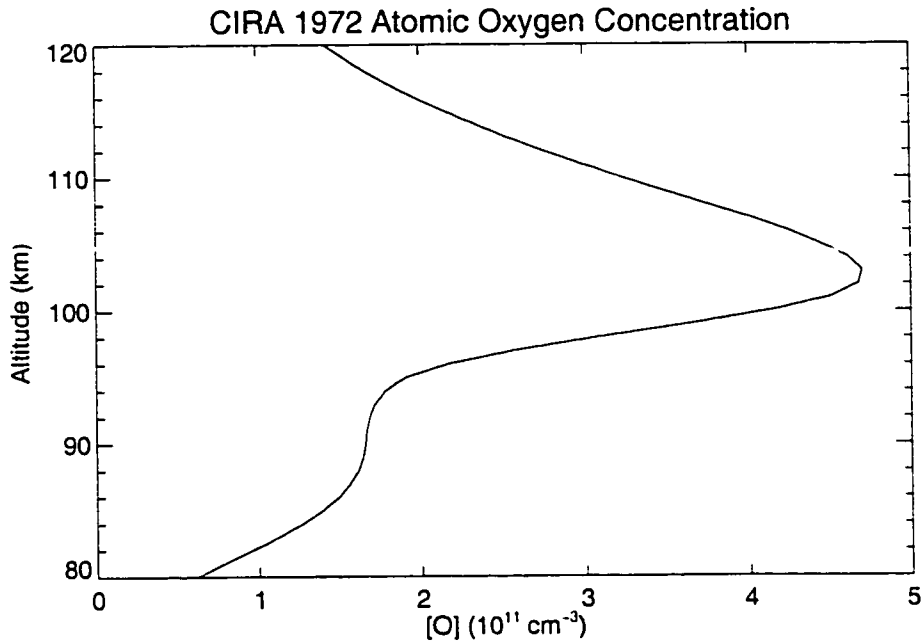


Figure 1.1: Annual mean atomic oxygen concentration as reported in the CIRA 1972 reference atmosphere [COSPAR, 1972].

illustrate the general characteristics of the distribution: the rather sharp peak in oxygen concentration near 100 km and the sharp drop-off in density below this peak.

The main source of atomic oxygen in the atmosphere is the photodissociation of molecular oxygen by sunlight. Several portions of the solar UV spectrum are involved, but the strongest photodissociation occurs in the Schumann–Runge region of the spectrum. Between 60 and 90 km, absorption by the Schumann–Runge bands occurs for the UV wavelength range $1750 < \lambda < 2060 \text{ \AA}$, while above 90 km absorption by the Schumann–Runge continuum in the $\lambda < 1750 \text{ \AA}$ range is the primary source of atomic oxygen [Allen *et al.*, 1981; Tohmatsu, 1990]. The maximum dissociation coefficient in the Schumann–Runge continuum region reaches $\sim 9 \times 10^{-5} \text{ s}^{-1}$ above $\sim 120 \text{ km}$, a full order of magnitude larger than the maximum dissociation coefficient ($\sim 10^{-7} \text{ s}^{-1}$) from the band region [Tohmatsu, 1990], meaning that the region of highest atomic oxygen production occurs at a much higher altitude than the observed concentration peak. This discrepancy illustrates the importance of dynamical process in the middle and upper atmosphere.

Atomic oxygen moves from its production level to lower altitudes through vertical diffusion. The magni-

tude of this motion is defined by the diffusion coefficient, K , as:

$$K = -\frac{\phi}{n_a(df/dz)} \quad (1.1)$$

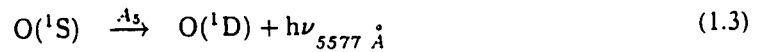
where n_a is the background atmospheric concentration and ϕ and (df/dz) are the flux and the mixing ratio gradient of a given tracer. This coefficient can be determined either directly by observationally tracking a tracer species or indirectly by following a tracer's evolution in an atmospheric model. *Hunten* [1975] suggests a typical value of $K = 10^6 \text{ cm}^2 \text{ s}^{-1}$ is appropriate for the region near the mesopause.

The dependence of K upon height (z) helps explain the peak in atomic oxygen near 100 km. Specifically, if local production of O is negligible and it comes downward from ~ 120 km, there must be a region of low K to allow the species to pool up and create the peak. If K were constant all throughout this altitude region, the flow of oxygen would remain steady and no accumulation would occur.

1.2.2 Green line chemistry

Nightglow

Our current understanding of the generation mechanism for the nighttime green line emission began with *Chapman* [1931], who proposed the following three body collision process followed by radiation:



$\text{O}({}^1\text{D})$ and $\text{O}({}^1\text{S})$ are the first and second states above the ground state of atomic oxygen, at 1.98 and 4.17 eV, respectively. Because of the long lifetime of the $\text{O}({}^1\text{S})$ state (~ 1 sec [*Garstang*, 1956]), a low density is needed to allow this species to radiate before it is deactivated by collisions; this density requirement implies a high emitting altitude.

Barth and Hildebrandt [1961] measured the reaction rate (k_0) for (1.2) in the laboratory. Using their result, along with molecular and atomic oxygen densities near 100 km, they calculated an upper limit on the emission intensity that was smaller than the observed intensities by a factor of 10^3 . This led *Barth* [1961] to suggest an alternate two-step mechanism for the generation of $\text{O}({}^1\text{S})$:

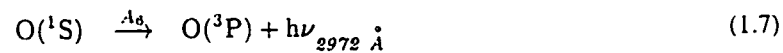


where M is an unspecified third body, and * signifies an excited state. This process then leads to the green line emission through (1.3). Note, however, that the overall reaction has the same reactants and products as the Chapman reactions in (1.2) and (1.3).

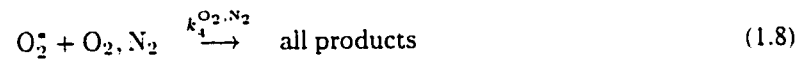
Due to the previously mentioned long lifetime of O(¹S), the species is prone to further chemical and physical interactions before it has a chance to radiate via (1.3). In general, any loss of a precursor to the radiation is called quenching. The most common quenching process for O(¹S) is [McDade *et al.*, 1986]



Note that reaction (1.6) is the reverse of reaction (1.5). Also, there is loss of O(¹S) through radiation at wavelengths other than 5577 Å:

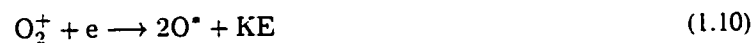


In addition, other processes may occur which result in a decrease in the production of O(¹S), such as [McDade *et al.*, 1986]:



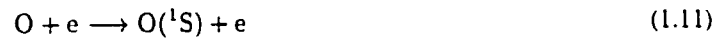
Rate coefficients for the contending production mechanisms have been remeasured and refined for several years (for a more complete history, see reviews by Bates [1978] or Greer [1988]), and both production mechanisms have moved in and out of favor. At present, the Barth mechanism has emerged as the leading contender, and more attention has been focused on determining the identity of the O₂^{*} excited state [McDade *et al.*, 1986]. For the remainder of this work, the Barth mechanism is presumed to be the primary source of the green line emission.

There are two other sources of nighttime green line emission in the middle and upper atmosphere. First, there is an additional green line emission layer which results from dissociative recombination of O₂⁺ ions in the ionosphere:



where the O^* can either or both be the (1S) or the (1D) state. The $O(^1S)$ generated will then radiate via (1.3). This emission is typically much fainter than the main green line and it occurs in the 150 – 200 km region [Gulledge *et al.*, 1968; Tohmatsu, 1990].

Additionally, there is the green $O(^1S)$ emission that is the signature of the aurora. $O(^1S)$ is generated from a variety of sources, some of which are



and



A thorough summary of the sources leading to the production of $O(^1S)$ can be found in Chapter 7 of Rees [1989].

Dayglow

Although it is not the focus of this work, we take a moment here to distinguish the generation mechanisms for the daytime green line emission from the nightglow. During the daytime, extreme ultraviolet (EUV) photons in the 200 – 600 Å range ionize species in the upper atmosphere, leading to the production of electrons. These electrons may then interact with atomic oxygen through the collisional excitation reaction shown in (1.11). In addition, $O(^1S)$ may be generated through dissociative recombination of molecular oxygen ions:



The altitude profile for the daytime green line emission is significantly different from that obtained during the nighttime. While the strongest feature is still a sharp peak located near 100 km, the daytime peak is much stronger than at night. Additionally, there is substantial emission occurring in a broad altitude range from ~ 125 – 200 km [Shepherd *et al.*, 1997].

1.2.3 Calculated emission rate

From the Barth reactions, one can calculate an expression for the volume emission rate (based on *McDade et al.* [1986]):

$$V_{1S} = \frac{A_5 k_1 k_2 [O]^3 [M]}{(A_4 + k_4^{O_2} [O_2] + k_4^{N_2} [N_2]) (A_6 + k_5 [O_2])} \quad (1.15)$$

As the above expression shows, the volume emission rate for O(¹S) is strongly related to the atomic oxygen concentration. This strong dependence is what makes the green line emission such a useful tracer of the atmosphere near 100 km. Any processes that alter the production or loss rates of atomic oxygen in the region should manifest themselves as a change in the emission rate as well as the peak emission height. These processes may either be chemical (i.e., variations in O₂ dissociation, changes in the quenching rate) or dynamical (i.e., variations in the diffusion rate which allow more or less oxygen to pool up near 100 km, horizontal transport of chemical species by other means) in nature.

1.3 Focus of this work

After the preceding discussion of the earlier studies done on the green line emission, one obvious gap is evident: with the exception of the early work by Lord Rayleigh and his colleagues, there have been no global long term studies of the nightglow at 5577 Å with the aim of developing the wide climatological behavior of the emission and the implications of this climatology in atmospheric investigations. As mentioned earlier, the green line emission is closely tied to other processes at work near the mesopause. Previous results on the seasonal behavior of this emission have been used to support the importance of changes in turbulence and vertical diffusion caused by the interaction of breaking atmospheric gravity waves with the local atmosphere. These claims need to be re-examined with the aim of providing boundaries on these quantities, based on the variations in emission intensity that they can generate. To accomplish this task we have amassed and will analyze an extensive collection of long term mid-latitude green line observations.

Once the climatology of the green line has been established from published and new data and the broader implications of this climatology to atmospheric dynamics and chemistry are explored, the significance of any deviations from this climatology can be addressed. The year-to-year variation of the seasonal behavior will provide useful insight into the necessary conditions that allow certain processes to become dominant.

Chapter 2

INSTRUMENTATION

The data analyzed in this dissertation span more than seven decades, and thus it is not unexpected that many changes and improvements in instrumentation have occurred over the course of these measurements. It is important to know and understand all instruments, present and past, which have contributed to the total measurement base. In a broad sense there have been three different categories of instruments. The first category, used in the Lord Rayleigh measurements in the 1920s and 1930s, required the human eye because the brightness of the night sky was visually compared to a radioactive source of constant intensity. This instrument took advantage of the excellent ability of the eye to judge equal brightness levels. The next generation of instruments was used from the 1940s to 1970s; these were electronic photometers using quantum detectors, which permitted the first automatic recording of airglow brightnesses. These instruments also used interference filters that passed a narrower bandwidth than the filters used by Lord Rayleigh. Measurements could be taken continuously with these newer photometers, thereby eliminating the need for a full time observer. Finally, measurements taken after the late 1970s often were made with high-resolution spectrometers. Designed mainly for spectral determinations of winds and temperatures, spectrometers also provide high-resolution emission intensities. The following sections will describe these three classes of instruments and their effects on the measured brightness levels.

2.1 Visual Photometers

As mentioned earlier, the first long term multi-station airglow measurements were undertaken by Lord Rayleigh in the 1920s and 1930s. The same instrumental design was used at all stations and is discussed below.

The methodology used by Lord Rayleigh and his observers entailed comparing the visual brightness of the sky (selected at a particular wavelength with filters) to that from a set of known and stable brightness sources. Figure 2.1a–d shows the combination of filters used to select out the green line emission at 5577 Å. The product of these three components makes up Rayleigh's 'visual auroral filter' [Rayleigh, 1924; Hernandez

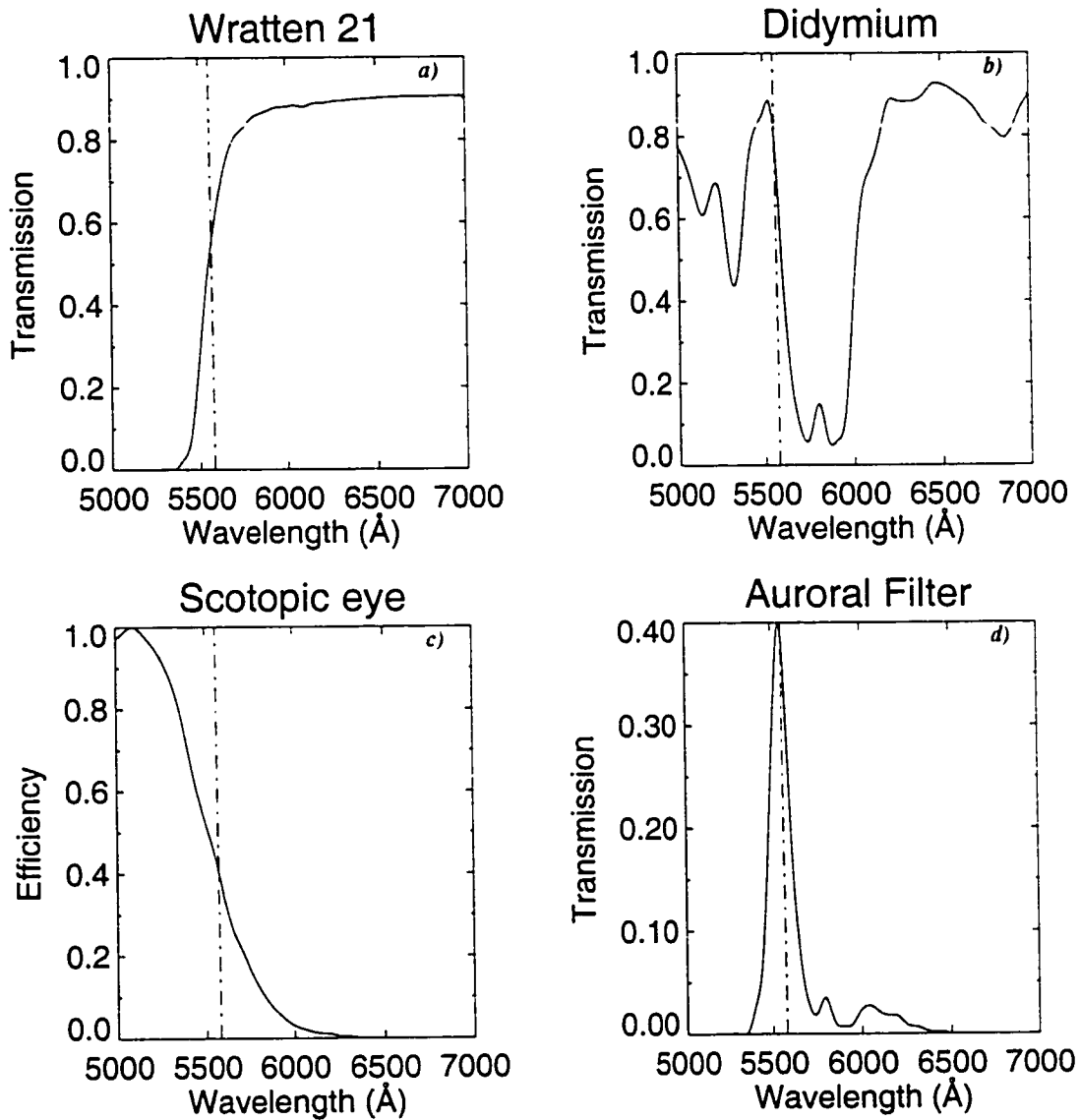


Figure 2.1: Lord Rayleigh's visual auroral filter for observing the green line brightness. Components are described in the text. The vertical dot-dashed line indicates the position of the emission line.

and Silverman, 1964]. A Wratten 21 filter (Figure 2.1a) [Eastman Kodak Company, ca. 1970] was used to cut off the blue end of the spectrum below 5400 Å. This was combined with a didymium rare-earth filter (Figure 2.1b) which has relatively high transmission around 5500 Å and drops off sharply towards the red [Hoya Corporation, ca. 1980]. Finally, the dark-adapted eye itself (Figure 2.1c) has a transmission curve that peaks around 5100 Å and decreases smoothly towards the red [Levi, 1980]. As is seen in Figure 2.1d, the resultant filter transmits quite well near the desired 5577 Å line and drops off reasonably quickly. The chosen normalization shown for the auroral filter is based on Rayleigh's determination that the filter transmitted 40% of the 5577 Å emission line [Rayleigh, 1924]. The equivalent box filter can be constructed by computing the total area under the final filter curve shown in 2.1d and assuming an ideal transmission of 100%. For Lord Rayleigh's auroral filter, the equivalent box filter would have a width of ~ 68 Å.

Figure 2.2 shows a night sky spectrum (taken at Apache Point Observatory, New Mexico) from 5000 – 7000 Å, overplotted with Rayleigh's auroral filter (arbitrarily scaled). As can be seen, while the O(¹S) emission line at 5577 Å is by far the strongest feature in the region, the 'tails' of the filter still transmit considerable background radiation. The identity of other spectral features are indicated. The strong mercury and sodium features from 5400 – 5900 Å are contamination from street lamps and other local lighting sources which would not have been present during Lord Rayleigh's time. Figure 2.3 shows high resolution spectra taken at a dark site (Mauna Kea, Hawaii) for the 5430 – 5615 Å region of the night sky showing the absence of the contamination features of mercury and sodium near the 5577 Å green line [Osterbrock et al., 1996].

Figure 2.4 (modified from [Rayleigh, 1924, fig. 2]) shows the instrumental setup for Rayleigh's visual photometer. The light of the night sky, after passing through the auroral filter (B), illuminated one-half of a field of view (D). The other half was illuminated by a radioactive uranium salt container of constant brightness (A). In each measurement, either the sky or the radioactive source would appear brighter to the eye. Neutral-density filters of known opacity would then be placed in front of the brighter source until the two sides appeared equally bright. (Both possible positions of the neutral-density filters are shown as C.) Rayleigh's measurements were therefore recorded as the number of neutral-density filters that were required to equalize the two sides, with interpolations made between steps.

Rayleigh later calibrated his visual photometers to determine the actual intensity of the green line [Rayleigh, 1930]. He found the typical green line emission *passing through his photometer* to be ~ 68 R (in modern-day units: 1 Rayleigh = 10^6 photons cm^{-2} column^{-1} s^{-1} [Hunten et al., 1956]). As part of his

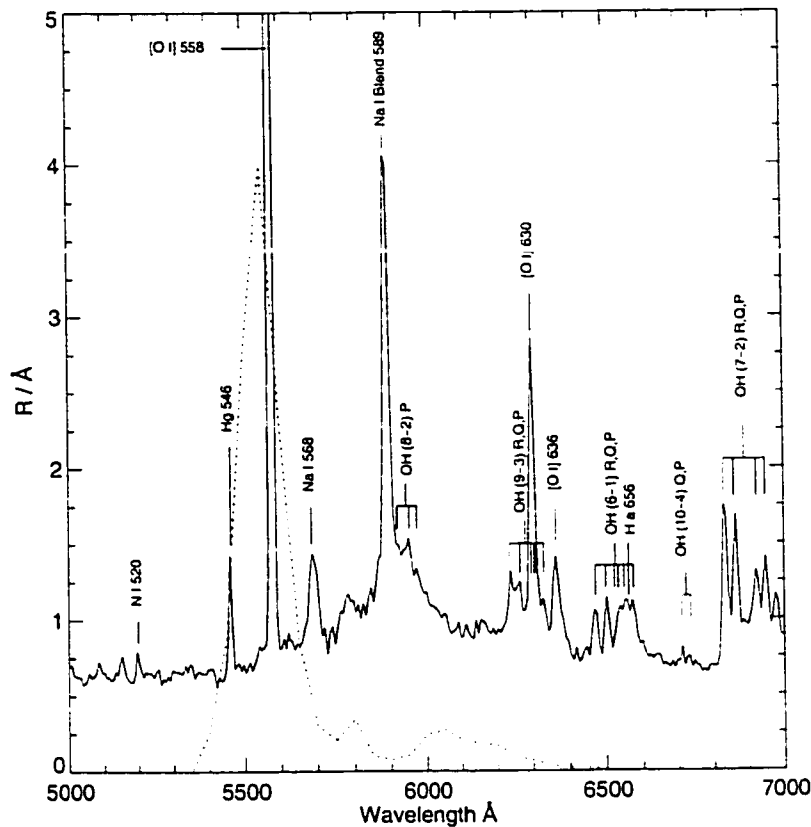


Figure 2.2: Night sky spectrum from 5000–7000 Å, along with Rayleigh's auroral filter (dotted line). The vertical position of the auroral filter is arbitrary in this figure. Spectrum taken at Apache Point Observatory, courtesy of E. Deutsch.

work, he measured the overall light transmitted by his auroral filter and found it to be comprised of 37% line emission and 63% continuum background. If 68 R of line emission represented 37% of the total light entering the filter, the remaining 63%, or 116 R, emission includes both the background continuum, scattered light, and, owing to the large field of view of Rayleigh's apparatus, emission from stars in the viewing field. Referring again to Figure 2.2, one can see that the 5577 Å emission line sits atop a background continuum level. Considering the filter width of ~ 68 Å this background amounts of a level of ~ 1.7 R/Å, well within the range of continuum levels found by *Broadfoot and Kendall* [1968] and *Krassovsky et al.* [1962] (0.6 R/Å and 2 R/Å, respectively) some 30 years later. An additional check of Rayleigh's calculation has been made by

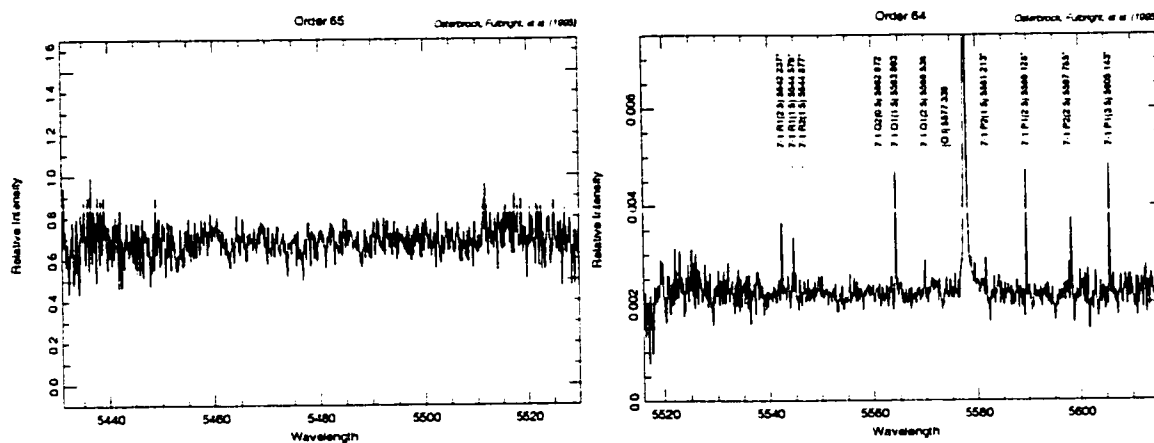


Figure 2.3: High resolution night sky spectra covering the 5430–5615 Å region taken at Mauna Kea, HI, where there is no contamination from artificial light sources. Note that the 546 nm Hg line and the 568 nm Na I line that were present in Figure 2.2 are not present, just as they would have not been present during Lord Rayleigh's observations. (From *Osterbrock et al. [1996]*).

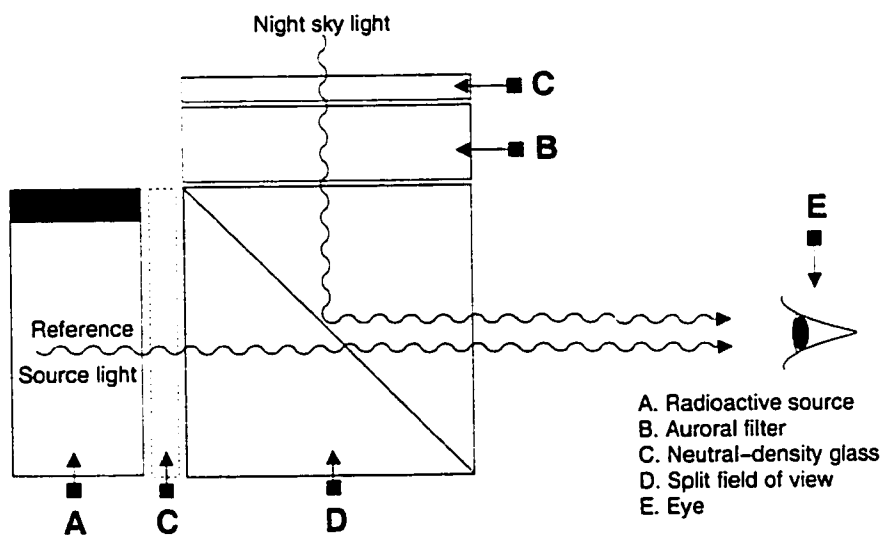


Figure 2.4: Visual photometer used by Lord Rayleigh and his collaborators (based on [Rayleigh, 1924, fig. 2])

passing a sky spectrum observed at Apache Point Observatory (E. Deutsch, personal communication) through the auroral filter. Integrating under this resultant curve coincidentally gives a total non-line emission of ~ 119 R, in reasonable agreement with Lord Rayleigh's estimates of the line/background ratio.

The measurements of Lord Rayleigh and his colleagues were later re-analyzed and the brightness units converted to modern-day Rayleighs by *Hernandez and Silverman* [1964]. In addition to converting the opacity-step measurements to Rayleighs, corrections were also made to recalibrate all the measurements to one common instrument and to remove any effects of external light contamination. Their investigation showed the validity and usefulness of such an extensive data collection.

2.2 *Electronic Photometers*

Several varieties of electronic photometers were used to obtain the data examined in this dissertation. While each type of photometer works differently, some basic issues need to be addressed for all of them. First and foremost is the need to understand how these instruments were calibrated, both relatively within each instrument (to maintain a consistent operating environment) and absolutely (to allow for inter-station comparisons). The subsections below will discuss the instruments and how the calibration issue was addressed in each case.

2.2.1 *Turret Photometer*

The photometer discussed here is described in *Purdy et al.* [1961]. The instrument itself was quite simple, allowing measurements to be taken in four colors while looking at a fixed, single direction with a 5° field of view. The optical arrangement is shown in Figure 2.5 [*Purdy et al.*, 1961]. From left to right, light from the sky passes through the following elements: a colored glass transmission filter and an interference filter (labeled 5 and 6 in the figure), objective lens (1,2), field lens (3,4), and a photomultiplier tube (1P21). The objective lens forms the image of the sky, while the field lens acts to evenly illuminate the photomultiplier tube. The colored glass transmission filter and interference filter are housed in the 'turret' assembly, which rotates according to the color of interest.

To select the desired color, four interference filters of ~ 50 Å FWHM were typically used: three for isolating the desired emission (5577 Å, 5893 Å, or 6300 Å) and one for providing an estimate of the con-

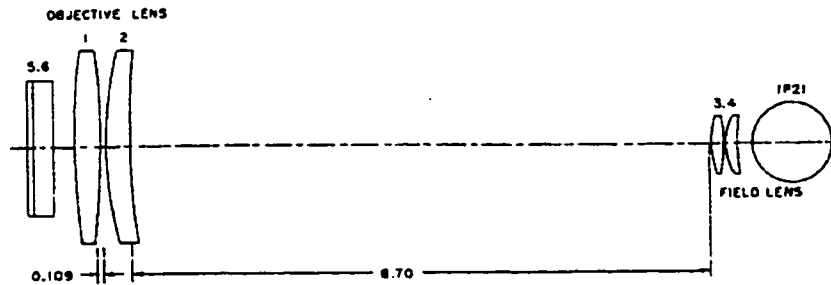


Figure 2.5: Optical elements of the turret photometer. From left to right: colored glass transmission filter, interference filter, objective lens, field lens, photomultiplier tube (from [Purdy *et al.*, 1961, fig. 4]).

tinuum level (5300 Å). While any 50 Å filter still transmits a large amount of background light, these filters represented an improvement over the filters used earlier by Rayleigh.

Observations were made sequentially through each of the four filters, with each color's measurement taking 75 seconds. This means that $\sim 5 - 6$ minutes elapsed between each green line observation. Within each color, three separate 25 second observations were taken. First, a measurement was made with the shutter closed to provide a baseline level. Then, a calibrating standard source was observed for use in monitoring the instrument's stability. Finally, sky observations were taken.

The relative brightness of the 5577 Å green line emission was determined from the difference of recordings of the 5577 Å filter with the 5300 Å continuum filter. However, the absolute brightness was still ambiguous. To address this issue, calibrations were often made using star crossings (see *Roach* [1956] for details). This was either done directly or by comparison with another photometer that had been star-calibrated.

2.2.2 Mobile Automatic Scanning Photometer (MASP)

A variation of the turret photometer was developed in the 1970s as the MASP instrument, described fully in *Kleckner et al.* [1981]. This photometer was developed to serve a dual purpose: taking airglow and auroral measurements at night as well as making solar observations during daylight hours. The nighttime measurements were taken during azimuthal scans at a sequence of varying elevation angles, so that the end result would be a full-sky 'map' of the emission being observed. The optical path of the MASP photometer is shown in Figure 2.6 [*Kleckner et al.*, 1981, fig. 1], showing the configuration for taking both solar and air-

glow measurements. Under daylight conditions, light passing through F1 reaches mirror M3, which then sends the light off through aperture A1 and on to detector D1. For airglow or auroral observations, the F1 and M3 components were removed, providing a clear path into aperture A2 and detector D2.

Calibration of the MASP photometers was similar to that used with other instruments: a light source of known calibration was used to illuminate the detector of the photometer. The calibration of the standard lamp was carried out in two ways. Primarily, the standard source was calibrated with a known radioactive phosphor source. A phosphor source has an inherent intensity which is dependent on wavelength, and this intensity is expressed in Rayleighs/unit-wavelength. The interference filters transmit a portion of the true source's intensity, and this response was then used to calibrate against observational results. This calibration, therefore, required a detailed knowledge of the filters' transmission properties as they were used in the instrument (which may differ from those properties measured under ideal laboratory conditions). *Kleckner et al.* [1981] quoted an absolute calibration accuracy of $\sim 20\%$. As a secondary check of the calibration, the lamp was also compared with two additional off-site standard sources. Details of the calibration scheme can be found in *Kleckner et al.* [1981] and in *Smith and Alexander* [1968].

As in the turret photometer, various wavelengths were available for observation: 5577 (O^1S), 6300 (O^1D), 4861 (H_β), 4278 (N_2^+), and 5350 Å (continuum). The advance in filter technology is evident in the filters used in the MASP project: the 5577 Å and 6300 Å filters had FWHM = 10 Å, the 4861 Å and 4278 Å filters had FWHM = 20 Å, and the continuum filter at 5350 Å had a FWHM = 30 Å. The standard operating scheme was to take scans at 10, 15, 20, 30, 50, and 90° elevation angles with a given filter; this sequence took just over two minutes (only the zenith measurements have been used here). For a five filter set, a full sequence took 10.33 minutes. The field of view of observation was 2.5°. Depending upon the level of auroral activity, a set of observations was taken either every 12 or every 20 minutes.

2.2.3 Tilting Photometer

One of the basic assumptions made when using a turret or MASP photometer is that the continuum level represented by the measurement near 5300 Å is the same (with proper scaling) as that underlying the 5577 Å emission line, more than 400 Å away. Inherent in this assumption is the idea that this scaling is constant with time, which has not been fully proven [*Gadsen and Marovich*, 1973]. This method of correcting for the

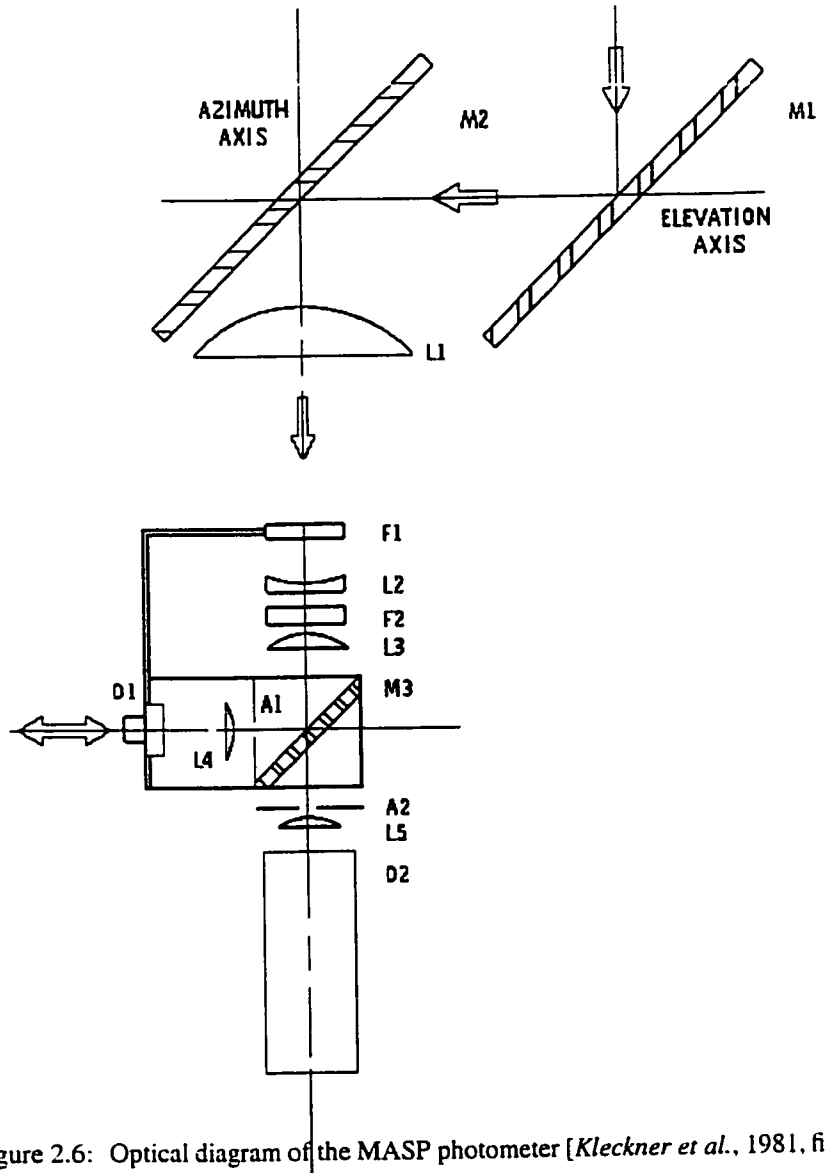


Figure 2.6: Optical diagram of the MASP photometer [Kleckner et al., 1981, fig. 1]

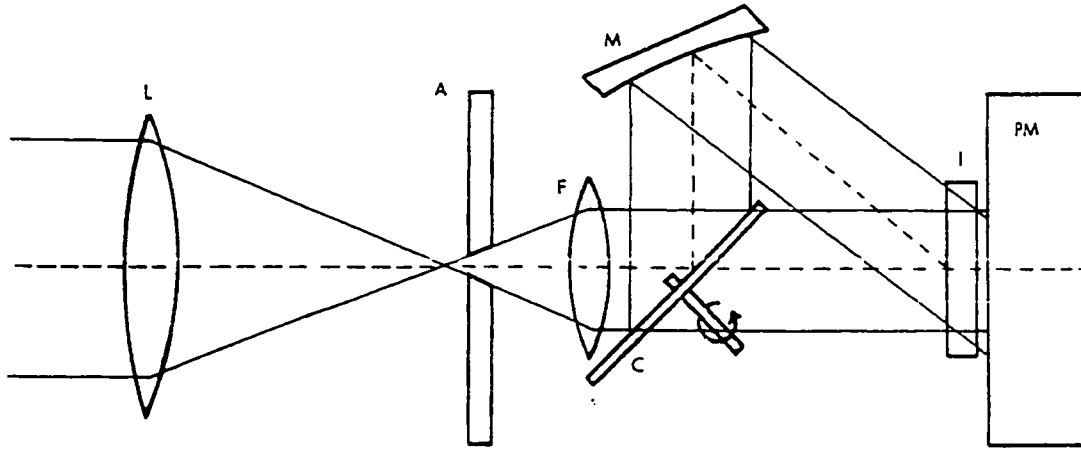


Figure 1. Schematic of Photometer Optics for Continuum Subtraction (L) Objective Lens, (A) Aperture, (F) Field Lens, (C) Chopper, (M) Mirror, (I) Interference Filter

Figure 2.7: Optical diagram of a tilting photometer [Greenspan, 1964, fig. 1]

continuum emission, therefore, may have shortcomings because the continuum level as observed through the 5300 Å filter may not represent the true continuum at 5577 Å.

Filosofo et al. [1965] took a different approach to the continuum issue with their tilting, or 'continuum compensating', photometer. Nominal central-wavelengths cited for interference filters are based on normal incidence. If the angle of incidence deviates from normal, however, the wavelength will be shifted towards the blue end of the spectrum. The tilting photometer exploited this feature to measure both the 5577 Å emission line and the nearby continuum level through the same filter. Figure 2.7 shows the optical arrangement of the *Filosofo et al.* [1965] design [Greenspan, 1964, fig. 1]. The field of view of this instrument was 3°.

As can be seen from the diagram, there are two different sets of light rays that reach the interference filter – one set that travels directly to the filter and a second set that gets reflected up to the mirror so that it reaches the filter at an oblique angle. The difference that this makes is easily seen mathematically. Interference filters are Fabry-Perot etalons with very small spacing, and they follow the basic etalon equation:

$$m\lambda = 2\mu d \cos\theta \quad (2.1)$$

where m is an integer (half-integer) for constructive (destructive) interference, λ is wavelength, μ is the index of refraction of the material, d is the thickness of the etalon, and θ is the angle of incidence. Subtracting this general case from case of normal incidence ($\theta = 0$) leads to $\Delta\lambda = \lambda_o \frac{\theta^2}{2}$, where $\Delta\lambda$ is the change in central wavelength resulting from a non-normal incidence angle and λ_o is the central wavelength of the normally incident ray. One more adjustment needs to be made to this relationship. The angle in the above equation is the angle *within* the material, whereas an incidence angle is usually given as the angle that light *enters* the etalon (i.e. in air). Snell's Law is used to convert the above angle (θ) to its equivalent air value ($\alpha = \theta\mu$).

In the arrangement above, *Filosofo et al.* [1965] had $\alpha = 20^\circ$. Typical values of μ for interference filters are ~ 2 . The relationship between the effective filter width as a function of angle of incidence can be given by

$$\left(\frac{\omega}{\omega_o}\right)^2 - 1 = \left(\frac{\theta\phi\sigma_o}{\mu^2 d\sigma}\right)^2 \quad (2.2)$$

where ω_o is the filter's width with no tilting (normal incidence), ω is the width with tilt and field of view angles θ and ϕ , respectively. σ_o is the peak wavenumber of the untilted filter, and μ is the filter's index of refraction [*Hernandez*, 1986]. Using this relationship, the effect of non-normal incidence for green line ($\lambda_o = 5577 \text{ \AA}$) observations in this configuration can be calculated to be $\Delta\lambda \sim 85 \text{ \AA}$.

While using non-normal incidence does generate the desired result of shifting the transmission curve off the emission line in order to get a reading of the nearby continuum level, there is one major drawback: in addition to shifting the curve, non-normal incidence also broadens it. For a full discussion, see *Hernandez* [1986]. The effects can be seen in Figure 2.8, which shows both the line and the continuum profiles reported by *Filosofo et al.* [1965]. As can be seen, the broadening of the continuum curve leads to overlap with the emission line curve.

Calibration routines for the tilting photometer were similar to those previously discussed. These included calibrating with standard sources in the laboratory as well as comparisons with other photometers.

2.3 Birefringent Photometer

In all of the photometers discussed so far, much concern has been expressed over the amount of background radiation inherent in each measurement and the steps that were taken to separate the desired emission from this

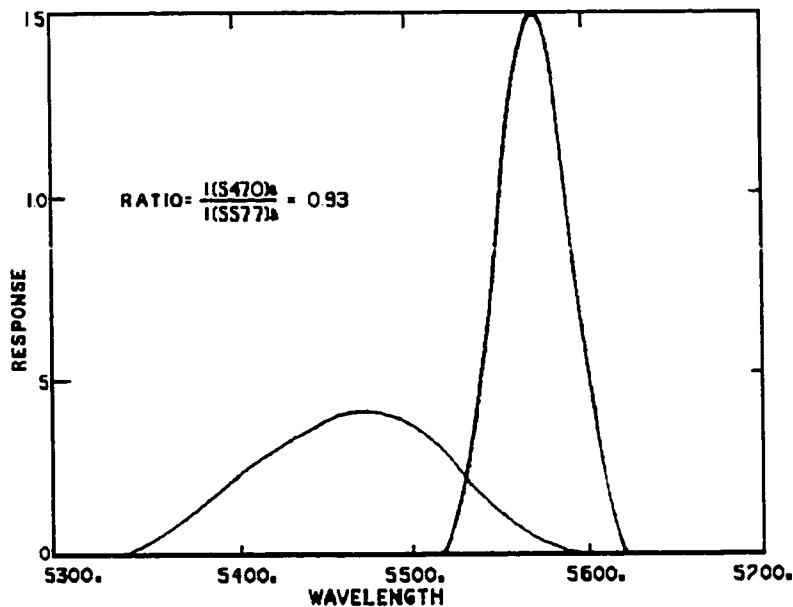


Figure 2.8: Transmission curves for normal (line) and tilted (continuum) incidence angles [Filosofo *et al.*, 1965, fig. 4]

background. The birefringent photometer solved this problem by modulation (or scanning) of the spectrum, using the optical properties of birefringent materials to select out the particular wavelength of interest.

The key component of this instrument is the birefringent crystal used in a Lyot-Öhman wide angle configuration (6° field of view) [Lyot, 1933; Öhman, 1938]. Light propagates through isotropic materials at the same speed, regardless of the orientation of the substance. In anisotropic materials light propagates at different speeds depending upon the direction of its travel (i.e. the index of refraction varies as a function of orientation). Such materials are referred to as being birefringent. Each axis has a different index of refraction, which leads to retardation of the light beams depending upon the direction. When the two rays emerge from the material and are superimposed, there will be a phase difference. The relative retardation, or phase difference, of the two light rays can be expressed as $\Delta\phi = \frac{2\pi}{\lambda_0}d(|n_o - n_e|)$, where λ_0 is the wavelength of the incident light, d is the length of the material, and n_o and n_e are the ordinary and extraordinary indices of refraction.

The optical arrangement of the birefringent photometer used to collect the data at Sacramento Peak is

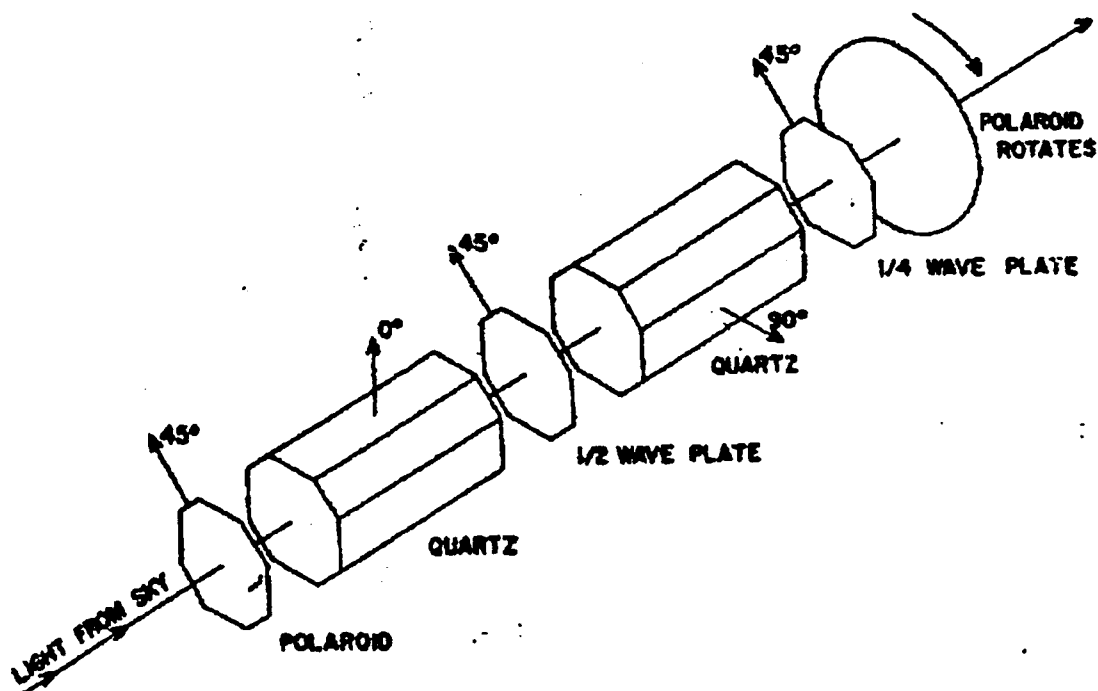


Figure 2.9: Optical components of the birefringent photometer [Dunn and Manring, 1956, fig. 2].

illustrated in Figure 2.9 [Dunn and Manring, 1956, fig. 2]. Incoming light is linearly polarized and then passes through two quartz crystals separated by a half-wave plate. A quarter-wave plate after the final quartz changes the light to elliptical polarization. The final optical component is a rotating polarizer. As this polarizer rotates, emission from the line is modulated, showing peaks at specific rotation angles, while that from the background continuum is approximately constant at all angles [Koomen *et al.*, 1956]. The modulation signal, therefore, represents the radiation present in the line only, without the need for complicated background subtraction routines.

Measurements were obtained using 0, 40, 55, 70, 75, and 80° zenith angles, with each azimuth scan taking six minutes. In contrast to many of the other photometers that were restricted to observe only in dark-moon conditions, the line isolation characteristics of the birefringent photometer allowed observations to be taken under much more liberal conditions. The instrument used in the Sacramento Peak observations was reported to be capable of taking measurements 'during full moon if a region of 20 degrees centered about the moon is

excluded' [Dunn and Manring, 1956].

Continuum exclusion, the feature that made the birefringent photometer so attractive for airglow measurements, also made the instrument a challenge to calibrate. Several methods were ultimately developed and used for the data set studied in this dissertation. The first method, described by Jones [1965], involved direct comparison of brightness levels recorded by the birefringent device with another photometer that had its own calibrated standard source, such as the turret photometer discussed above. The second and third methods, detailed by Hernandez and Layman [1965] and Dandekar *et al.* [1965], use a modulated standard source and a second polarizer, respectively. The recorded modulation of the line after passing through the birefringent element provides a direct calibration of the instrument. For the data studied in this work, both calibration methods were used: during the observation years, comparison with the turret photometer was periodically carried out, and the final data were also adjusted after the instrument was directly calibrated following the observation years.

2.4 Fabry–Perot Spectrometers

The Fabry–Perot spectrometer is a useful tool for studies of the atmosphere using airglow emissions as tracers, with roots as far back as Babcock [1923]. Such instruments have been typically used to measure Doppler widths and shifts of spectral lines, which relate to kinetic temperatures and motions of the emitting medium. The area under the line profiles is a measure of the emission intensity and is the quantity used here.

The essential component of the Fabry–Perot spectrometer is the etalon, a pair of precisely spaced parallel (partially transparent) mirrors. All light entering the etalon at a given angle will undergo numerous reflections, with the transmitted and focused light forming regions of destructive and constructive interference (depending upon the mirror separation). Figure 2.10 illustrates the ray paths for a given angle of incidence. When all beams of a monochromatic source entering the etalon at a given angle of incidence are considered, the resultant pattern is a complete ring; when all angles are considered, a set of concentric rings is formed, as shown in Figure 2.11.

Referring again to the etalon equation, $m\lambda = 2\mu d \cos\theta$, taking for simplicity the case of normal incidence ($\theta = 0^\circ$), and holding the index of refraction constant at $\mu = 1$, one can see that a change of order Δm can be achieved by a corresponding change of mirror separation Δd . In particular, to achieve a one order change

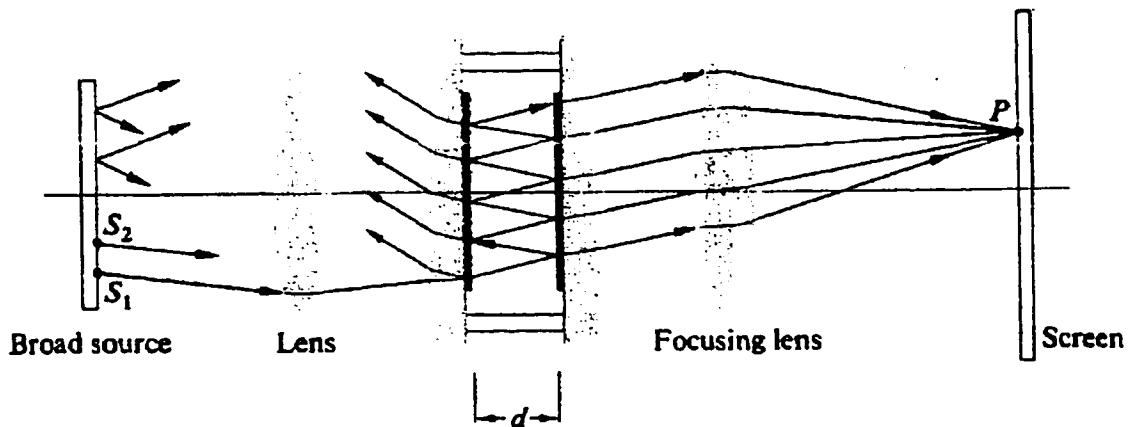


Figure 2.10: Ray diagram for a Fabry-Perot etalon [Hecht and Zajac, 1974]

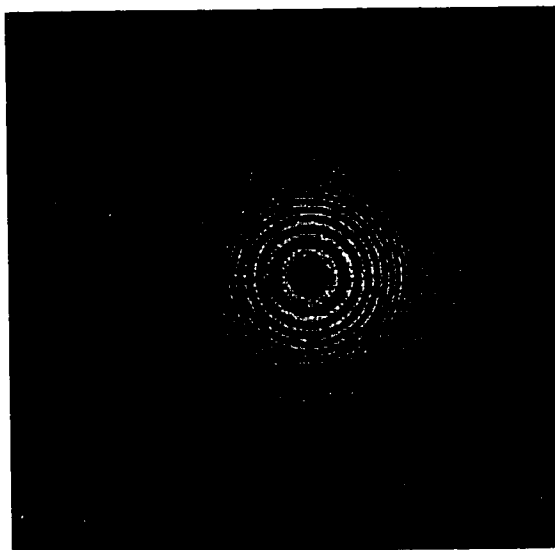


Figure 2.11: Fringes from a Fabry-Perot etalon [Hecht and Zajac, 1974]

($\Delta m = 1$), the change in plate spacing must be $\Delta d = \frac{\lambda}{2}$. With this change, the Fabry–Perot spectrometer is capable of modulating a line source, which makes the instrument an excellent choice for airglow studies.

The change in plate separation can be achieved through the use of piezoelectric crystals, whose lengths change depending on the voltage applied to them. These materials allow for a specific, known motion of one plate in relation to the other. Figure 2.12 shows the setup of the plates and crystals [Hernandez, 1986]. Each plate is supported by an invar steel holder. The basic spacing of the etalon is maintained by the coarse adjusting nuts, while the differential screws above the top plate allow for a more precise alignment of the plates. The bottom plate is mounted upon three piezoelectric crystals, so it is the motion of this bottom plate that varies the etalon spacing.

Another great advantage of piezoelectric crystals is that they allow for automatic dynamical adjustment of the parallelism of the plates. Since a change in order for the instruments used in this work is achieved by an actual change in spacing (as opposed to holding the spacing fixed and changing the index of refraction, for example), it is crucial to have a means of maintaining the parallelism of the plates as they are moved. This is achieved through electronic feedback circuitry [Hernandez and Mills, 1973]. This feedback circuit has proven very successful for achieving the long term stability needed to make precise measurements of the Doppler shift and widths of airglow emission lines.

Figure 2.13 shows a typical emission profile taken with the Fabry–Perot spectrometer located at Mt. John, New Zealand. Line-of-sight wind velocities can be obtained by comparing the position of the peaks in a profile with those from a non-moving reference profile using the principle of the Doppler shift. Wind blowing towards the observer will shift the peaks toward the blue side of the reference peaks, while wind blowing away will move the peaks toward the red side. After removing the instrumental profile, which reflects the best knowledge of how the instrument itself affects the measured data, Doppler temperatures can be calculated from the width of the profile, while the area under the line profile gives a measure of the emission intensity.

Observations are count limited, meaning that integration continues until a minimum count level has been reached. Typically, integration times range from $\sim 3 - 15$ minutes.

All measuring devices have effects on the quantity being recorded, and the Fabry–Perot spectrometer is no exception. If the precise nature of these effects is understood, they can be removed from the observations, leaving only the desired quantity [Hernandez, 1977, 1986]. In this work, this amounts to quantitatively knowing the effect the instrument has on the measured line profiles and removing this effect so that the profiles

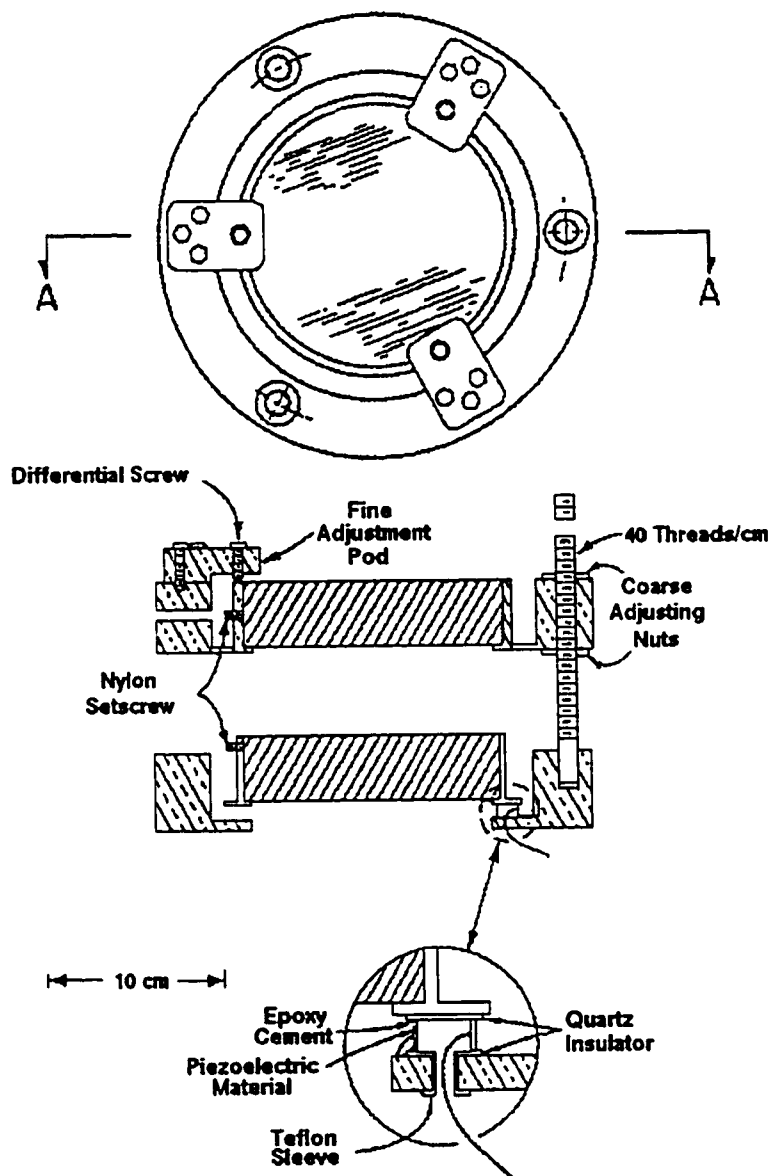


Figure 2.12: Mechanical setup of a Fabry-Perot etalon [Hernandez and Mills, 1973]

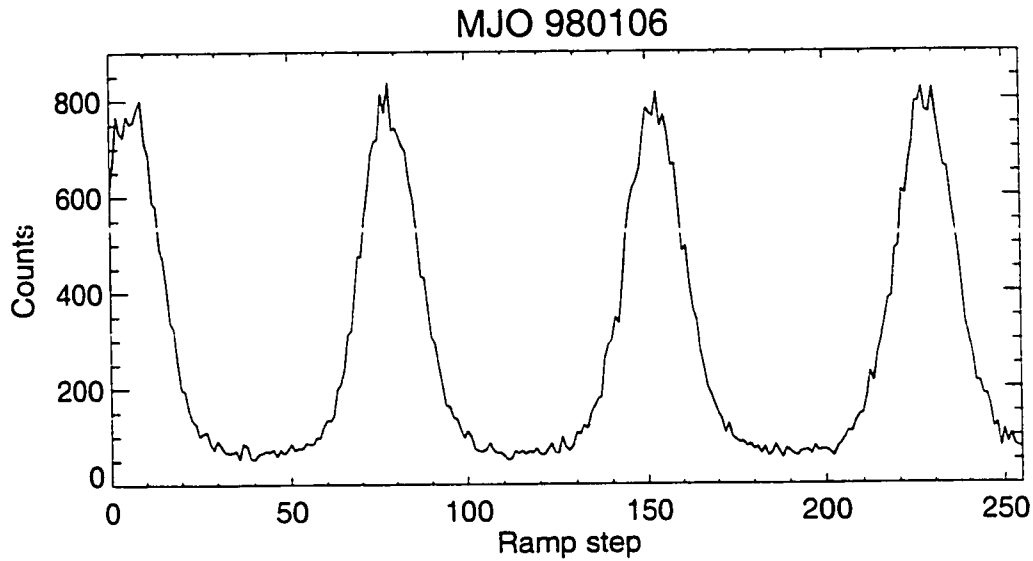


Figure 2.13: Emission profile measured by a Fabry-Perot spectrometer

are then strictly the result of the airglow emission. This is primarily done with a single frequency laser source, whose line profile has negligible width. As actually measured through the spectrometer, however, the laser profile has an apparent definite width. Therefore, the observed profile reflects the instrumental response that needs to be removed from the sky measurements. Laser profiles are observed regularly throughout daylight hours in order to monitor the stability of the instrument.

Other calibrations are made less frequently. Roughly once a year, the reflectivity of the plates and the dead time of the electronics is remeasured. In addition, the aging of the interference filters is monitored yearly. As filters age, their transmission can decrease, their width broaden, and their central wavelength can drift. These effects can show up as a decrease in brightness that might otherwise be attributed to geophysical variations in emission intensity. Because of the precise nature of the measurements being made, these calibration steps are a crucial part of insuring both the precision and accuracy of the observations.

Chapter 3

DATA AND ANALYSIS

This chapter will briefly describe the data sets used in this dissertation and the analysis performed on them. About one-half of the data sets have been published previously in the literature, while the rest are unpublished. The geographical location of the observatories used in this work is shown in Figure 3.1. As can be seen, the coverage here is nearly global, with data sources on six continents. Although the majority of the stations are in the northern hemisphere, there is a reasonable representation of southern stations as well.

3.1 Long term data sets

Long term data sets are the core components of this study. In order to develop a climatological understanding of any phenomenon, it is necessary to have data for a long enough term to characterize it. An interesting question we will examine is just how long of a data series is needed to achieve a stable climatology. For the purposes of this investigation, we have arbitrarily chosen eight years as a starting baseline time period. The issue of whether this starting value is a sufficiently long period will be addressed as part of this work, as will be seen later. Ten long term data collections have been analyzed in this study. Table 3.1 provides an overview of these sources, showing both the broad geographical spread of the stations and the extensive time coverage (over 10,000 nights of data from all over the world). Each station is discussed in more detail in the subsections below.

3.1.1 Lord Rayleigh's data

Lord Rayleigh and his colleagues undertook the first global study of the atomic oxygen emission at 5577 \AA in the 1920s. The data were taken with visual photometers as described earlier. The results of these studies can be found in *Rayleigh* [1924] and *Rayleigh* [1928]. These measurements continued into the 1930s, leading to long term measurements at three stations: Terling, England (TER); Cape of Good Hope, South Africa (CAP); and Canberra, Australia (CAN) [*Rayleigh and Spencer Jones*, 1935].

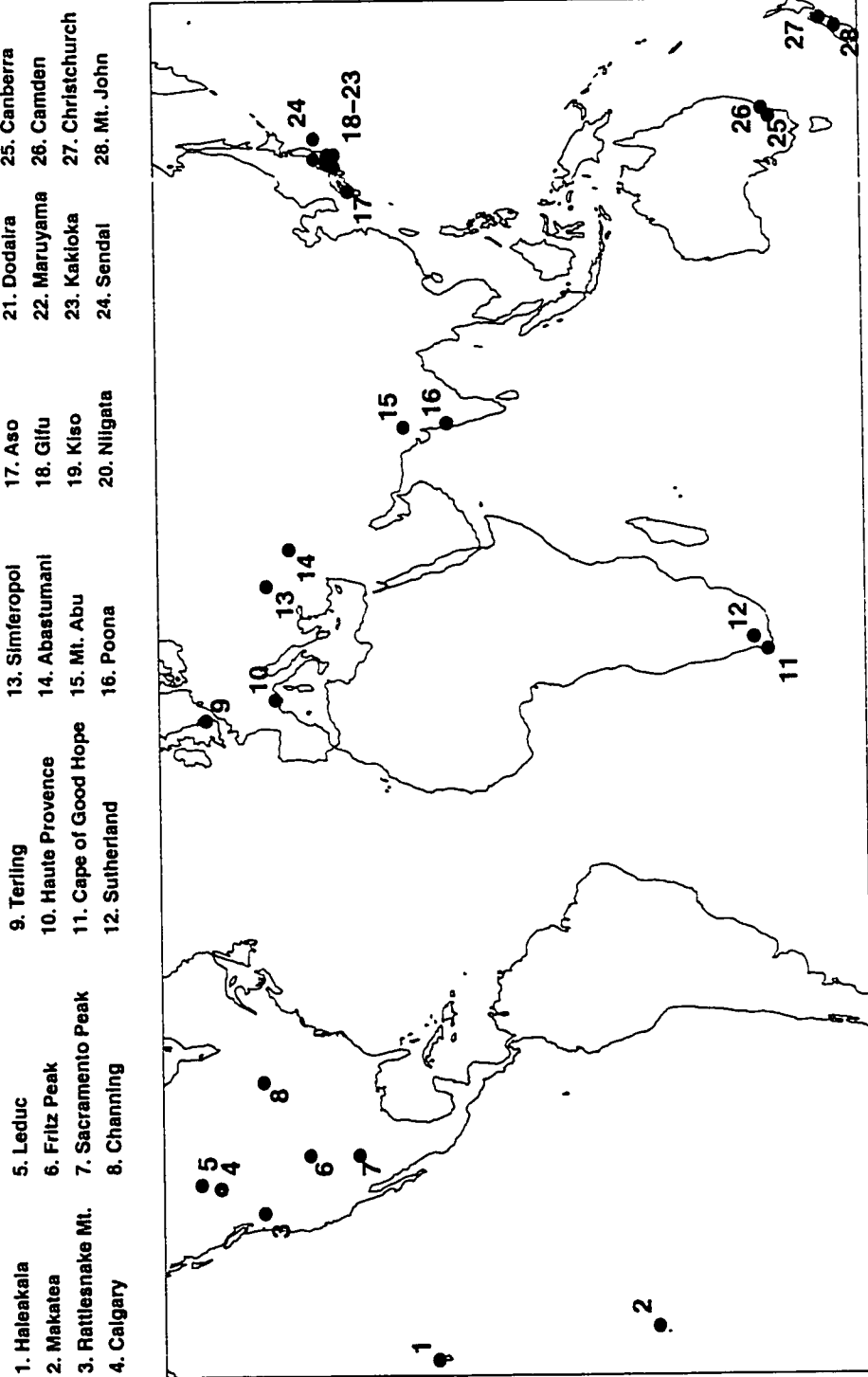


Figure 3.1: Global distribution of datasets in this study.

The typical observational technique was to make one measurement per night near 2300 local time during the two week period about the new moon. It is important to note here that due to the high latitude (52° N) of Terling, the sky was not sufficiently dark (never reaching astronomical twilight at 18° solar depression angle) during the summer months for observations to be taken. Capetown and Canberra were not affected in this way.

Hernandez and Silverman [1964] later re-examined the work of Lord Rayleigh and his collaborators and converted their measurements into the now common unit of brightness, the Rayleigh. As part of their study, all existing original data records from Lord Rayleigh's work were obtained. Due to fire at the Rayleigh laboratory in the late 1920s, some of the original records are missing. For example, most of the daily measurements at the stations were lost, leaving only multi-night averages available for use. These averages were taken over an observing period near each new moon, and there are typically between 8 – 14 nights in each average, depending on weather. The particular dates contributing to each average are uncertain: only the 'central' date and the total number of nights in the average are given. How these unknown factors are considered in the analysis of the data is discussed below. Although this collection of data is old, Lord Rayleigh and his colleagues took great care to assure the consistency of the observations, and they still are the longest green line studies ever undertaken.

3.1.2 *Sacramento Peak*

Observations of several airglow emission lines were made at Sacramento Peak, New Mexico (SAC) from 1953 – 1963, using a birefringent photometer as described in the previous chapter. Part of this data set was included in the International Geophysical Year (IGY) campaign in 1957 – 1959. Several published studies have used this data set, among them *Manring and Pettit* [1955]; *Hernandez and Silverman* [1964]; *Yao* [1962]; *Rosenberg and Zimmerman* [1967]; and *Brenton and Silverman* [1970].

3.1.3 *Fritz Peak spectrometer*

A Fabry–Perot spectrometer operated at Fritz Peak, Colorado (FPO) in the mid–1970s, and approximately nine years of green line observations are used in this work. As discussed in the instrumentation chapter, interferometric spectrometers are ideally suited for making precise observations of wind velocities and temperatures at airglow heights, and these quantities were the primary focus of the work done at Fritz Peak

[Hernandez, 1982; Hernandez and Roble, 1979, 1984, 1995]. In the course of measuring a line profile, the intensity of the emission is proportional to the area under the profile, and these intensities are analyzed for the first time in this work. These intensities have not been calibrated, and therefore are expressed in counts rather than Rayleighs. However, since the focus of this work is the variation in brightness, counts are adequate, provided that the instrument characteristics (i.e. filter quality, photomultiplier tube response, reflectivity) are stable and reasonably well-known. Brightness data from the Fritz Peak spectrometer span the period from 1977 – 1985, and include only known clear nights, as reported by an observer on the premises.

3.1.4 Mobile Automatic Scanning Photometers (MASP)

Battelle Pacific Northwest Laboratories began the MASP program in 1979 as part of the International Magnetospheric Study of 1979 – 1980. The program consisted of airglow observations at seven North American locations through a collection of Mobile Automatic Scanning Photometers (MASP) and is described in *Kleckner et al.* [1983]. These measurements were extended for several years after the original campaign, and two of the stations (Rattlesnake Mt., Washington (RAT) and Channing, Michigan (CHA)) were in isolated, dark-sky locations and have sufficient coverage to be included as part of the long term analysis in this dissertation. The MASP data were generously provided by Don Slater at PNL.

Because these were automated observatories, measurements were taken under all moon and weather conditions. Initial investigation of the data from these stations revealed that the nightly emission intensities were strongly influenced by the moon, even when only zenith measurements are considered. We therefore use measurements through the continuum filter as an indication of the amount of background light present. For each green line observation, a fraction of the nearest (in time) continuum observation is subtracted in order to remove much of the background light. This fraction is selected for each station individually to optimize the removal. Once this background level is removed, the green line emission intensities no longer exhibit the strong moon effect.

Reconstructing weather conditions is another challenge for the MASP data sets, as site based weather reports are unavailable. We therefore use observations taken at stations in the Solar and Meteorological Surface Observation Network (SAMSON), made available by the National Climatic Data Center. Observations of the total cloud cover, reported in tenths of the sky, were made every hour. For each night of observations, we take the average of cloud cover observations made between 1800 – 0600 LT. We arbitrarily chose to keep all

nights where the average cloud cover was less than or equal to 0.9. This cutoff level may seem quite high, but since we are only using the zenith measurements in this work, the photometer only viewed a small portion of the sky, and since we have no information on the location of the cloud cover, we strive to not eliminate any data unnecessarily. This cutoff level for these stations leaves us with 45 – 50 % of the original nights. For our other long term stations, where weather conditions were recorded as part of the observations, typically 20 – 30 % of the available nights are considered clear. While our retention rate is higher, we cannot justify a more stringent criterion.

This weather consideration is only possible for the two long term stations. For Rattlesnake Mt. (46.4°N, 119.6°W), we were able to use weather observations taken at Yakima (46.6°N, 119.5°W) through 1990, and for Channing (46.1°N, 88.7°W), the nearest complete weather observations were taken at Houghton (47.2°N, 88.5°W).

3.1.5 Kiso

The World Data Center C2 in Tokyo provided one of the longest collections in this study – eleven years of 5577, 5893, and 6300 Å airglow observations from Kiso (KIS), Japan taken over the period of 1979 – 1990. This is a particularly useful period because it overlaps with other observations (Fritz Peak and the MASP observatories). Information about this data set is otherwise scant. However, the overall behavior and noise characteristics at Kiso are comparable to those from other stations. An illustration of this is shown in Figure 3.2, which compares the raw nightly average brightness at Kiso and Fritz Peak from 1979 to through 1985. In general, the two stations clearly show the same behavior of increasing brightness roughly through 1982 followed by decreasing brightness throughout the rest of the period (the differing vertical scales are not relevant: Kiso data are presented in Rayleighs while the data from Fritz Peak are in counts). Even considering that the exact observation dates do not match, many of the smaller scale features also appear at both stations, such as the rise just prior to 1980, the peaks in mid 1983 and 1984, and the minimum in 1985 followed by increasing brightness.

Another illustration of this similarity can be seen in Figure 3.3, which shows the correlation between the two stations. The ratio of two week averages divided by the calendar mean is plotted for each station. Given that the time coverage of the two data sets are not exact (1979 – 1991 for Kiso, 1977 – 1985 for Fritz

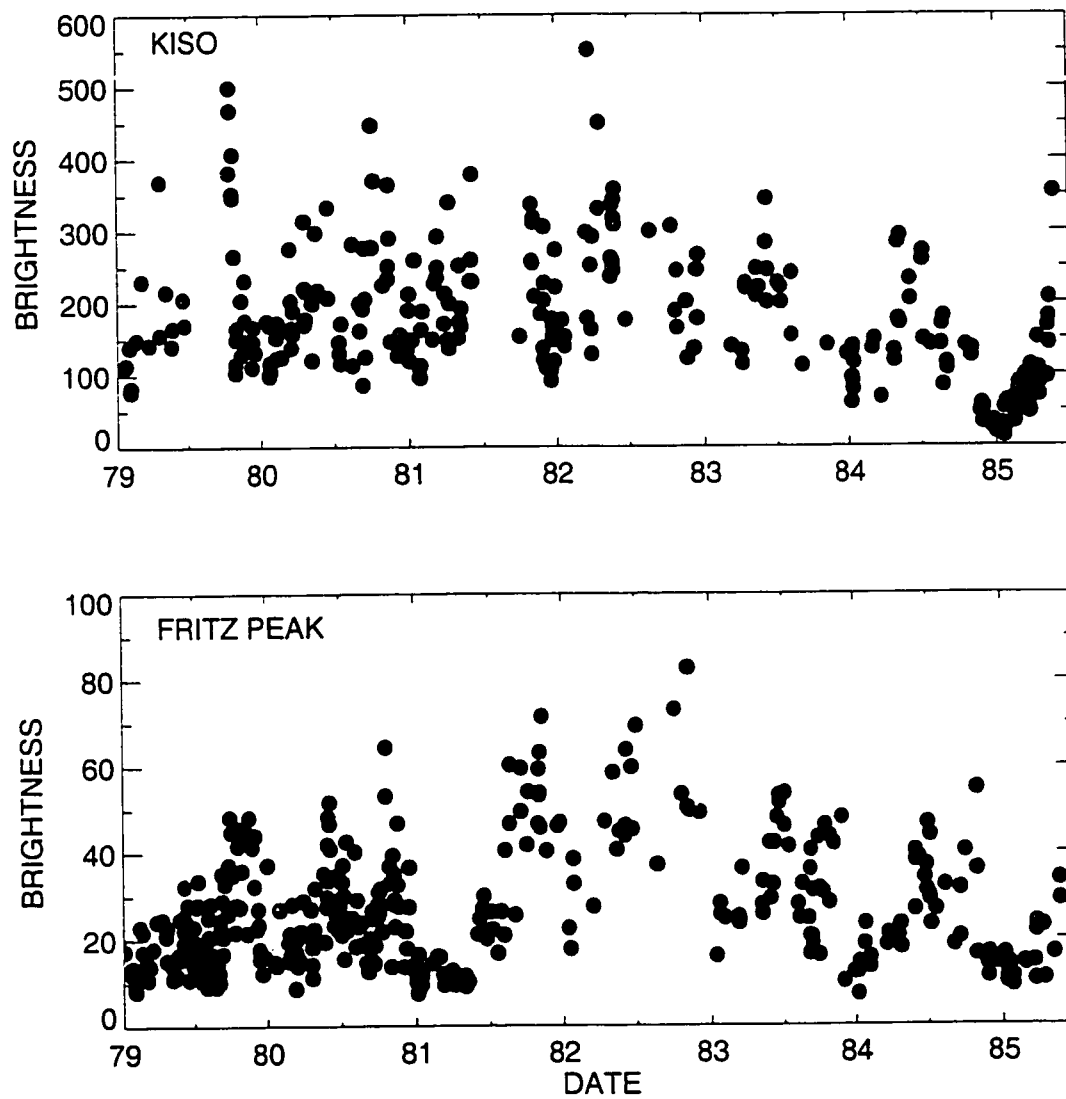


Figure 3.2: Raw nightly brightness averages for Kiso and Fritz Peak, 1979 – 1985.

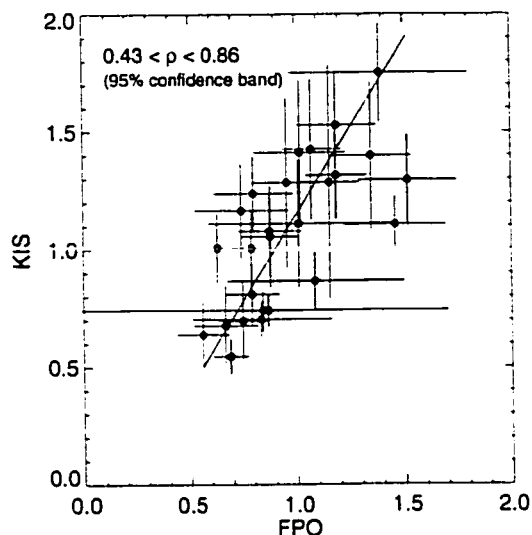


Figure 3.3: Comparison of Fritz Peak and Kiso data sets. The ratio of two week averages to the yearly mean is plotted for each station.

Peak), and realizing that local effects are likely, we take this level of correlation to be indicative of at least the similarity in data quality at the two stations.

3.1.6 Mt. John

Airglow observations have been carried out by a Fabry–Perot spectrometer at Mt. John (MJO), New Zealand since 1991. The instrumental setup and observational plan are identical to that used to obtain the Fritz Peak spectrometer data. Some results from wind and temperature analyses can be found in *Hernandez et al.* [1995a] and *Hernandez and Smith* [1995], but the intensity aspect has not been examined to date. Only clear weather data, as reported by the astronomers working at the observatory, are used in this study.

3.2 Supplemental short term data sets

While the main focus of this work is to investigate the long term climatology of the green line emission, shorter term data sets (of duration at least one year) have proven to be quite useful for addressing related questions. Table 3.2 summarizes the short term data used in this dissertation. As can be seen, several of the

Table 3.1: Summary of long-term airglow datasets

Code	Station	Geog. Location		Inv. Latitude	Date Coverage
TER	Terling	52.0 N	1.0 E	48.6 N	1923.6–1934.3 [†]
RAT	Rattlesnake Mt.	46.4 N	119.6 W	52.6 N	790508–901017
CHA	Channing	46.1 N	88.1 W	57.4 N	790819–900102
FPO	Fritz Peak	39.9 N	105.5 W	48.9 N	770812–850524
KIS	Kiso	35.8 N	137.6 E	28.7 N	790101–901224
SAC	Sacramento Peak	32.5 N	105.5 W	41.3 N	530510–630628
CAP	Cape of Good Hope	33.9 S	18.5 E	42.0 S	1925.8–1933.1 [†]
CAN	Canberra	35.3 S	149.1 E	45.6 S	1925.8–1934.0 [†]
MJO	Mt. John	44.0 S	170.5 E	51.2 S	910209–991117

[†] Multi-night averages.

data collections fill in geographic gaps not covered by our long term observations. We also have used these data to look for changes in the seasonal emission behavior over many decades at one particular location (such as MJO/CHC, KIS/JAP, OHP), and, with the inclusion of measurements taken under both the IGY and IQSY campaigns, to investigate whether there is any significant difference in brightness levels under varying solar conditions. Although we cannot address these questions fully using only our long term data, they can be approached with the addition of these shorter length collections.

The scientific community has conducted two main programs of airglow monitoring: the IGY campaign from 1957 – 1959 and the IQSY campaign from 1964 – 1965. The aeronomy portions of these campaigns were global studies of several airglow emissions ([OI] 5577 Å, NaI 5890 – 5896 Å, [OI] 6300 Å, OH 8400 Å, N₂⁺ 3914 Å), one during a maximum of the solar cycle and one during a minimum, undertaken to study the effects of solar activity on the emissions and to determine whether the emissions have a geographical dependence.

Several different types of instruments were used in these campaigns, including the turret, tilting, and birefringent photometers previously described. Measures were taken to develop a standard method of calibration and data presentation in both studies [Roach, 1956, 1968]. The data from these campaigns were originally published in tabular form [Yao, 1962; Smith *et al.*, 1968]; recently, however, data entry projects undertaken by the National Geophysical Data Center (NGDC) have made the data available electronically, greatly increasing

their usefulness and allowing them to be incorporated here. We are grateful to Helen Coffey of the NGDC for her assistance in making these digitized observations available to us.

Thirteen data sets from the IGY campaign and nine from the IQSY campaign are included in this work. These stations are widely spaced around the world, with latitudes ranging from $\sim 45^{\circ}\text{N}$ to $\sim 34^{\circ}\text{S}$. In many cases, a station was involved in both studies. At many of these stations, the data coverage is insufficient to draw any conclusions regarding the seasonal behavior of the green line emission. To improve matters, several stations have been grouped in order to form a 'regional' station. In particular, the closely spaced Japanese stations of Niigata, Kakioka, Dodaira, Gifu, Maruyama, and Aso have been combined to form a single Japan station; Simferopol and Abastumani have been combined into West Asia (WAS); Mt. Abu and Poona have been combined into India (IND); and Haleakala and Makatea have been combined to form a Pacific (PAC) station. Also, the IGY and IQSY runs for Haute Provence (OHP) and Sendai (SEN) have been merged into a single data set for each station.

In addition to data from these organized campaigns, data from four additional locations were used. Photometer data from Haute Provence (OHP), kindly made available by Gerard Thuillier, provide a contemporary set of measurements to go along with the long term data at Mt. John, while photometer observations from Fritz Peak provide additional time coverage to the later interferometer data from that site. Data from Sutherland (SUT), South Africa were originally published in *Burnside and Tepley* [1990] as a comparison with data from Arecibo (not included here because it is an equatorial station). Considerable effort was made by Craig Tepley to recover the digital records of these observations and make them available to us. Spanning four years in the mid-1970s, this tilting photometer data set is quite close in location to the early Rayleigh measurements taken at the Cape of Good Hope in the 1920s and 1930s, and thus provides a means of looking for long term changes in the emission behavior. A similar comparison can be made with the addition of data from 1962 – 1964 in Christchurch. These observations, first analyzed by *Neff* [1965], were made about a hundred kilometers away from the current observatory at Mt. John, New Zealand. The original data notebooks were generously loaned to us by Sam Neff. A mean value of the green line intensity at Christchurch (185 R) was also given by *Rayleigh* [1928], based on a year's worth of observations beginning in 1926.

Two additional data sets are listed in Table 3.2: Leduc (LED) and Calgary (CAL). These two Canadian sources were part of the MASP program, but we were unable to obtain adequate weather records for these stations and therefore have not included them in the full analysis. They are listed for completeness: if such

records are someday found, then these two data collections would be useful.

3.3 Analysis

When working with data gathered in various ways from different types of instruments, one obvious challenge is developing a method of analyzing them collectively. For example, the data from the IGY and IQSY campaigns are presented as hourly average values, meaning that the individual measurements that contributed to these averages have essentially been lost. Observations from the interferometers, on the other hand, are count limited, so the number of observations in any given hour varies according to the strength of the emission. At the other extreme, the existing data from Lord Rayleigh's work is comprised of multi-night averages of single-observation nights. Also, while the data from some sites have been converted into Rayleighs, that is not the case for all of the sites, where counts are commonly presented. This section first outlines the general process that was followed to bring all the data into a common format for comparison. Certain data sets required variations of this process, and these special cases are considered next. Following that is a discussion on geomagnetic activity and how it fits into the analysis routine.

Data are initially presented as a time series of brightness measurements. Figure 3.4 shows the raw nightly averages for two stations, Kiso and Mt. John. The data have been arbitrarily scaled for presentation purposes, so the emission vertical scales should not be taken as equal for the two stations. Also plotted in the figure is the solar 10.7 cm flux. The variation of green line intensity with solar flux has been investigated previously [Rosenberg and Zimmerman, 1967] and will be re-examined later.

Since most of the data are presented in local time, any data sets originally in UT are converted to local time. Then, if there are multiple measurements in a given night, they are combined into a single nightly average value, weighting by measurement uncertainties where available.

3.3.1 Statistical analysis

The most straightforward way of finding significant variations in a data series is through statistical analysis [Bracewell, 1965]; however, for this analysis to be valid, the data must satisfy certain assumptions [Hernandez, 1999]. Ideally, the time series should be long, preferably of infinite length, a condition that is not approached in real world situations. Harmonic analysis presumes that time series are cyclical in nature. If this is not the case, various tapering techniques have been used to diminish a discontinuity between the start and

Table 3.2: Summary of supplemental airglow datasets

Code	Station	Geog. Location		Inv. Latitude	Date Coverage
LED	Leduc	53.2 N	113.3 W	61.1 N	811101–841224
CAL	Calgary	50.9 N	114.3 W	58.4 N	830114–880312
SIM	Simferopol	44.8 N	34.0 E	39.9 N	570721–591223
OHP	Haute Provence	44.0 N	5.7 E	38.2 N	640104–650902 570629–591104
OHP	Haute Provence	44.0 N	5.7 E	38.2 N	920730–950806 970203–990515
ABA	Abastumani	41.8 N	42.8 E	36.9 N	570704–591028 640106–651104
FPO	Fritz Peak	39.9 N	105.5 W	48.9 N	570701–591204 48.9 N 690314–750218
SEN	Sendai	38.1 N	144.6 E	30.8 N	570821–591221 640106–651116
NII	Niigata	37.7 N	138.8 E	30.6 N	570701–590806 640105–650927
KAK	Kakioka	36.2 N	140.2 E	29.0 N	570728–591204
DOD	Dodaira	36.0 N	139.2 E	28.8 N	640414–651127
GIF	Gifu	35.4 N	137.0 E	28.3 N	570721–591230
MAR	Maruyama	35.0 N	140.0 E	27.8 N	570705–590601
ASO	Aso	32.9 N	131.0 E	26.0 N	570801–591123 640213–640813
ABU	Mt. Abu	24.6 N	72.7 E	18.4 N	571017–581216 641124–651229
HAL	Haleakala	20.7 N	156.2 W	21.3 N	640110–651230
POO	Poona	18.5 N	73.9 E	11.6 N	590109–591230
MAK	Makatea	16.4 S	148.3 W	15.1 S	640106–651117
SUT	Sutherland	32.4 S	20.8 E	23.4 S	730126–770324
CAM	Camden	34.0 S	150.7 E	44.0 S	570630–580914
CHC	Christchurch	42.5 S	172.6 E	49.1 S	620529–640405

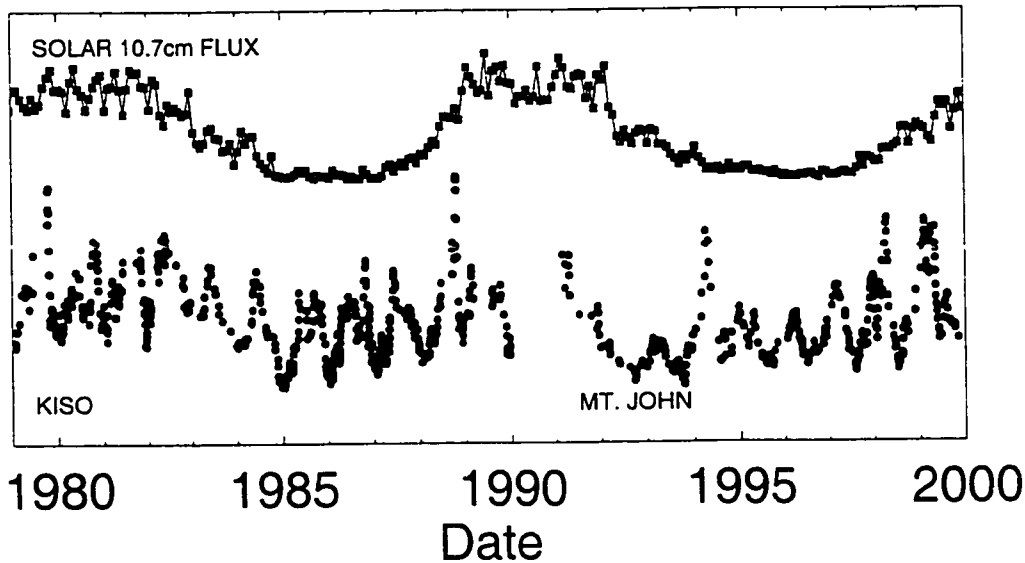


Figure 3.4: Original time series of green line brightness for Kiso and Mt. John, along with a measure of solar activity (10.7 cm flux). Data have been formed into nightly averages and have been slightly smoothed for presentation purposes.

end of the series [Blackman and Tukey, 1959]. While it is possible to work with unevenly spaced data (such as the case in this work, where weather or instrumental problems do not permit observations every night), it is necessary that the gaps themselves not be periodic in nature. If they are periodic, they may show up as significant oscillations in the power spectrum of the series. Also, spikes (or discontinuities) in a data series will be treated as delta functions in the time domain. This leads to the spreading of power over all frequencies in the frequency domain, effectively increasing the background level of the frequency spectrum.

Given these restrictions on series length and data quality, only a few of the data series used in this work are suitable for a statistical analysis. Periodograms for the nightly average values of the data series shown in Figure 3.4 (eleven years at Kiso and nine years at Mt. John) have been calculated, and the results can be seen in Figure 3.5. For details of the methodology, see Hernandez [1999]. The 95% significance level as computed by the Fisher-g test [Fisher, 1929] is also indicated. Both Kiso and Mt. John show a strong annual oscillation, and Kiso also has a statistically significant half-year oscillation.

In those cases for which statistical analysis is possible, the most significant feature is the yearly variation.

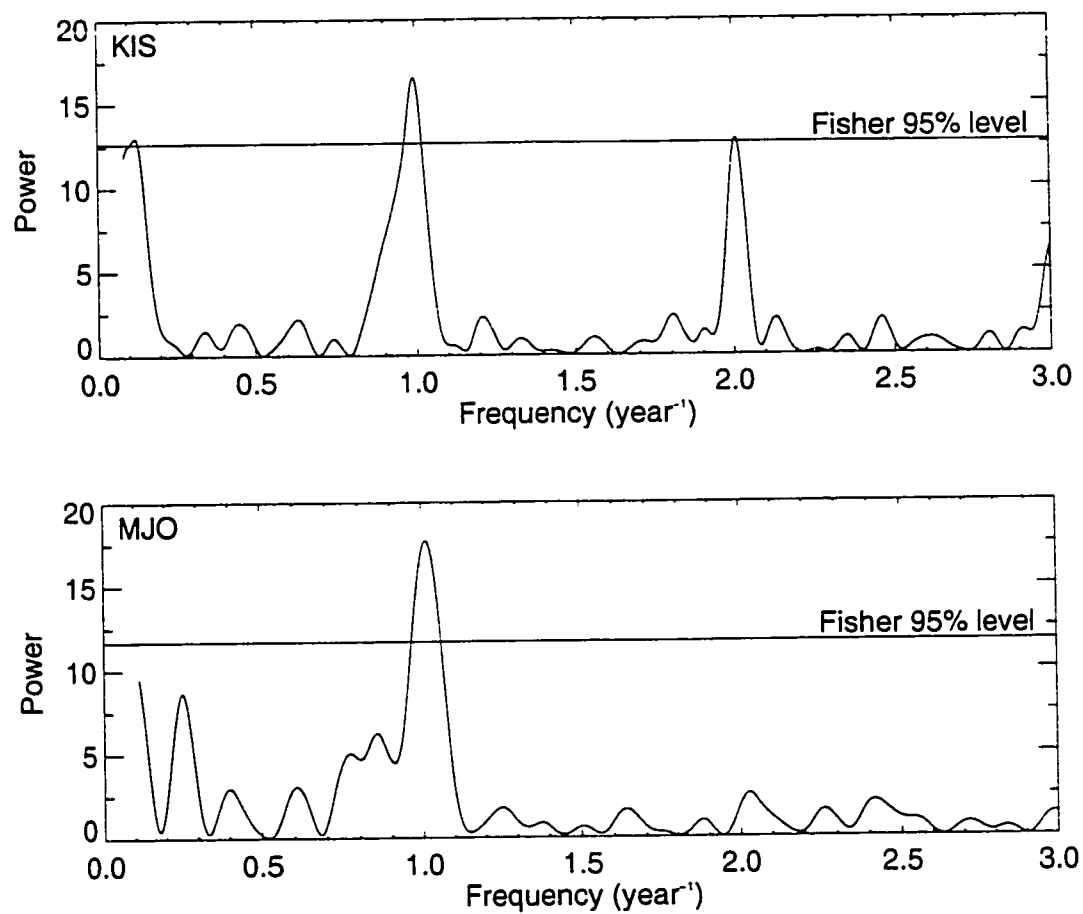


Figure 3.5: Periodogram for the Kiso (KIS) and Mt. John (MJO) data sets. The significance level is computed from the Fisher-g [Fisher, 1929] test. Both data series show the strongest power at one year, while Kiso also exhibits a barely significant six month oscillation.

This result formed the basis for the reduction of the remainder of the data sets. For this task, we have used the technique of superposed epoch, as will be described below.

3.3.2 *Superposed epoch analysis*

Analysis using superposed epochs is commonly used to as a way to fill in observational gaps in data series. However, it is crucial to consider the inherent periodicities of the data when selecting the superposition period.

Based on our periodogram results, which show a strong one year periodicity in several of the data sets, we have chosen to use a one-year superposed epoch analysis for the remainder of the data sets. While this choice for a superposition period is reasonable since it is based upon one of the significant frequencies, it does have implications. Looking again at the top plot in Figure 3.5, there is significant power at $\sim 0.1 \text{ yr}^{-1}$, although this peak is not completely resolved. Whether this peak is truly of a geophysical nature or is simply related to the length of the data series (11 years) is unknown and will be discussed later. The power spectrum for Mt. John also shows increasing power at the low frequency end of the spectrum, although it is below the 95% significance level. By choosing a one year superposition period, we are effectively ignoring all information that may be contained at frequencies lower than this choice. One might argue that there is no significant information in the Mt. John data series below one year, but we do not know the true nature of the rising power near $\sim 0.1 \text{ yr}^{-1}$. Certainly, there is significant information below one year in the Kiso data which will be effectively ignored in a superposed epoch analysis. However, since we are unable to use periodogram statistical analysis for most of our data sets, superposed epoch is our best option.

Our superposed epoch method is as follows: Each nightly average is divided by its respective calendar-year mean, so that the final quantity is a unitless ratio reflecting the difference of each night from the yearly mean. This step allows for the comparison of all data sources, regardless of units of measurement. All normalized years are then superposed and the results are placed into bi-weekly groups to create a 'typical' year's behavior. This final result represents the yearly, long term, coherent climatology of the green line yearly variation.

Figure 3.6 shows a comparison of the green line emission's seasonal variation as established by both the superposed epoch technique and through direct statistical analysis for Kiso and Mt. John. The plotted points and lightly shaded region represent the superposed epoch result and its 95% confidence band, while the smooth line shows the curve constructed from the significant oscillations found by statistical analysis. No

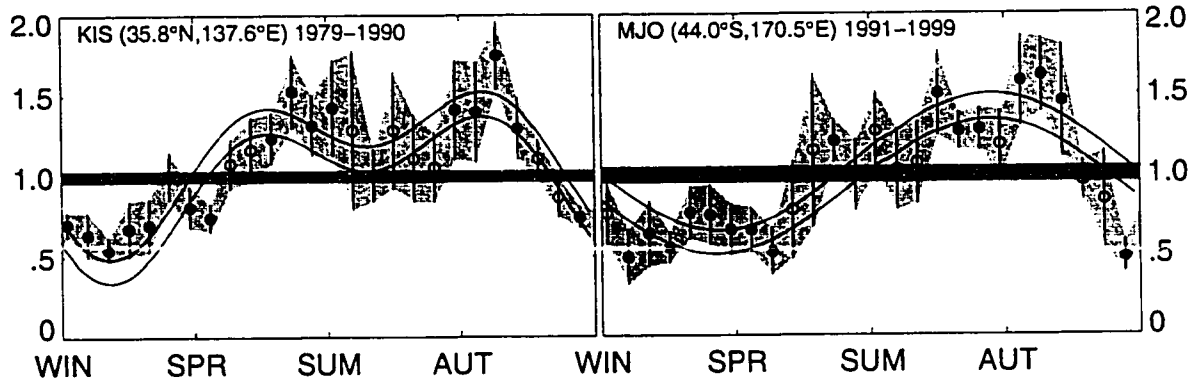


Figure 3.6: Comparison of the annual (and semi-annual for Kiso) significant variability of the green line emission as computed by both direct statistical analysis (between the smooth lines) and by superposed epoch (points and shaded region). Points from the superposed epoch curve represent the bi-weekly values of the normalized yearly variation of the emission intensity. Filled in symbols are those points which are different from the yearly mean value (darkly shaded region at ordinate = 1) at the 95% significance level. The agreement between the results confirms the reasonable applicability of the superposed epoch technique for these two stations. Tick marks indicate the beginning of each season, such that the plot starts and ends at the winter solstice.

systematic cause was found to explain the differences in the width of the confidence bands throughout the year, so it is likely that these differences represent the true variability of the emission. The strong similarities between the results from the two methods confirms that the technique of superposed epoch is a reasonably valid alternative analysis method for data sets unsuitable for periodogram statistical analysis, and that superposed epoch analysis reasonably reproduces the significant features found by the more direct periodogram results.

Figure 3.7 shows the results of our investigation of the effects of ignoring the long term oscillations by performing a superposed epoch analysis. We show in this figure two curves that were generated from the periodogram results in Figure 3.5 for the Kiso data. Curve a) is generated by forming a harmonic function out of the three significant oscillation at 0.1, 1, and 2 yr^{-1} frequencies, while b) includes only the 1 and 2 yr^{-1} power. Additionally, curve c) is the 2 component harmonic function generated by fitting the individual points of our superposed epoch result (as shown in Figure 3.6). While there is some difference in the amplitude of the variation, in general, the agreement illustrates that our results do not substantially change the general behavior by choosing a superposed epoch analysis.

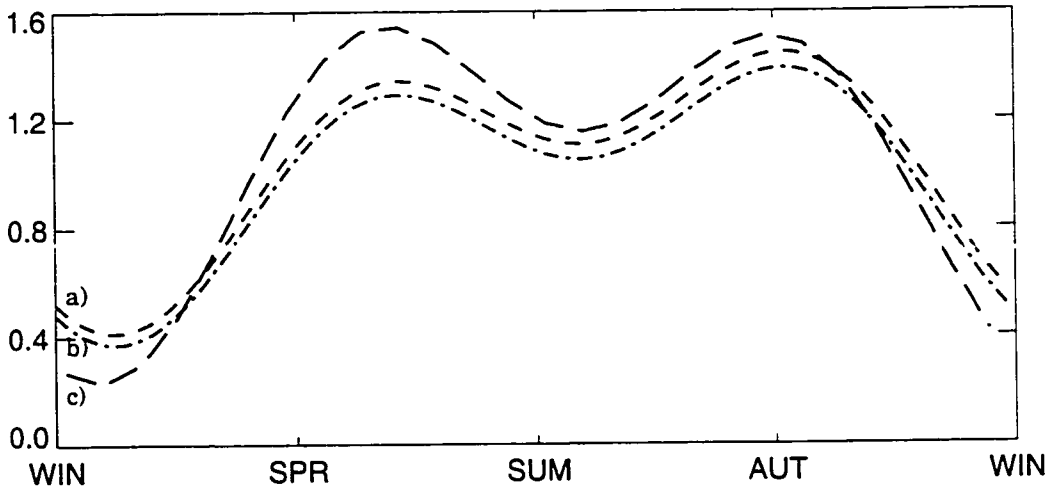


Figure 3.7: Examination of the effect of ignoring the long term power on the resultant seasonal variation at Kiso. Curve a) is the harmonic function constructed from the 3 significant oscillations shown in Figure 3.5 at Kiso, while curve b) is made from only the 1 and 2 yr^{-1} oscillations. Curve c) is the harmonic fit to the superposed epoch results shown for Kiso in Figure 3.6.

3.3.3 Variations of the analysis routine for special cases

The superposed epoch analysis procedure just described is the most generally applied routine. However, because data sets were collected and presented in various ways, this procedure could not be followed for all stations. This section will outline those cases where variations from the above analysis were needed.

Intermediate hourly averages

Data from the IQSY and IGY campaigns were presented as hourly averages. We therefore needed to investigate the validity of forming a single nightly value out of data already presented in average form. While either method should provide nearly identical means, we examined the impact of this intermediate averaging step on the calculated confidence bands by performing both methods of analysis on the Sacramento Peak data. The result is shown in Figure 3.8, where the two methods are compared. As expected, the results show negligible differences, confirming that data sets which are given as hourly averages can be analyzed in a consistent manner with those data presented as individual measurements.

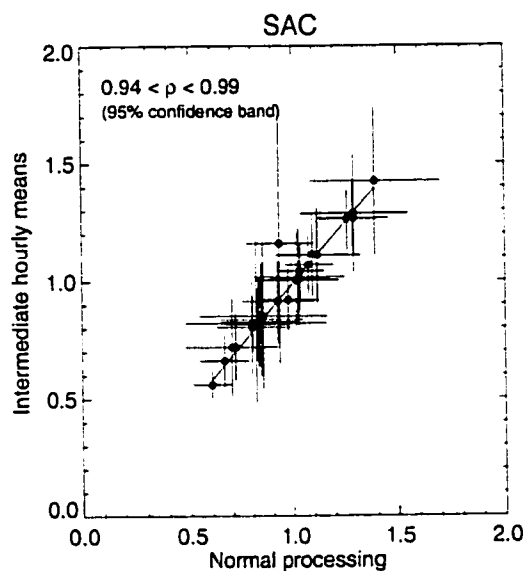


Figure 3.8: Comparison of analysis variations on the SAC data. Nightly averages formed from hourly averages are plotted versus nightly averages formed from individual measurements.

The use of measurement uncertainties

Another issue that bears investigation is the treatment of measurement uncertainties. The spectrometer data taken at Fritz Peak and Mt. John are the only two data sets that include uncertainties with each observation. Since the other data sources do not have a measure of uncertainty, it is necessary to examine the effects of including this information during the analysis. Figure 3.9 shows the result of this investigation. Data from Mt. John were analyzed as detailed above, but in one case all measurement uncertainties were ignored, giving equal weight to all observations, and in the other case the observations were weighted by the given uncertainties. The equal weighting case reflects how all the other data sets were treated, given the absence of measurement uncertainties. The figure shows no appreciable difference in the two approaches; therefore, uncertainties have been used whenever available.

Variation for Rayleigh data

A slight modification of the above process is required when dealing with the early Lord Rayleigh measurements (TER, CAM, CAP). Data from these stations are given as multi-night averages. Centered about the

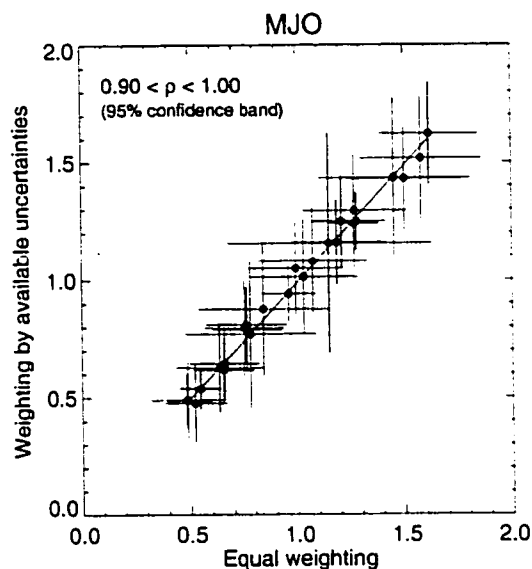


Figure 3.9: Comparison of analysis variations on the MJO data. Analysis using equal weighting versus analysis using weighting by measurement uncertainties.

new moon, these averages typically include 7 – 10 nights, where one measurement was taken per night. The exact dates of the individual observations that contribute to the average are unknown, but we do know the number of nights included in each average. For these locations, the years are simply superposed and the weekly bins subsequently formed. It is important to note that care must be taken when interpreting the results from Terling, due to the summertime gap in observations.

3.3.4 Geomagnetic Activity

The influence of geomagnetic activity on the green line emission was one of the earliest subjects examined by researchers. Most often examined was the relationship between the green line emission intensity and the geomagnetic activity index K_p . As summarized by *Christophe-Glaume* [1965] and *Silverman* [1970], many results suggested that the correlation with geomagnetic activity is dependent upon geomagnetic latitude, insofar as there appears to be a threshold level of K_p at which the dependence begins. At high latitudes (above $\sim 40^\circ$ geomagnetic latitude), the emission increases with increasing geomagnetic activity once K_p is above $\sim 3 - 4$. As the geomagnetic latitude decreases, this threshold level increases, such that at Sacramento Peak

(geomagnetic latitude $\sim 45^\circ$), K_p must reach 8 before the green line intensity becomes significantly correlated [Silverman *et al.*, 1962].

A full investigation of this dependence is beyond the scope of this work, largely due to observational differences at the various locations. As previously discussed, there are two additional sources of green line emission which result from electron interactions, one from dissociative recombination of molecular oxygen ions and the other from auroral sources. These emissions typically occur at higher altitudes than the airglow level at 97 km, but all ground based observations collect light from a vertical column and include all sources of the emission from along such a column.

High resolution spectrometer observations make it easy to distinguish between emission at 5577 \AA generated by these secondary mechanisms because of the high resolving power needed to measure the Doppler temperature of the emitting region [Hernandez, 1971]. Emission originating from a higher altitude than the 97 km region will show a characteristically higher temperature, reflecting the conditions of the higher emission altitude. With these instruments, it is therefore possible to recognize and minimize emission from these secondary sources, and so our data from the Fritz Peak and Mt. John spectrometers have been screened in such a manner. The other instruments used to gather the data used in this study do not have this capability. In some cases, observations were not made when auroras were visibly present, but in other instances, sub-visual auroras would make this determination insufficient. The end effect of these variations in observational method is that data from some stations have already been filtered to eliminate high activity measurements, meaning that we are unable to fully address the issue of the correlation between the emission intensity and strong geomagnetic activity.

To assure that our results are not biased by the inclusion of 'event induced' correlations at some stations and not at others, we have taken efforts to remedy these differences. For the purposes of this work, we have chosen to exclude all measurements taken under high geomagnetic conditions. The geomagnetic indices a_p and A_p were chosen as indicators of activity. The a_p index is a three-hour measurement of the amount of variation in geomagnetic activity (beyond the normal diurnal or latitudinal variations) on a planetary scale (hence the subscript p). Each day's a_p values are averaged into a daily A_p value. These indices have been recorded since 1932 (see *Mayaud* [1980] for details). Prior to 1932, an index called magnetic character (C_i) was used. Yearly summaries of this index were published in *Terrestrial Magnetism* (e.g. *Van Dijk* [1932]). This (C_i) index can be converted into A_p via tables given by *Lincoln* [1967], with the end result being that

A_p values are available for all the data presented here.

For the purposes of this work, we have selected A_p (or a_p) = 30 as the cut off level for elevated geomagnetic activity. This level is roughly equivalent to $K_p \geq 4^+$ [Menvielle and Berthelier, 1991]. A K_p of $3^+ - 6$ is generally thought of as signifying active conditions. Our selection of $A_p \geq 30$ ($K_p \geq 4^+$) is in line with findings that threshold value for a significant correlation of green line intensity with geomagnetic activity is latitude dependent, with $K_p \sim 4$ being the lowest value at which the dependence begins near 50° latitude [Silverman, 1970].

Another reason for choosing the $A_p = 30$ threshold value comes from the inherent properties of the indices themselves. One well known feature of geomagnetic activity is the semiannual oscillation that appears in virtually every magnetic index, known as the Russell–McPherron effect [Russell and McPherron, 1973]. During times of southward oriented interplanetary magnetic field, there is increased coupling between the earth's magnetosphere and the solar wind. This configuration occurs around the equinoxes, leading to the semiannual oscillation in activity indices. The timing of this oscillation coincides with the times of highest auroral activity, so one might reasonably expect that the influence of the activity–related green line sources might also be strongest at these times.

Figure 3.10 shows power spectra for the A_p index for the years 1979 – 1991 (the same yearly range as the observations at Kiso). The top plot is the spectrum produced when all days are included, and it shows that in addition to unresolved significant power at the low frequency end (possibly due to the length of the data series itself), there is a significant oscillation at 2 yr^{-1} . This oscillation is still significant when only those days with $A_p < 40$ are used. However, as shown in the bottom three plots, once the cut off level is $A_p < 30$ or below, the oscillation falls below the 95% significance level. (Note also that at the lowest A_p cutoff level of 10, the power spectrum shows no significant oscillations. This is because such stringent filtering leaves a much smaller and therefore noisier data sample.) Since the phase of this oscillation matches that suggested by the Russell–McPherron effect, we therefore conclude that choosing a cutoff level of $A_p = 30$ reasonably eliminates those green line observations which may be contaminated by high geomagnetic activity events such as auroras.

Because there may be a delay between the rise in geomagnetic activity and its subsequent effects, we have chosen to look at the level of A_p for the day prior to each observation, along with the individual a_p levels on the day of the observation up until the time of the last measurement. This method of choosing the

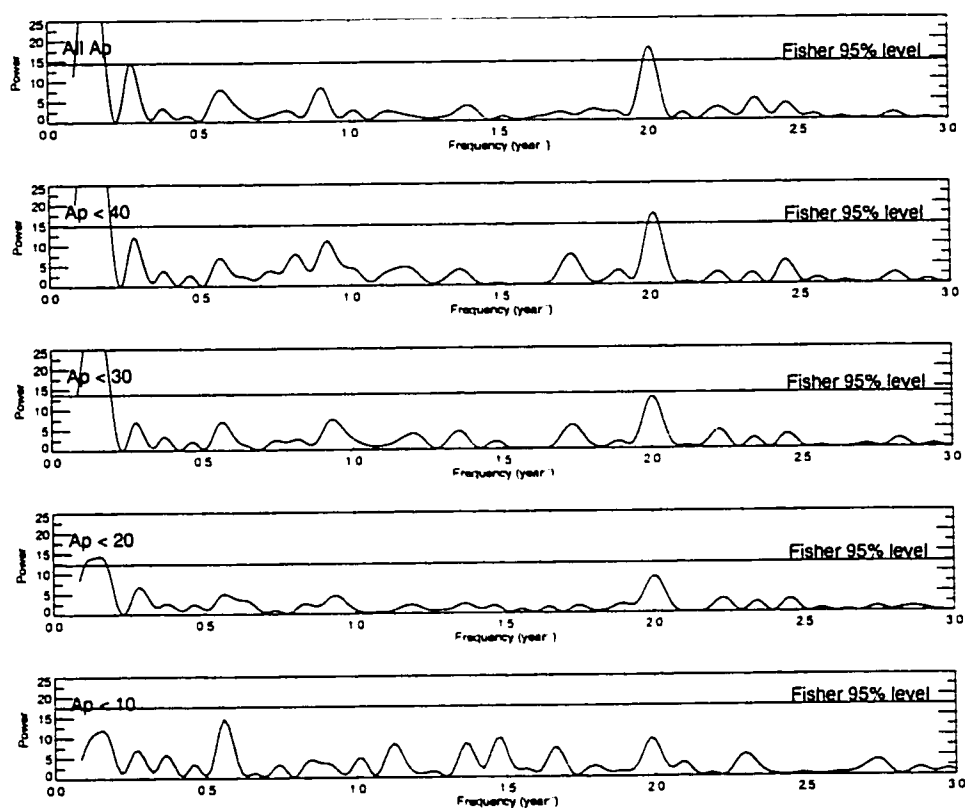


Figure 3.10: Power spectra for the A_p time series for the period 1979 – 1991. The top plot includes all days, regardless of A_p level, and shows significant low frequency and 2 yr^{-1} power. The second plot is the power spectrum for the time series for all those days where $A_p < 40$, and the same significant oscillations are found. Once the cut off level has reached 30 and below, however, the half-year power is no longer statistically significant, as shown by the bottom three plots.

periods for which to check A_p and a_p levels is necessary because there may be some lag time between the rise of geomagnetic activity and any effects it may have on the airglow emission [*Hernandez, 1976*]; also, it is quite possible that conditions could become disturbed after observations have ceased for the night, and the appropriate cut off time needs to be taken into consideration.

Because of the ambiguity of the exact observation dates in the Lord Rayleigh data, a different criterion has been used for his observations. As mentioned earlier, while exact dates are unknown, the number of days included in each average is a known quantity. Combining this number with the knowledge that the observations were taken around new moon periods, a reasonable guess can be made as to the range of dates involved. A_p levels are checked for each date within this probable range, and any range containing $\geq 50\%$ active days (as defined above) is marked as having high activity. With this criterion, very few average values from these data collections end up being marked as elevated.

With the above process, we are left with a data collection where we are reasonably confident that the effects of large geomagnetic events (such as aurora) are removed. With this 'screened' data set, we can then investigate the question of whether there is a significant correlation between geomagnetic or solar activity with the green line emission on a climatological time scale (i.e. not event driven). We will address this question in the next chapter.

Chapter 4

RESULTS AND DISCUSSION

The seasonal behavior of the 5577 Å oxygen emission for the nine long term stations is shown in Figure 4.1. As described earlier, the data have been screened to eliminate high geomagnetic activity nights. The plots are arranged by geographic latitude in left to right, top to bottom order. The abscissa scale is presented according to season so that the six month difference between northern and southern hemisphere stations is eliminated. While there certainly are variations among the stations, there are several predominant features common to a majority of them. The most common feature evident at nearly every station is the peak in green line brightness occurring shortly after the autumnal equinox. This peak typically is 50 – 70% brighter than the mean annual brightness and lasts for ~1 – 2 months, followed by a decrease in intensity to 25 – 50% of the mean value that persists throughout winter and into spring. Many of the stations also exhibit a maximum close to the summer solstice, although this feature shows much more variation than the fall peak. At some stations (RAT, CHA) this is the strongest yearly variation, while it is not as prominent at other locations (FPO, KIS, SAC).

The two southern hemisphere Lord Rayleigh stations (CAP, CAN) show much less variation than the other stations. This is most likely due to the absence of nightly measurements as discussed in the analysis chapter, which would tend to smooth out many variations. However, the locations of the significant departures from the mean value at these stations are consistent with those of the other stations.

One valid concern when examining these results is that there is an inherent bias in comparing measurements made at the same local time each night (such as at the Rayleigh stations) with full night averages at other stations. As pointed out in the introduction, many studies of the nightly variation in the green line emission (e.g. *Roach and Pettit* [1951]; *Christophe-Glaume* [1965]; *Brenton and Silverman* [1970]; *Fukuyama* [1977]) have shown that the brightness peaks during the night, and that this peak may not be constant with season or latitude. With this knowledge, it is conceivable that taking a single measurement at the same local time throughout the year might select points at various positions relative to this peak. Also, a similar effect

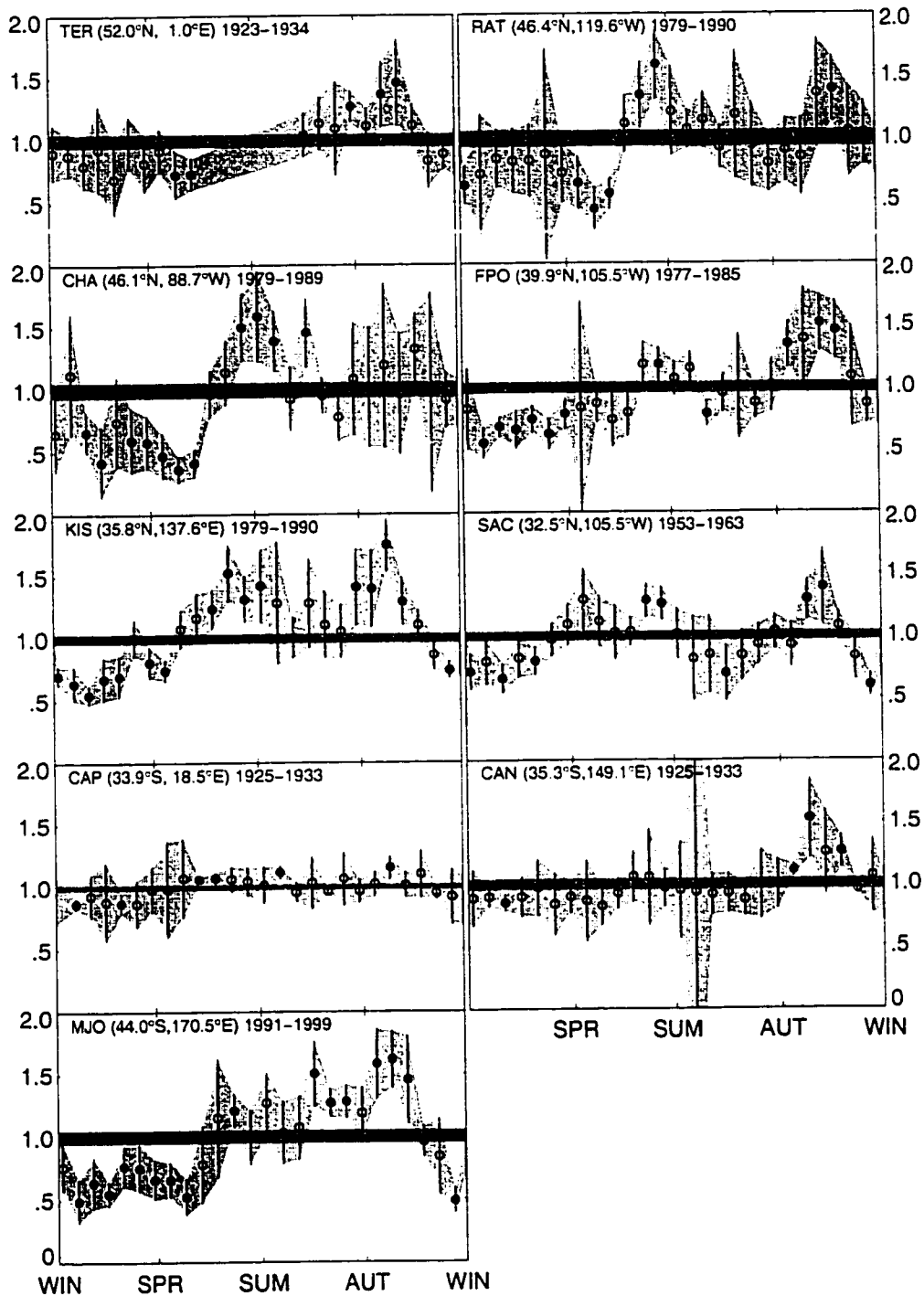


Figure 4.1: Seasonal behavior of the green line brightness at nine long term stations. Plots are in left-to-right, top-to-bottom order from highest northern latitude to highest southern latitude. Data have been screened to eliminate days with high A_p .

might be found due to the varying lengths of the night during the summer and winter months.

To insure that our results were not strongly biased in such a way, we have investigated the hourly dependence of the seasonal variation. The results of this investigation are shown in Figures 4.2 and 4.3. In Figure 4.2, we show the effect of different lengths of night upon the final seasonal variation. The top left panel shows the seasonal variation which results when only the measurements from 2350 – 0050 LT are used to form the nightly average value. Each subsequent plot shows the results when an additional two hours of observation are included in the nightly average, and the final panel shows the variation when all measurements from 1950 – 0450 LT are averaged. The strong similarity in the final variation suggests that our results are not biased against any specific feature of the nightly variation.

To examine this issue another way, we show in Figure 4.3 a comparison of the seasonal variation that emerges from the standard analysis described earlier with the results produced by forming the nightly averages using only those measurements taken between 2230 – 2330 LT. By forming nightly averages in this way, we closely mimic the observational methods used to obtain the Terling, Cape, and Canberra measurements (where a single observation was made near 2300 LT). As can be seen, using only those measurements near 2300 LT does not produce significant variations in the results, confirming that the older Rayleigh observations can be combined with the more modern data sets to broaden our long term data coverage.

Based on earlier studies [*Barbier, 1959; Fukuyama, 1977; Cogger et al., 1981*], a springtime maximum was to be expected. The data in Figure 4.1 show a minimum instead. The absence of this spring maximum on a climatological scale has large implications for identifying the dominant processes operating near the mesopause, as will be discussed later.

The seasonal variations at our short term stations are shown in Figure 4.4. While the results are much noisier than at the longer term stations, a number of similarities can be seen. In particular, the most common feature is again the rise to a maximum near the fall equinox followed by a drop-off to low wintertime levels.

A few of these stations also show a significant peak between the spring equinox and the summer solstice (India, Pacific, Sutherland). In further sections we will discuss some possible reasons why such a feature does not appear on a climatological time scale.

The short term stations also allow us to investigate whether the seasonal behavior of the green line emission has changed significantly over the course of many decades at several locations. We show such a comparison in Figure 4.5, which shows the behavior at five pairs of closely spaced geographic locations: FPO_OLD

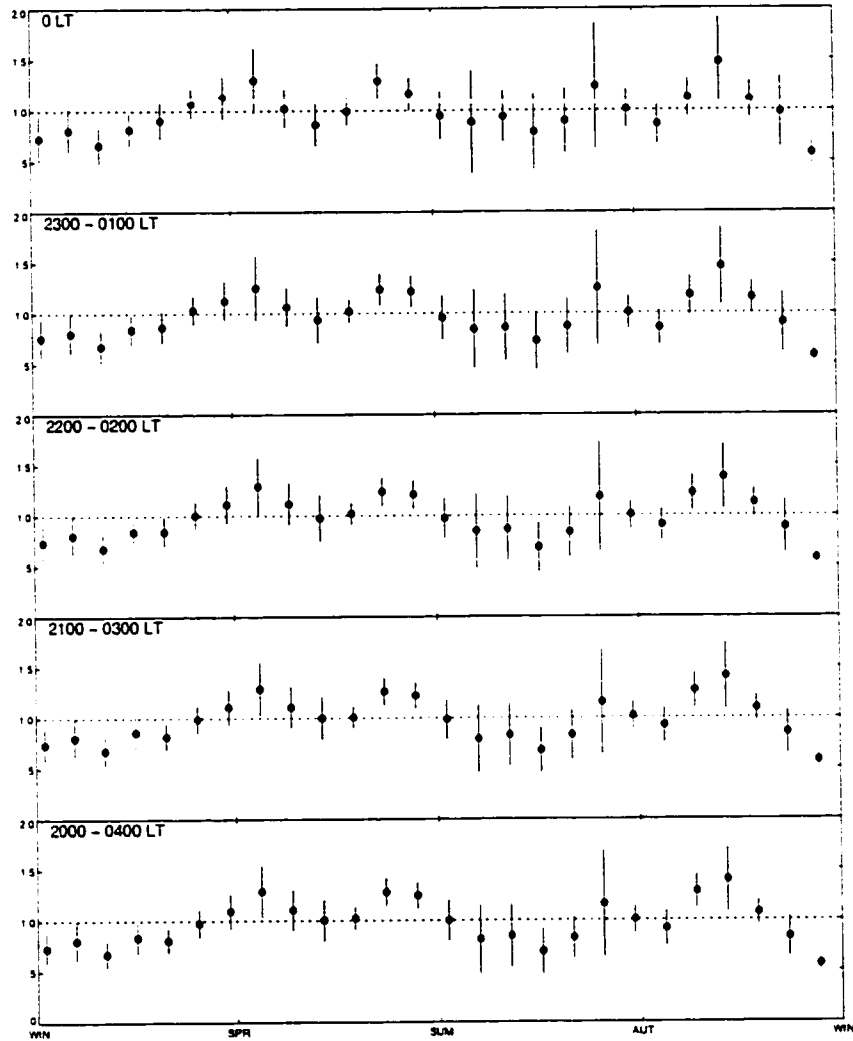


Figure 4.2: Effects on the seasonal behavior at Sacramento Peak due to varying the length of each night's observation period. The top left panel shows uses only those measurements averaged from the 2300 LT hour. Each panel adds one hour earlier and one hour later, so the final panel uses the 2000 – 0400 LT hour measurements.

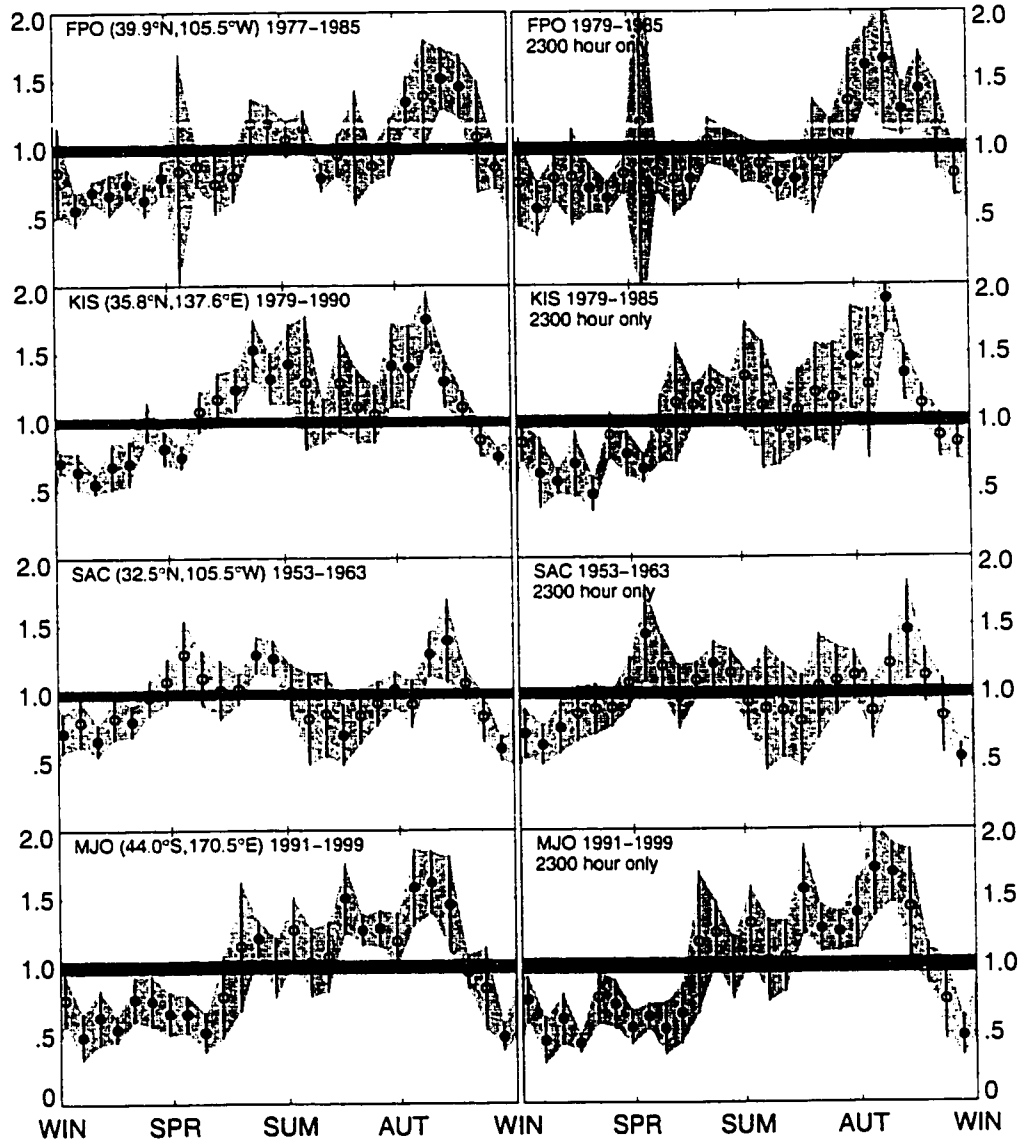


Figure 4.3: Comparison of the results of the normal analysis (left column) with results from using only measurements near 2300 LT to form the nightly average brightness values (right column).

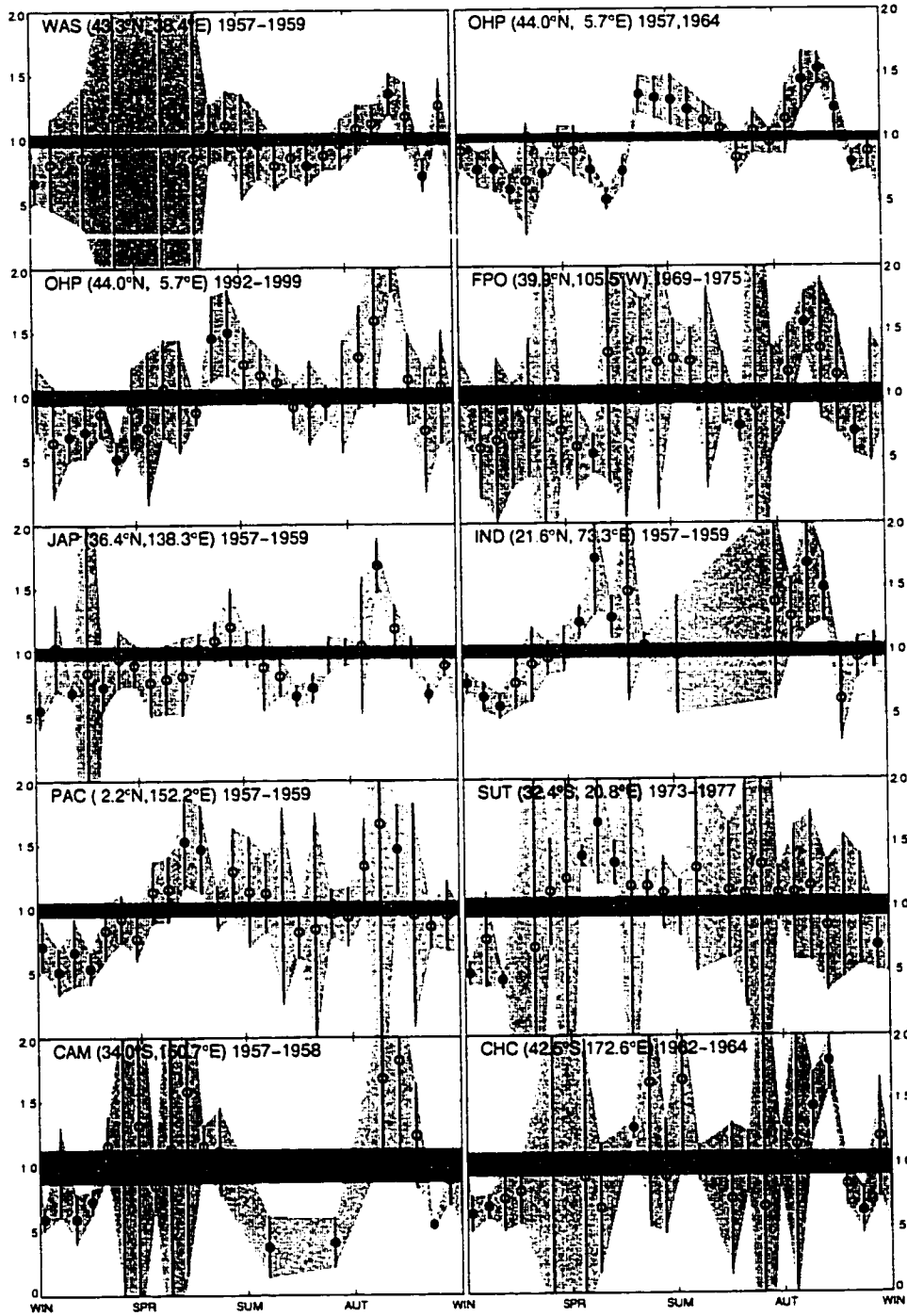


Figure 4.4: Seasonal behavior of the green line brightness at ten short term stations. Plots are in left-to-right, top-to-bottom order from highest northern latitude to highest southern latitude. Data have been screened to eliminate days with high A_p .

(1966 – 1975)/FPO_NEW (1977 – 1985), OHP_OLD (1957 – 1959, 1964 – 1965)/OHP_NEW (1992 – 1999), JAP (1957 – 1959, 1964 – 1965)/KIS (1979 – 1990), CAP (1925 – 1933)/SUT (1973 – 1977), and CHC (1962 – 1964)/MJO (1990 – 1999). At least one station in each pair is a short length data series (both in the case of OHP), so the large confidence bands reflect the strong year-to-year variability in the emission behavior, making a quantitative comparison not possible. However, we can see qualitatively that there are no drastic changes at a given location over an extended period of time. In particular, there are strong similarities between the short term Japan combined station with the modern Kiso observations. Additionally, one can see that the early IGY and IQSY results from Haute Provence are quite similar to the behavior there in the 1990s, and both sets of observations here confirm the overall findings of *Barbier* [1959] and *Christophe-Glaume* [1965] at this location of strong summer and fall maxima. While these researchers also claimed to observe a very weak spring time maximum as well, our results show that this variation is not significant for our periods of study. Other areas do seem to show differences in the amount of overall variation, as seen in the early Rayleigh data at the Cape of Good Hope compared with the four year data series at nearby Sutherland, or the variations in the short term observations in Christchurch as compared with the long term climatology at Mt. John. The apparent enhanced variability of the southern hemisphere stations with respect to the northern hemisphere stations will be discussed later.

4.1 Implications of the missing springtime emission maximum

As previously discussed, airglow emissions can provide useful constraints on atmospheric models. The seasonal behavior of the green line emission, for example, has been used as supporting evidence for the importance of internal gravity wave breaking near the mesopause. The findings from this work do not support the seasonally symmetrical behavior of the emission that results from including the parameterization of breaking gravity waves in Garcia and Solomon's (1985) atmospheric model. We will explore this idea and re-examine the assumptions made in their model in the context of our new observational results.

Internal gravity waves are atmospheric oscillations whose main restoring force is buoyancy. These waves typically have horizontal wavelengths of tens to hundreds of kilometers, vertical wavelengths of $\sim 5 - 15$ km, and periods of a few minutes up to approximately an hour [Andrews *et al.*, 1987]. These waves are thought to be generated in the lower atmosphere as winds cross over orographic features such as mountains [Lilly and

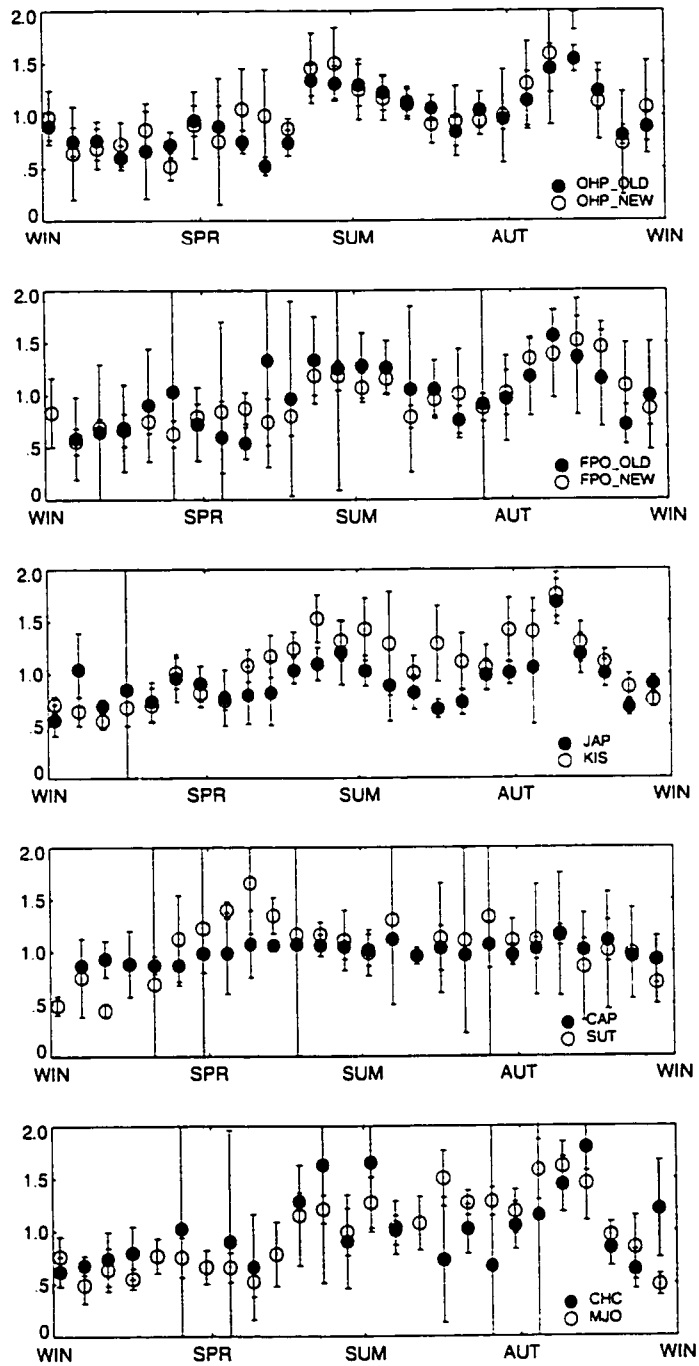


Figure 4.5: Seasonal behavior of the green line brightness at five pairs of closely spaced geographic stations. From top to bottom, the plots show OHP (1957 – 1959, 1964 – 1965)/OHP (1992 – 1999), JAP (1957 – 1959, 1964 – 1965)/KIS (1979 – 1990), CAP (1925 – 1933)/SUT (1973 – 1977), and CHC (1962 – 1964)/MJO (1990 – 1999).

Kennedy, 1973; *Nastrom and Fritts*, 1992] or by weather phenomena such as thunderstorms or fronts [*Jordan*, 1972; *Taylor and Hapgood*, 1988; *Pasko et al.*, 1997]. As these waves propagate vertically, they encounter a decrease in atmospheric density. In response to this, the amplitudes of the waves increase in order to conserve energy. Thus these waves are capable of bringing large amounts of energy into the middle atmosphere, as discussed early on by *Hines* [1960].

At some altitude, the amplitudes will reach a level at which they become unstable, and the waves can break. This breaking provides the means of distributing the wave's energy into the surrounding atmosphere. This energy can subsequently lead to an increase in turbulence and vertical diffusion, leading to a decrease in the emission intensity as described above. Only a brief development of these ideas will be presented here; for a much more detailed discussion, see the review article by *Fritts* [1984].

If seasonal variations in the strength of gravity wave breaking are significant, as a consequence there should be a corresponding variation in the green line emission. *Garcia and Solomon* [1985] found that by including gravity wave breaking in their dynamical model of the middle atmosphere, they could reproduce just such a variation, and they cited satellite measurements of the seasonal green line variation [*Cogger et al.*, 1981] to support their result.

In the first version of their model, *Garcia and Solomon* [1983] used a generalized friction term to represent the drag force of gravity waves on the zonal mean flow, and they used a vertical eddy diffusion profile that gave a value of the diffusion coefficient K from $\sim 1 - 4 \times 10^6 \text{ cm}^2 \text{ s}^{-1}$ in the 86 to 100 km altitude range.

As part of their work, *Garcia and Solomon* [1983] modeled the density profiles of several long-lived chemical constituents, including atomic oxygen. Their results produced an annual range of atomic oxygen that was well within the observational bounds from 80 to 100 km provided by *Offerman et al.* [1981]. The results from their model showed a very small annual variation compared to the nearly two orders of magnitude variation suggested by the observations, but note was made that the large annual variation might be instrumental in nature [*Garcia and Solomon*, 1983].

Two years later, *Garcia and Solomon* [1985] updated their model to include a parameterization of gravity wave breaking. Their choice of parameterization was that of *Lindzen* [1981], in which gravity waves generated in the lower atmosphere propagate upwards until they become convectively unstable. According to *Lindzen* [1981], this will occur when the total lapse rate reaches the adiabatic lapse rate. At this point, the wave will break and change the diffusion in the region.

Gravity waves can also transport chemical constituents if the constituents are either chemically active or if there is turbulent mixing along the wave trajectory [Schoeberl *et al.*, 1983]. Garcia and Solomon included the vertical component of this transport of a species μ as

$$F_{\mu}^* = -\frac{1}{\rho_s} \frac{\partial}{\partial z} \{ \rho_s [(\overline{w' \mu'^*})_{\text{chem}} + (\overline{w' \mu'^*})_{\text{diff}}] \} \quad (4.1)$$

where $(\overline{w' \mu'^*})_{\text{chem}}$ and $(\overline{w' \mu'^*})_{\text{diff}}$ are the net vertical fluxes from chemically active species and from turbulent mixing, respectively, and $\rho_s = \rho_0 \exp(-z/H)$, where ρ_0 is a reference density.

The spectrum of gravity waves used in the model of Garcia and Solomon [1985] was selected so that the waves would break at the 85 km level. They 'launched' 9 waves at the lower boundary and allowed each to propagate upwards. Each wave had a horizontal wavelength of 100 km and the phase speeds were $c = 0, \pm 10, \pm 20, \pm 30, \text{ and } \pm 40 \text{ m s}^{-1}$.

Inclusion of this parameterization of gravity wave breaking generated changes in the vertical eddy diffusion. In general, the addition of breaking gravity waves led to a decrease in the diffusion coefficient. The breaking waves also have a seasonal variation, resulting in a similar variation in vertical diffusion. Figure 4.6 shows the changes in diffusion coefficient from the original to the modified version of the model. The seasonal variations are clearly evident in the figure, with values of the diffusion coefficient near the mesopause level 50% lower than the no gravity wave breaking model. The effects are even more pronounced at the green line altitude near 97 km. K in the original model at this altitude is $\sim 2.5 \times 10^6 \text{ m}^2 \text{ s}^{-1}$. With the addition of breaking gravity waves, this value drops to between $0.8 - 1.2 \times 10^6 \text{ m}^2 \text{ s}^{-1}$, depending on season. The seasonal variations are complicated at this altitude, with both equinoxes and the winter solstice values being $\sim 50\%$ lower than the summer solstice value. Clearly, one would expect that such a seasonal variation in the level of vertical diffusion would be evident in tracers of chemical composition in the region.

Such experimental evidence was cited in Garcia and Solomon [1985] from ISIS-2 satellite observations of the green line intensity as published by Cogger *et al.* [1981], and is reproduced in Figure 4.7 (from Garcia and Solomon [1985], Figure 14). Mid-latitude green line brightnesses were observed over a roughly two year period, and the resulting seasonal variation showed large emission peaks at the equinoxes, with the springtime peak a factor of ~ 3 higher than solstice levels and the fall peak a factor of ~ 2 higher. As can be seen, the gravity wave breaking model also generated these peaks, with only a small time discrepancy between the model and observational fall peak. Therefore, since including the effects of breaking gravity waves

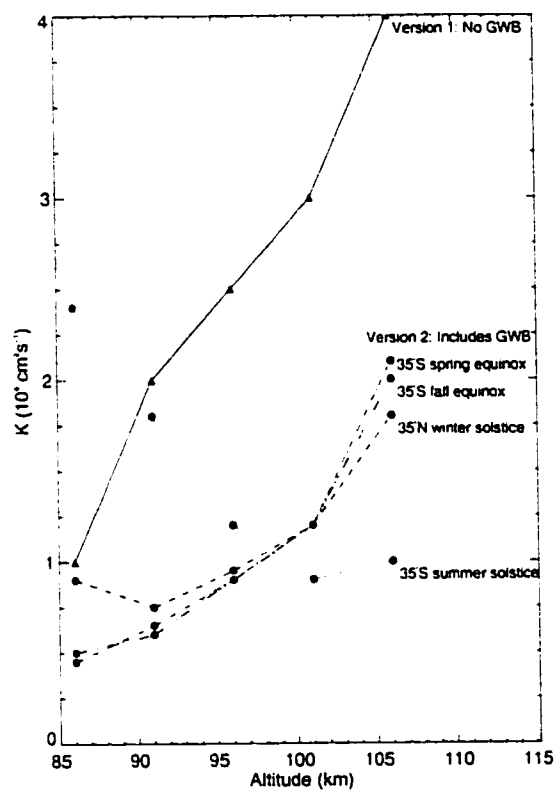


Figure 4.6: Altitude variation of vertical eddy diffusion (K). Version 1 is the profile used in *Garcia and Solomon* [1983], with no temporal or latitudinal dependence. Version 2 is the diffusion coefficient that results when gravity wave parameterization is added to Version 1 [*Garcia and Solomon*, 1985].

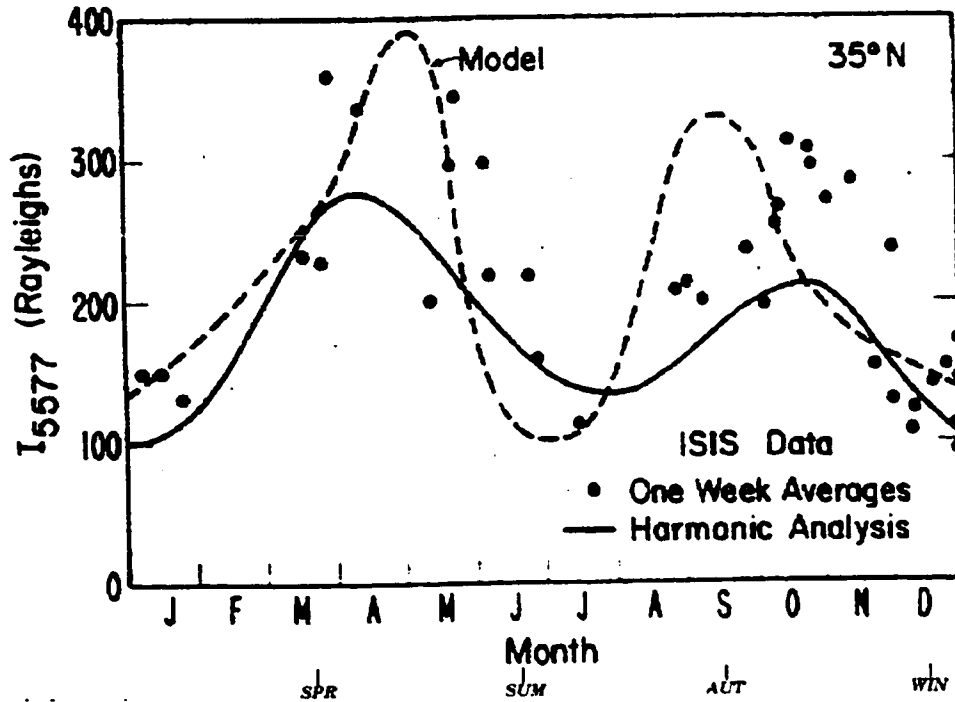


Figure 4.7: Comparison of ISIS-2 weekly green line emission levels [Cogger *et al.*, 1981] with the Garcia and Solomon's GWB model (from [Garcia and Solomon, 1985, fig. 14]).

enabled the model to reproduce the observed seasonal behavior of the green line emission (and therefore the underlying atomic oxygen concentration), this result was touted as strong support for the importance of gravity waves to the mesopause region.

However, our climatological-scale results shown here present a different result. Given that the long term coherent behavior lacks a significant springtime maximum (see, for instance, Figure 4.1), any process which in theory leads to such a peak must be re-examined. Stated another way, from our climatology developed in this present dissertation, seasonal variations in green line emission due to changes in vertical diffusion produced by breaking gravity waves in the model do not reproduce the (climatologically) observed variations in the green line emission intensity. This can easily be seen by comparing the model curve in Figure 4.7 with the harmonic fits shown in Figure 3.6. The link between these breaking gravity waves and the emission has largely been made [Garcia and Solomon, 1985; Elphinstone *et al.*, 1984] through the changes in vertical

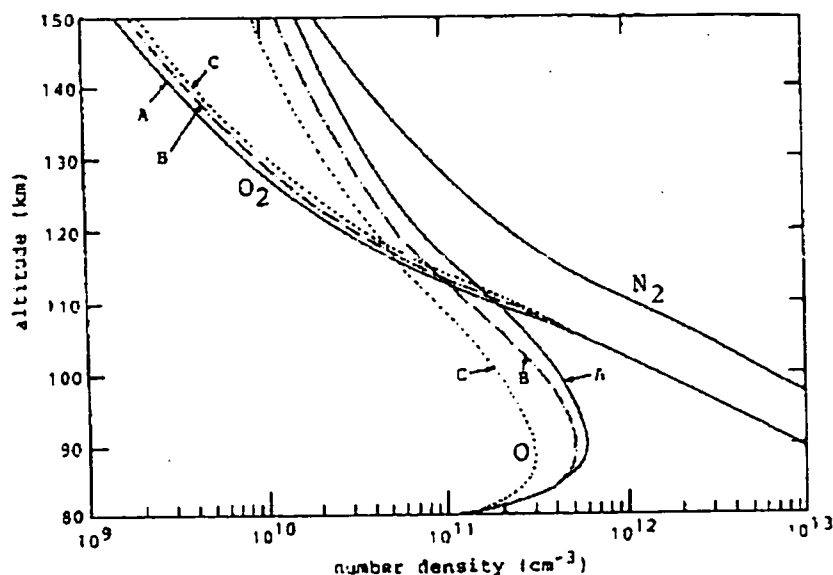


Figure 4.8: Variation of atomic oxygen concentration caused by changes in the eddy diffusion coefficient. A: $K = 2.5 \times 10^6 \text{ cm}^2\text{s}^{-1}$, B: $K = 5 \times 10^6 \text{ cm}^2\text{s}^{-1}$, C: $K = 7.5 \times 10^6 \text{ cm}^2\text{s}^{-1}$ [Tohmatsu, 1990, fig. 4.20].

diffusion that they would generate, which in turn would move more atomic oxygen out of the emission region (lower brightness) or allow more to accumulate in the same region (higher brightness).

Referring back to the equation for the green line volume emission rate presented in equation 1.15, one can compute that, to zeroth order, the concentration of the green line is proportional to the cube of the atomic oxygen density. From the climatology presented here, this means that the winter level of the green line brightness is roughly one-third that of the fall peak level, which corresponds to a $\sim 30\%$ reduction in the atomic oxygen concentration. Tohmatsu [1990], based on work by Ogawa and Shimakazi [1975], showed that in order to reduce the oxygen concentration near 97 km by 20% (from $\sim 4.7 \times 10^{11}$ to $3.8 \times 10^{11} \text{ cm}^{-3}$), the diffusion coefficient would need to double from $2.5 \times 10^6 \text{ cm}^2\text{s}^{-1}$, as shown in Figure 4.8. Because the Ogawa and Shimakazi [1975] calculations are only for steady state conditions, and therefore do not represent seasonal variations in the profile, these numbers only provide a rough estimate for quantifying such an effect. However, it is likely that an even greater change would be required to reach a 30% reduction in the atomic oxygen concentration as seen in our fall to winter behavior.

Returning to the Garcia and Solomon's gravity wave breaking model, if we assume that the fall equinox

at 35°N would be the same as the spring equinox at 35°S, then from *Garcia and Solomon* [1985], the value of the diffusion coefficient K at that time at 96 km is $\sim 0.9 \times 10^6 \text{ m}^2 \text{ s}^{-1}$ (see Figure 4.6). Moving to the winter solstice, the model has a diffusion coefficient at 96 km of $\sim 0.95 \times 10^6 \text{ m}^2 \text{ s}^{-1}$, amounting to a change of only $\sim 5.5\%$. Comparing this change to the results from *Ogawa and Shimakazi* [1975], we conclude that such a small change in diffusion is unable to explain a three-fold change in emission brightness as seen in our data.

In addition, several other researchers [*Chao and Schoeberl*, 1984; *Coy and Fritts*, 1988; *Schoeberl et al.*, 1983] have suggested that the diffusion coefficients generated by the model of *Garcia and Solomon* [1985] are too large, and that there may not be such large seasonal variations in the diffusion [*Hocking*, 1988]. Since a simple model which incorporates the changes in the diffusion coefficient (caused by proposed changes in gravity wave activity at mesospheric heights) is insufficient, then we must search for effects other than vertical diffusion that may result from the influence of breaking gravity waves.

4.2 An additional effect of gravity waves in the upper mesosphere/lower thermosphere region

In addition to affecting constituent populations through vertical diffusion, gravity waves are also believed to influence greatly the underlying circulation of the upper mesosphere/lower thermosphere region through advection. As gravity waves propagate vertically, they are able to carry horizontal momentum upwards as well. A detailed discussion of linear gravity wave theory can be found in *Lindzen* [1981]; *Andrews et al.* [1987]; and *McLandress* [1998], which is the basis of the explanation given here. The horizontal momentum flux (τ) that a gravity wave can carry in traveling vertically is given by

$$\tau_u \equiv \rho_s \langle u' w' \rangle \quad (4.2)$$

where

$$\langle u' w' \rangle \equiv L_x^{-1} \int_0^{L_x} u' w' dx. \quad (4.3)$$

L_x is the horizontal wavelength and is equal to $2\pi/k$; u' and w' are perturbation (residual from the mean) zonal and vertical velocities, and $\rho_s = \rho_0 \exp(-z/H)$, with ρ_0 is the surface density. This form may be reworked into

$$\tau_0 \approx \frac{1}{2} \frac{\rho_s N}{\bar{\omega}} w_B^2 \quad (4.4)$$

where ρ_s is the surface density, N is the buoyancy frequency, $\tilde{\omega}$ is the wave's intrinsic frequency, and w_B is the amplitude of the wave.

The vertical variation of this momentum flux produces a force which affects the underlying zonal wind. This force has the following form:

$$F_u = -\frac{1}{\rho} \frac{\partial \tau_u}{\partial z}. \quad (4.5)$$

The above expression shows that if the wave's momentum varies with height, a force exists in the zonal direction. Depending on the direction of the wave motion, this force will either augment or decrease the underlying zonal motion.

Not all gravity waves are able to propagate to mesosphere/thermosphere heights. Gravity waves may encounter critical levels where they are absorbed by the surrounding medium. Such critical levels occur where the phase speed of the wave matches that of the background zonal wind [Andrews *et al.*, 1987]. Since the zonal wind profile varies with height, a range of critical levels may absorb much of a gravity wave spectrum generated by a low altitude source. Only waves which have phase speeds above or below the zonal wind speeds from the source up to a given height will reach that height. Since the zonal winds have a variation throughout the year, this filtering results in a seasonal variation of gravity wave propagation to the upper mesosphere region.

An example of this variability can be seen in Figure 4.9 from *McLandress* [1998], which shows the expected differences in gravity wave vertical propagation at the winter and summer solstices. At the winter solstice, the zonal wind is strongly directed eastward throughout most of the stratosphere and mesosphere, with a speed range of $0 - 60 \text{ m s}^{-1}$ (this range is marked by the dashed vertical lines). Any gravity waves with phase speeds within this range will encounter a critical level as they move upward and will be absorbed. Only those waves with easterly phase speeds or strongly westerly phase speeds ($c < 0$ or $c > 60 \text{ m s}^{-1}$) will be able to reach the mesopause region. At the summer solstice, the wind pattern has been found to be different, so that the only gravity waves capable of penetrating to the mesopause are those with $c < -60$ or $c > 30 \text{ m s}^{-1}$.

At the equinoxes, the wind patterns are not as well defined, as shown in Figure 4.10. The zonal average wind profiles for the spring (left) and fall (right) equinoxes were generated through the HWM-93 atmospheric model [Hedin *et al.*, 1991, 1996], and are plotted in a comparable way to the profiles in Figure 4.9. The shaded regions mark the range of gravity wave phase speeds that will be able to reach the mesopause level.

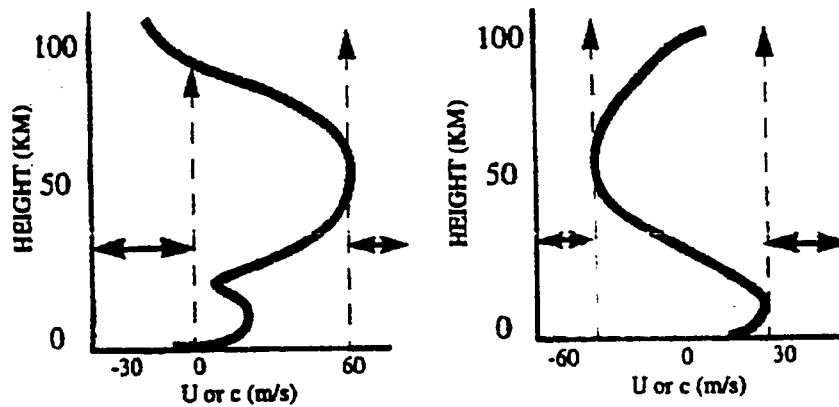


Figure 4.9: Winter (left) and summer (right) solstice variations in the extent of vertical propagation of gravity waves, from *McLandress* [1998]. Only those waves with phase speeds in the regions marked by solid horizontal arrows are able to reach the upper mesosphere; the remainder of the waves will encounter critical levels and be absorbed.

Comparing these equinox results with the solstice profiles, one can see that a much broader range of gravity waves will be able to reach upper mesosphere/lower thermosphere heights at the equinoxes. As a result, the extent of the drag force applied to the zonal flow by the gravity waves in this region will differ from the solstice conditions.

Holton and Schoeberl [1988] investigated the relative importance of gravity wave drag (advection) and diffusion in terms of the transport they generate. They found that, for chemical tracers with large scale heights and long chemical lifetimes (greater than ~ 10 days), advection is the dominant process; therefore seasonal variations in such tracers are more likely to be caused by variations in the mean meridional circulation that occur as a result of the gravity wave drag force.

While the chemical lifetime (τ) of atomic oxygen is only about one day at the mesopause, it increases rapidly with altitude to a value of τ a few weeks near the green line emission layer at 97 km [*Brasseur and Solomon*, 1986]. The scale height for the species is ~ 10 km. With these values, the atomic oxygen population near 97 km could arguably fit into the regime of the 'long-lived' chemical tracer referred to by *Holton and Schoeberl* [1988]. Our results, therefore, appear to provide confirming evidence of the relative importance of advective over diffusive processes on a climatological time scale. However, this proposition must wait for

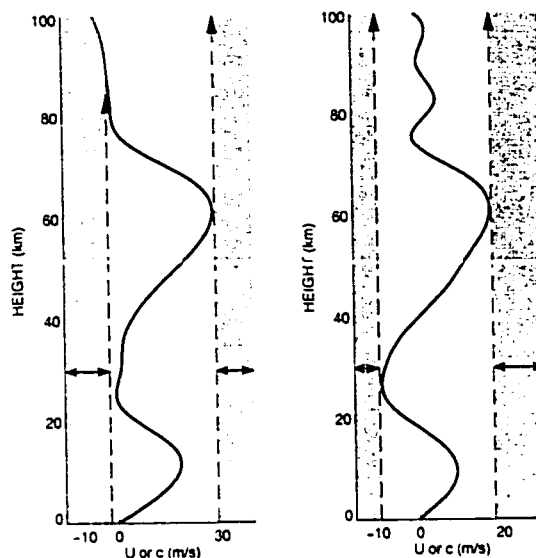


Figure 4.10: Spring (left) and fall (right) equinox variations in the extent of vertical propagation of gravity waves. Only those waves with phase speeds in the regions marked by solid horizontal arrows are able to reach the upper mesosphere; the remainder of the waves will encounter critical levels and be absorbed. Winds are computed from the HWM-93 atmospheric model [Hedin *et al.*, 1991, 1996].

further measurements of wind and gravity waves before it can be confirmed.

4.3 Variations of the green line emission with solar and geomagnetic activity

4.3.1 Solar activity

As reported in the introduction, several researchers have noted relationships between solar activity and the green line emission. Oftentimes, these studies have been concerned with only the emission's response to a specific event, such as a solar flare, or a more general connection with quantities such as sunspot area or number. With our data collection, we were able to investigate this concept on a long term basis.

Our results also indicate that a simple linear correlation between the emission intensity and solar activity is not appropriate. We then investigated an earlier result of Lord Rayleigh [Rayleigh and Spencer Jones, 1935] (and later confirmed by Hernandez and Silverman [1964]) that there is a hysteresis effect between the emission and solar activity, and our results appear in Figure 4.11. The six modern-day long term stations all exhibit a definite hysteresis effect, although the details of the relationship seem to vary. Coverage at six

locations is insufficient to determine whether this variation is due to the particular solar cycle (or a particular part of the solar cycle), in accordance with the results of *Rosenberg and Zimmerman* [1967], or whether they may be location effects, as suggested by *Fukuyama* [1977].

The variation of this relationship is also evident in Figure 4.12, which plots both the emission intensity and the solar flux separately. In this plot, the filled circles reflect the solar flux averages, while the open symbols show the green line intensity averages. At some stations (RAT, FPO) the emission definitely appears to lag the solar flux, but at other stations the situation is not as clear.

4.3.2 Geomagnetic activity

As previously discussed, due to variations in observational technique we found it necessary to remove all observations taken during times of high geomagnetic activity. This eliminated all possible 'event driven' influence between emission intensity and geomagnetic activity. We are able, however, to examine a related issue of how the inclusion of such events manifests itself in the climatological behavior.

Referring back to Figure 3.10, which shows the computed power spectra for various selections of A_p , one can see that the 2 year^{-1} oscillation becomes less important as the cutoff A_p level is lowered. This effect also appears in a power analysis of green line emission data taken at Kiso, as shown in Figure 4.13. However, since such an analysis provides information only about the relative importance of the frequencies, it is not clear whether this effect will manifest itself as obvious differences in the seasonal behavior. To investigate this, we present in Figure 4.14 the 12 year time series constructed from the significant 1 and 2 year^{-1} oscillations found in the Kiso data (as shown in Figure 3.5). The top panel shows the resultant series using our standard procedure of eliminating all days with high ($A_p > 30$) geomagnetic activity, while the bottom panel includes all observations, regardless of A_p . As can be seen, there are clear yearly variations in the relative amplitudes of the mid-spring and fall equinox peaks. However, the inclusion of all data appears to greatly enhance the amplitude of the mid-spring feature near (and for several years following) solar maximum. This can also be seen (although less easily) in the raw data, for example, by comparing how the ratio of the two features changes in 1979 or 1988/1989 depending on whether or not filtering has been done (see Figure 4.15). It is interesting to note that the ISIS-2 observations reported by *Cogger et al.* [1981] were made in 1971 – 1972, roughly three years past solar maximum. Comparing the harmonic fit to those data (shown in Figure 4.7) with the equivalent period in our figure (1983), one can see that the mid-spring feature is greatly enhanced if A_p

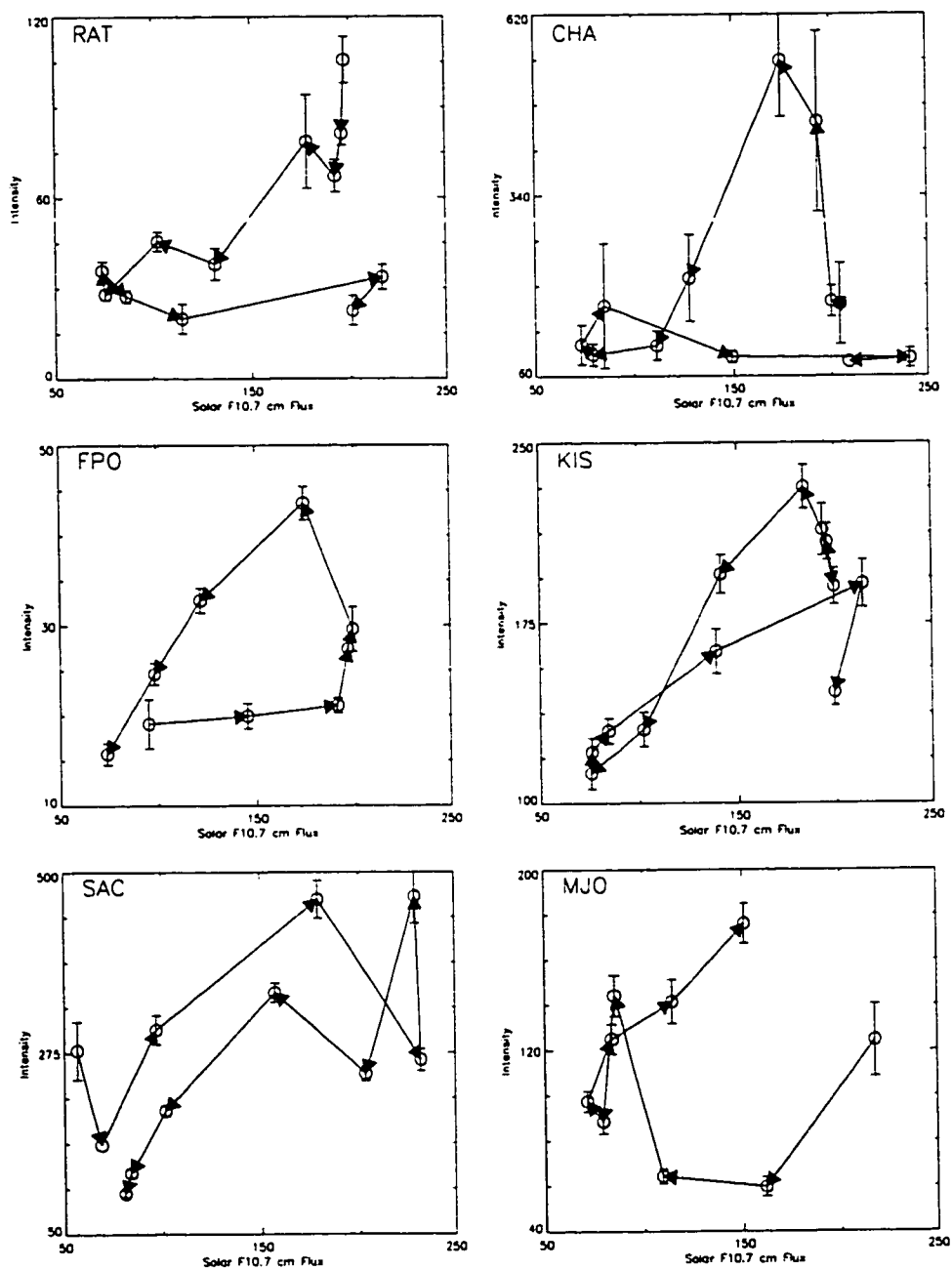


Figure 4.11: Intensity vs. solar 10.7 cm flux for our six modern day long term data samples. Yearly averages of both quantities are compared (where the intensity values may be either counts or Rayleighs), showing a clear hysteresis effect at all stations. Arrows connecting the data points indicate the direction with time.

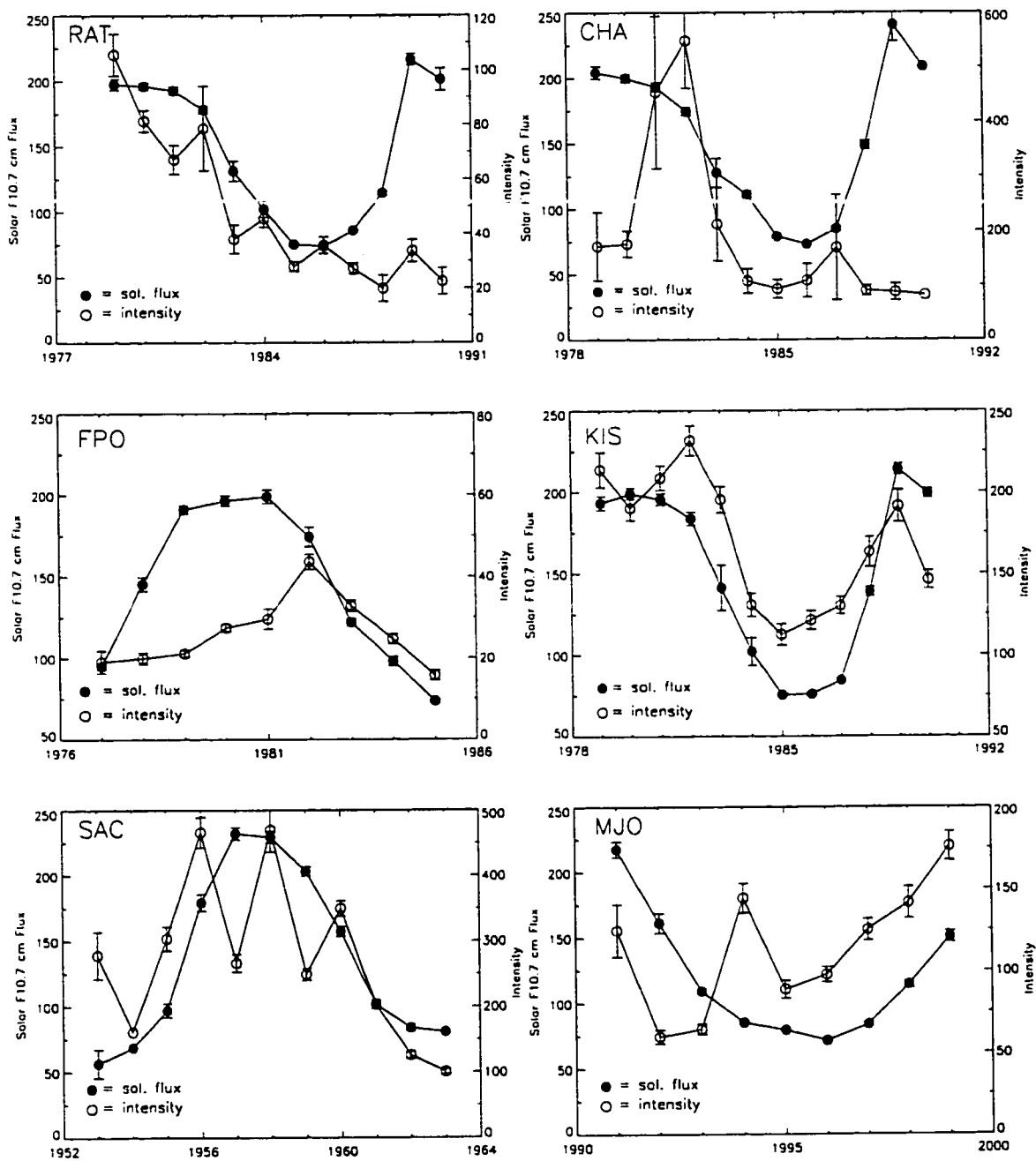


Figure 4.12: Intensity (open symbols) and solar 10.7 cm flux (filled symbols) for our six modern day long term data samples. Yearly averages of both quantities are plotted (where the intensity values may be either counts or Rayleighs).

filtering is not performed. This raises the possibility that the ISIS-2 data could also have included the effects of large geomagnetic events, and furthermore, that the exclusion of such data would remove the necessity of invoking a dynamical process to reproduce such strong mid-spring emission.

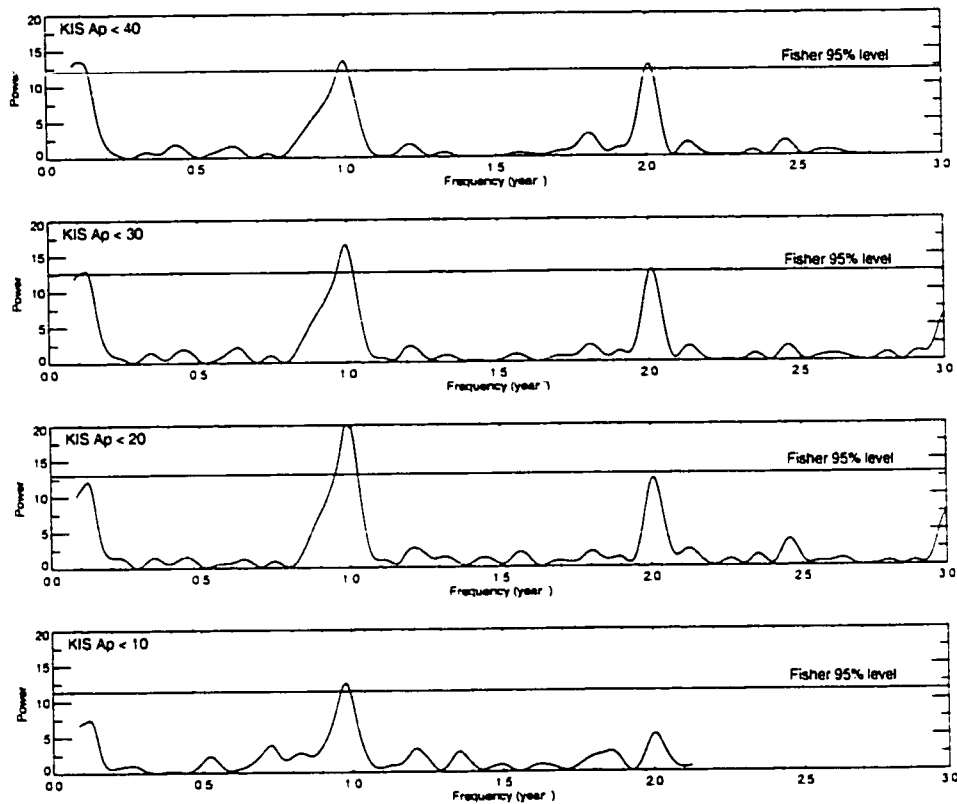


Figure 4.13: Power spectra for the Kiso time series. The top plot includes all days with A_p level < 40 , and shows significant low frequency, 1 yr^{-1} , and 2 yr^{-1} power. The second plot is the power spectrum for the time series containing those days where $A_p < 30$, and the same significant oscillations are found. Once the cut off level has reached 20 and below, however, only the one-year power remains statistically significant, as shown by the bottom three plots.

To further understand this difference in sensitivity to A_p filtering between the mid-spring and fall equinox peaks, we show in Figure 4.16 the results of correlating the amplitude of each peak with solar F10.7 cm flux for both activity filtered and non-filtered conditions. The top panel shows the amplitude of the mid-spring peak as a function of solar flux, and the bottom panel shows the same relation for the fall equinox peak. As was shown in the previous filter the amplitude of the fall peak does change with solar cycle, but this figure

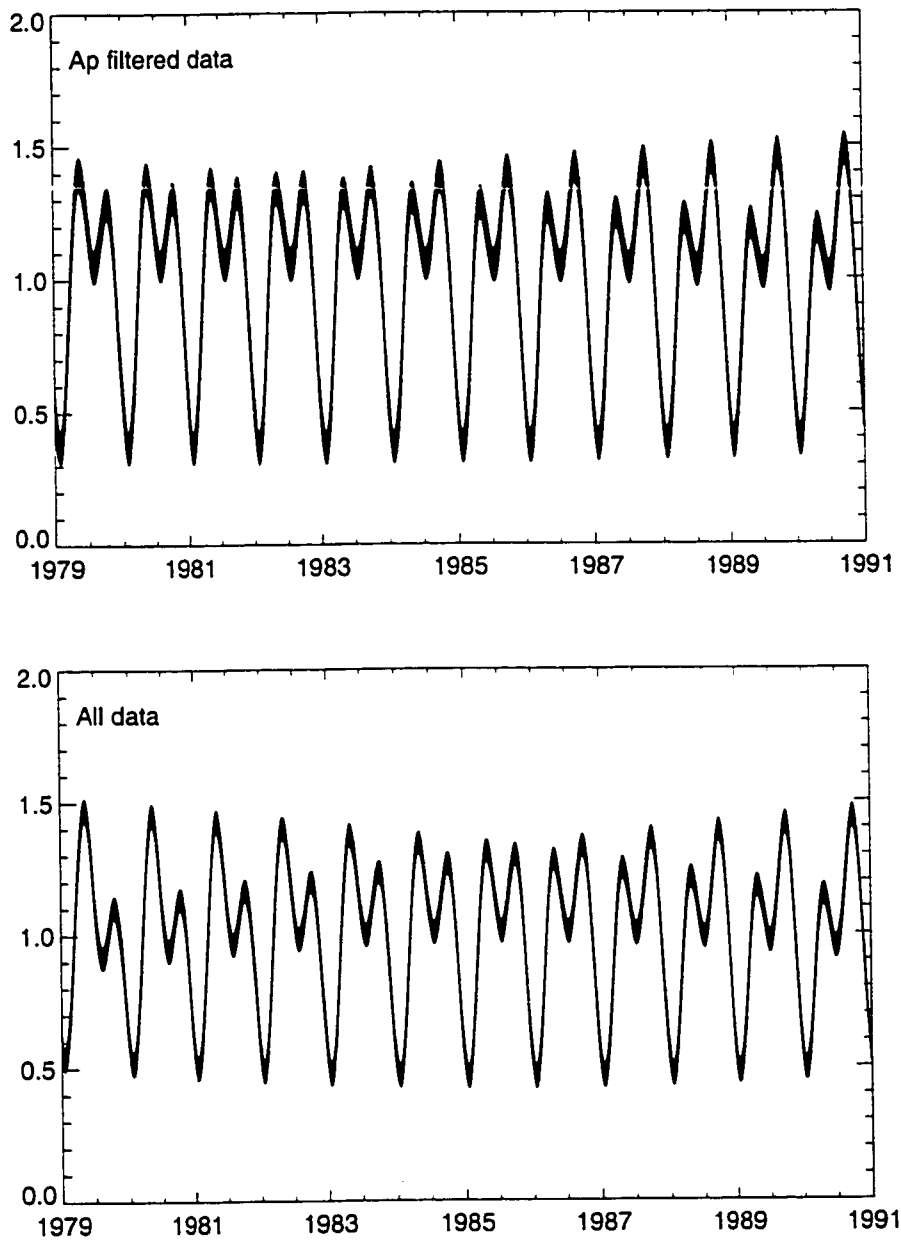


Figure 4.14: Reconstructed time series from the significant 1 and 2 yr^{-1} oscillations found in the Kiso data, for both A_p filtered (top) and non-filtered (bottom) conditions. The shaded region on each plot represents the 1σ bound on the function.

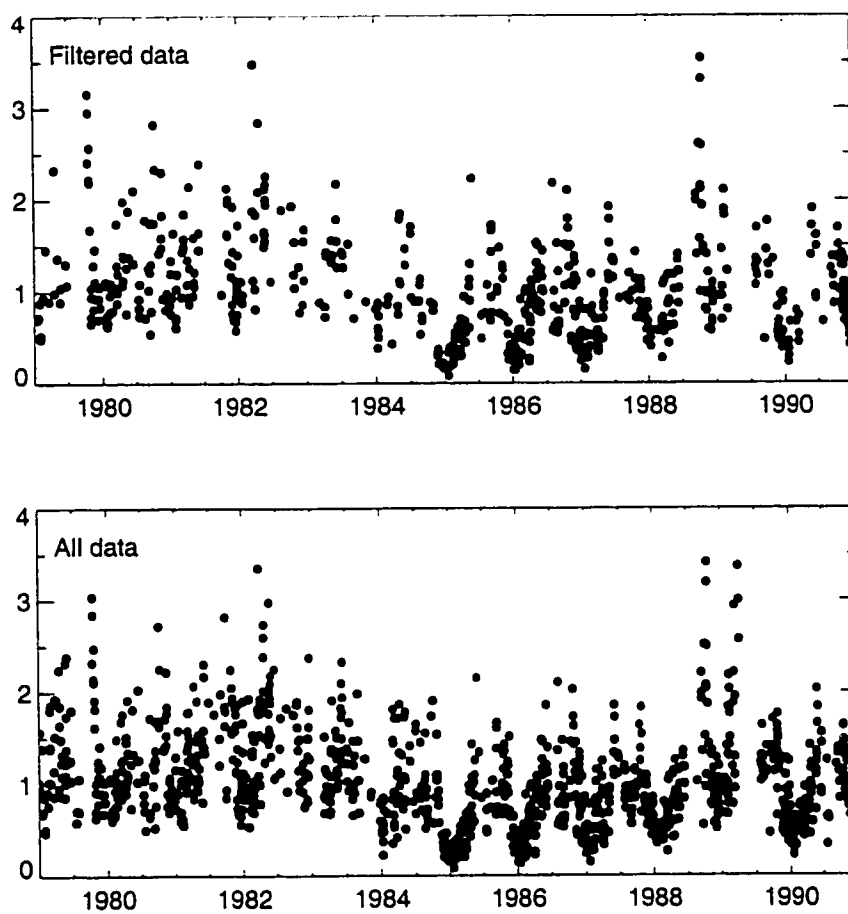


Figure 4.15: Raw nightly averages at Kiso, for both A_p filtered and non-filtered conditions, showing how the effect of filtering varies according to solar cycle phase.

shows that the relationship is fairly insensitive to whether or not A_p filtering is done. The situation is quite different for the mid–spring peak, however. The top panel clearly shows that the correlation between this peak and solar flux exhibits significantly different behavior when the high geomagnetic activity observations are removed. Furthermore, the non–filtered curve for the mid–spring peak is also quite similar to the curves for the fall peak, further stressing the uniqueness of the mid–spring peak’s response to activity filtering.

The implications of this difference are not understood, except perhaps to underscore that the influence of geomagnetic and/or solar activity on the green line emission may be more complicated than previously thought. With only one station and one solar cycle worth of observations, we cannot be certain about the whether this is an isolated behavior in either location or time. However, because we are attempting to establish and understand the climatological behavior of the emission, a further investigation of these effects with other stations over longer periods of time is called for.

4.4 Variations in hemispheric behavior

With the eight long term data sets available to us, we have been able to investigate the similarities and differences in our northern and southern hemisphere stations’ climatological behavior. While we do not have adequate data to establish a definitive ‘representative’ station for each hemisphere, we are able to qualitatively detail some characteristics that can be applied to our range of stations.

The strongest comment that we can make about the differences between the green line emission in the two hemispheres is that the northern hemisphere stations exhibit a more cohesive seasonal behavior over a broad latitude range than do the southern hemisphere stations. This is quite clearly shown in Figure 4.1. Ignoring the Terling data, due to the summertime gap in observations, the latitude range for the northern hemisphere covers $\sim 14^\circ$; this is slighter larger than the latitude range for our southern stations, $\sim 10^\circ$. Yet the seasonal behavior shows much less variation over this region than the southern hemisphere shows.

Nearly all the northern hemisphere stations examined here show an emission maximum near the summer solstice, although the magnitude of this maximum varies from station to station. These stations therefore appear to have a ‘double–peaked’ variation, with distinct peaks around the summer solstice and near the fall equinox.

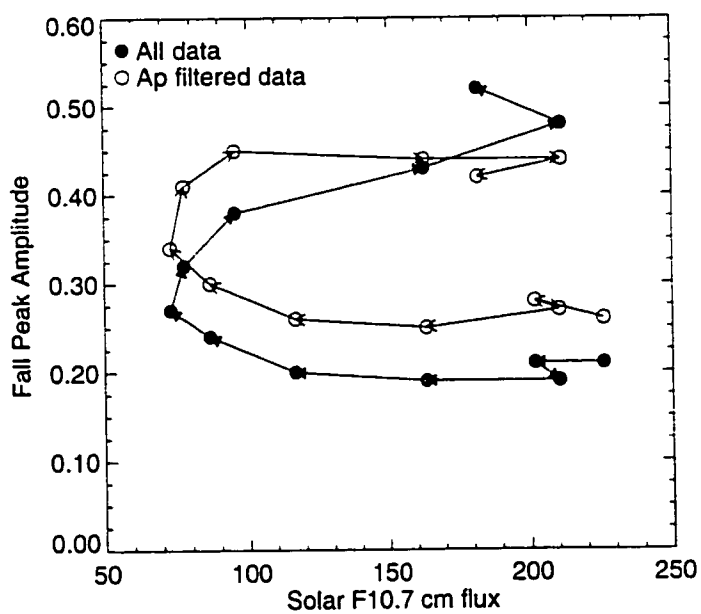
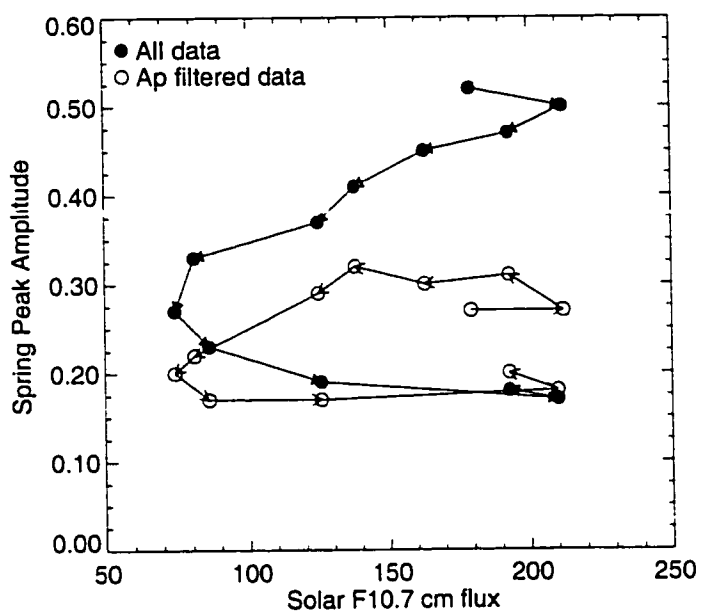


Figure 4.16: Relationship between the mid-spring and fall peak amplitudes with solar F10.7 cm flux for both A_p filtered (open symbols) and non-filtered (filled symbols) conditions. Arrows mark the time progression of the measurements.

Conversely, the summer hemisphere behavior as represented by our three long term data sets shows much more variation over a similar latitude range. Two of our stations (CAP, CAN) show very little variation throughout the year than their northern hemisphere counterparts (SAC, KIS), although Canberra has a significant maximum near the fall equinox, in agreement with the north. Mt. John, however, shows overall variations of comparable magnitude to the northern hemisphere stations, but the emission behavior here is more 'step-like', rather than double-peaked.

The summertime maximum in the green line emission is interesting in itself. As described in the introduction, many researchers have reported this feature, and its existence appears fairly intuitive: during the summer, there is increased solar UV interacting with the upper atmosphere, which would lead to increased photodissociation of molecular oxygen and therefore an increase in atomic oxygen. It is interesting to note, however, that current atmospheric models (among them MSISE-90 [Hedin, 1987, 1991] and TIME-GCM (R. Roble, personal communication) do not show a maximum in atomic oxygen concentration near the summer solstice at 100 km. In fact, they show a minimum at this time, reflecting the quick transport towards the winter hemisphere. However, given the strength of this feature at nearly all stations, this dynamically driven view is difficult to reconcile with our observations.

In addition to these qualitative differences, we also were able to perform quantitative statistical analyses to address differences found at two particular stations, Kiso and Mt. John. We noted in Chapter 3 that while both stations exhibited a significant annual variation, Kiso also showed a significant half-year oscillation. To confirm that this oscillation is not due to some poorly-placed periodic gaps in our data series, we have constructed a time series of noise using the same time base as our observations and analyzed it in the same fashion as our original data. We also re-constructed the data using only the one year and ~ 8 year significant oscillations to confirm again that the half-year oscillation was not an artifact of the data spacing. Our results from these investigations are shown in Figure 4.17, which show that the half-year significant oscillation seen at Kiso (as shown in the top portion of Figure 3.5) is a true geophysical feature that is not present in the Mt. John data series. Due to the previously mentioned differences in the seasonal variations among the three southern hemisphere stations available to us, we cannot make the claim that Mt. John is representative of all southern hemisphere stations. However, the power analysis performed just described suggests that there are statistical differences between these this particular (and reasonably representative) northern hemisphere station and this particular southern hemisphere station.

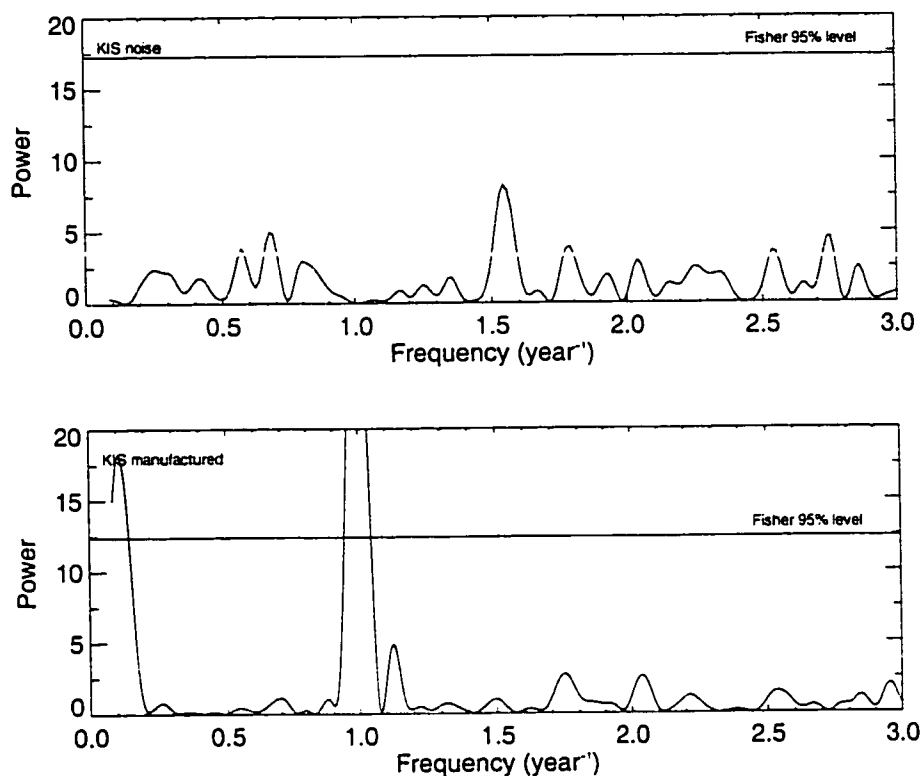


Figure 4.17: Power spectra constructed using the Kiso time base. The top plot is random noise, the bottom plot uses the one year and ~ 8 year significant oscillations found in Figure 3.5, along with noise. Since neither of these two reconstructions shows a significant half-yearly oscillation, we conclude that this feature, shown in Figure 3.5, is truly geophysical and not due to data spacing.

4.5 Departures from the climatological behavior

One of the most intriguing questions to emerge from the results presented here is where is the oft-cited spring emission maximum? In other words, what makes this feature insufficiently coherent to appear as part of the climatology? Since this feature has been reported by many researchers [Yano, 1967; Fukuyama, 1977; Cogger *et al.*, 1981], it was unexpected that it did not appear in the present climatological study.

To investigate this issue, we have looked at individual year behavior at several of our long term stations. While this approach leaves us much more vulnerable to the vagaries of weather and other observational disruptions, we can still get a reasonable idea of whether the emission behavior varies significantly from one

year to the next. We find that this is indeed the case, as shown in Figure 4.18, which shows the seasonal variations for 4 years of the Fritz Peak spectrometer data set. One of the years (1979) may show evidence of a peak near the spring equinox (although it is not strong enough to reach the 95% significance level), while the next year shows only a strong summertime peak. There is even one year, 1981, where the behavior closely resembles that of the southern hemisphere observations at Mt. John, where there is a rather step like seasonal behavior from low winter and spring levels up to a high summer/fall value. The fact that there is such substantial year-to-year variation in the emission only serves to underscore the importance of establishing the climatological behavior to cull out those processes which are coherent, rather than intermittent, such as the springtime feature appears to be.

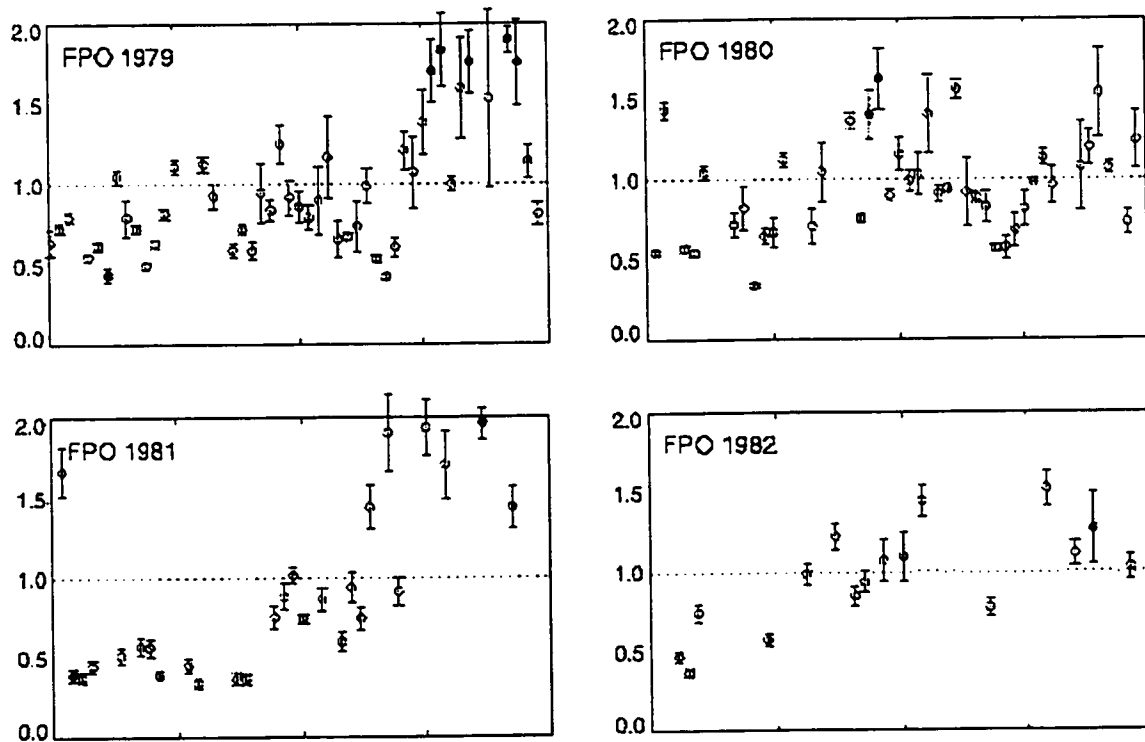


Figure 4.18: Seasonal behavior of the green line emission intensity at Fritz Peak for the years 1979 – 1982. Note the strong changes from year to year, signifying the inherent variability of the upper mesospheric region near 97 km.

One possible explanation for this feature may be related to the 'springtime transition' in atomic oxygen

airglow emissions, where there is a rapid increase in the emission over the course of a few days, followed by a sharp decrease that persists for several days. The feature was first described by *Shepherd et al.* [1999b], who observed it at two northern ground based stations at 42° and 41° latitude. They coordinated these ground based observations with global WINDII satellite measurements and found that contours of the emission rate changed from being aligned parallel to the equator before the event to a perpendicular alignment during the event. This alignment occurred along with large changes in the zonal circulation. *Shepherd et al.* [1999b] point out that changes in the zonal circulation led to a change in the mean vertical wind from downward to upward motion. Such changes in the vertical direction would have a direct effect on the chemical composition, moving constituents into and out of the emission region. In fact, they suggest that the large swings in the integrated green line intensity result from the formation of a second airglow layer near 92 km. They also connect these occurrences to the winter-to-summer wind reversal, which may also be related to enhanced gravity wave vertical propagation as described above.

Examples for three years (1992, 1993, 1995) were shown. Unfortunately, weather conditions at our Mt. John station prohibited observations that coincide with their measurements. It is possible that such events were the cause of the springtime green line maximum observed by *Cogger et al.* [1981] and others. Understanding the specific conditions which allow such transitions to occur may help explain why the springtime feature is not adequately coherent and does not contribute to the climatological behavior of the emission.

4.5.1 *Is this truly a climatological scale work?*

One important remaining question to be raised is whether the long term coverage of the data sets used in this work are long enough for us to claim solidly that we have uncovered the climatological behavior of the green line emission variation. In a sense, this is an unanswerable question, since we are aware of no data sources longer than ours still in existence. However, it is possible to look back on our data sets to see how the variation developed with the addition of more years of observation.

Figure 4.19 shows such an example. Plotted are four periodograms for the original Kiso time series. The top plot is the periodogram for the 1979 – 1982 period, showing significant power at a 2 yr^{-1} frequency. The next plot covers the 1979 – 1985 time period. The 0.5 year period has been joined with a 1.0 year period that just misses the 95% significance cutoff. The third plot is for the years from 1979 – 1988, and one can see that there is now significant power found at a long period of ~ 10 years. Finally, the last frame shows the

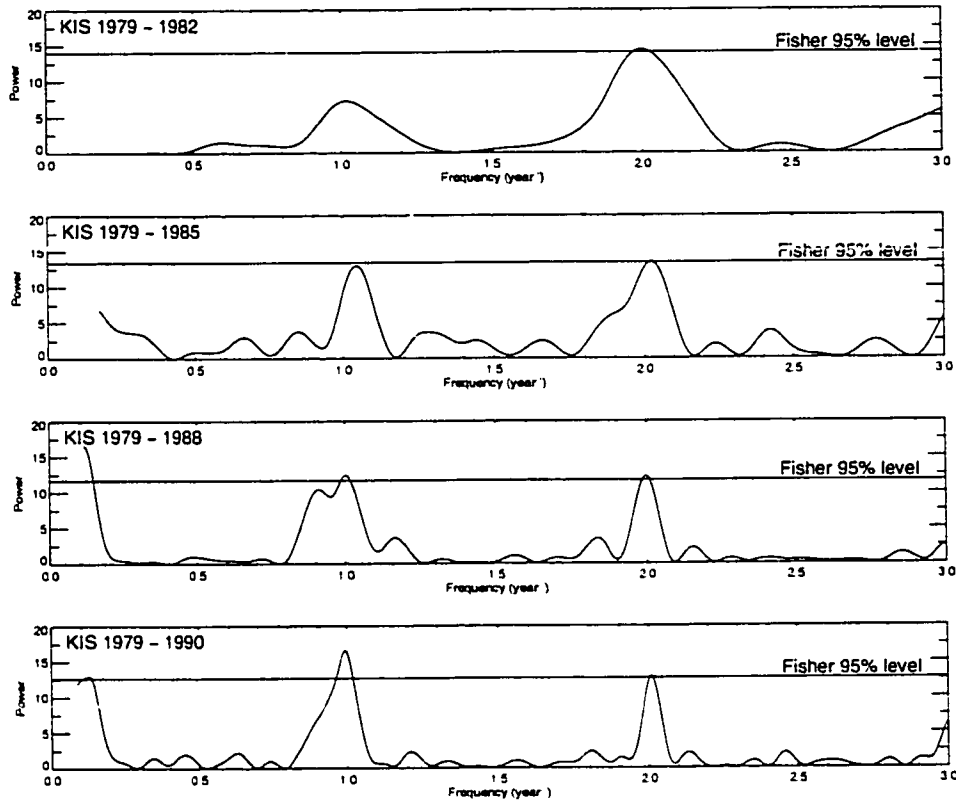


Figure 4.19: Periodogram for various subsets of the Kiso data series. The panels are, from top to bottom, 1979 – 1982, 1979 – 1985, 1979 – 1988, and 1979 – 1991. The effects of gathering a longer time series are clearly reflected by the fluidity of the locations of significant power.

full 1979 – 1991 time series. The same significant periods are found as in the third panel, but their relative importance has changed. One also sees that the frequency resolution increases with a longer series (i.e., note how the 0.5 year peak narrows). The last two panels show a growth of power at the low frequency end (at approximately the length of the time series), but because the peak is not fully defined, even in the final plot, we cannot make any strong claims about it.

The point of this figure is to illustrate how conclusions about the significant variations at a given station are dependent upon the length of the data series. Four years of observations may seem like an adequate length of time to draw conclusions about the climatological behavior of a process, but as demonstrated by the figure, this may not be the case. Indeed, even with eleven years of observations as shown in this example, we

are unable to say definitively whether the emerging peak at the low frequency end of the spectrum is a true climatological feature of the emission or an artifact due to the length of the data series under investigation.

As previously mentioned, this is a question that cannot be settled with the data available here. Unfortunately, we are unaware of any current plans underway (aside from the continuation of our observations at Mt. John) in the community to gather data at a single location for such an extended period of time that would allow this issue to be fully explored.

Chapter 5

CONCLUSION

We have presented an in-depth analysis of 9 long term mid-latitude collections of the 5577 Å green line data with the aim of establishing the climatological behavior of this emission. Based on our analysis, this understanding of the behavior of the atomic oxygen green line emission at 5577 Å is now becoming more clear. The most striking result from this climatological investigation is that the often claimed springtime maximum in the emission intensity does not statistically exist on a climatological time scale. This result is consistent at all but one of the locations we examined, leading to the conclusion that the absence of this feature is not an artifact of the locations we studied.

This result has several aeronomic implications: the first is that current chemical and dynamical models which predict both a strong springtime and autumnal maximum need to be changed to represent correctly the experimentally found climatological behavior observed here. Further, this finding calls attention to the need to re-examine the reported dominance of the effect of gravity wave breaking at these heights, given that one of the strongest pieces of supporting evidence for its large role has been the reproduction of a symmetrical spring and fall behavior.

The second implication of this result is that if the breaking of gravity waves is insufficient to explain the seasonal variation of the emission behavior, another explanation must be found. What is it about the fall peak that causes it to be a coherent feature, whereas the springtime feature is sporadic? Explaining this climatologically determined equinoctal asymmetry would go a long way to identifying the controlling processes in this region of the atmosphere. Our results appear to support the contention that advection, rather than diffusion, is the dominant mechanism operating in this region of the atmosphere.

Additionally, we have shown in this work that once observations taken during large geomagnetic events are screened out, the connection between the emission intensity and geomagnetic and/or solar activity becomes less clear. To examine this issue further, more data are needed to provide adequate statistics during all phases of the solar cycle. Also, we have shown that failure to exclude such geomagnetic events leads to a

springtime enhancement in the green line emission intensity. This fact may be one explanation for some of the historical references to a spring time maximum in the green line brightness.

We have demonstrated how periodogram analysis gives results which asymptotically approach a climatologically coherent result as the length of data examined increases. Our results show that statistically significant oscillations appear to settle down after 10 years of observations are used in the analysis. However, there are still unresolved oscillations at the low frequency end of the spectrum. Since we do not have any longer data series available, it remains undetermined whether this low frequency power is a true oscillation of a geophysical nature or whether it is an artifact due to the length of the time series. To settle this issue, observations spanning a few decades would be required.

The large year-to-year variability of the seasonal behavior may be related to such transient events at the springtime transition reported by *Shepherd et al.* [1999a]. While this feature is claimed to be quite common, it is not sufficiently coherent to be part of the climatology. Understanding such events may lead to an explanation of why they lack the coherence to emerge over the long term, which is related to the absence of a more general springtime maximum as discussed above.

Finally, from the distribution of mid-latitude stations used in this work, there is similarity in the fall-to-winter behavior over the long term at almost all stations. However, there are differences in the seasonal behavior within each hemisphere. In the north, the stations analysed in this work show similar seasonal behavior over a $\sim 14^\circ$ latitude range. Our three southern hemisphere stations, on the other hand, show greater variability over a comparable latitude range. In particular, the greatest variability seems to be associated with the spring/summer recovery. At most northern hemisphere stations, we see a distinct maximum during this season, while our limited southern hemisphere stations show a much smoother or step-line behavior between low winter/spring to elevated summer/fall levels. This difference appears statistically in our spectral analysis as the presence of a significant half-yearly oscillation at Kiso and the absence of the same at Mt. John. More analysis, along with additional data sets, is needed to determine whether this discrepancy represents some sort of broad hemispherical difference, local effects, or a combination of the two. We also have shown, using observations from the same or nearby stations separated by decades in time, that the typical behavior (regardless of hemisphere) has not undergone significant changes over that period.

The importance of a long-term ground based airglow measurements has received much attention lately with the beginning of the PSMOS (Planetary Scale Mesopause Observing System) project. The goals of the

project are as follows (taken directly from *Shepherd et al.* [1997]):

- To determine the large-scale dynamics of the mesopause region by decomposition of the observations into the mean flow, planetary scale perturbations, tides and gravity waves, and to study the interactions between these dynamical components
- To determine the zonally averaged temperature trend, and separate from it the influence of solar variability and other dynamical effects
- To determine gravity wave characteristics and their zonal variability, with the goal of identifying important gravity wave sources

The results we present in this work provide useful guidelines for this new project. An adequate description of the climatological behavior of the airglow emission requires observations extending beyond 10 years in duration, which in turn requires a strong commitment to maintain observations over such an extended period of time. We have shown that even eleven years may not be enough time for the significant oscillations to be fully resolved.

Equally important, however, is the necessity for maintaining records of instrumental performance to calibration changes. The most fundamental way of analyzing long period data series is through statistical analysis. This approach has fewer necessary assumptions than an approach like superposed epoch analysis, as discussed in Chapter 2. However, very few of our long term data series used in this work were sufficiently well documented and of sufficient quality to use the statistical method. For example, filter changes may lead to discontinuities from one night to the next, but unless such changes (e.g. exact date, how long the old filter had been degrading, transmission properties of the old and the new filter) are noted, they are nearly impossible to handle properly later on, especially given the inherent variability of the green line strength from night to night.

Meticulous weather records must also be kept. In our assembly of data, we have several additional long term data sets which were not analyzed since we have no information about the weather during the observations. Without such information being recorded in conjunction with the airglow measurements, the data sets remain unusable.

Provided a commitment can be made to address such issues over an extended number of years, we have shown that there is much to be gained from firmly establishing the climatological behavior of the airglow. In fact, it is a necessary precursor to addressing some of the goals put forth in projects such as PSMOS. For example, if attempts are to be made to isolate solar and dynamical effects upon the airglow to investigate underlying long term trends (related to global change, for example), the baseline for comparison must be the climatological behavior of the emission, which represents what the true long term picture is when these effects are included. The work presented here has begun to address some of these issues.

Increasing data coverage in the southern hemisphere would also be extremely beneficial to addressing the question of whether there are significant hemispherical differences in the green line emission climatology. Our study included one southern hemisphere station (Mt. John) with long term daily measurements (Capetown and Canberra collections are multi-night averages). As mentioned above, statistical analysis of this station showed only a significant annual oscillation, compared to the annual and semi-annual oscillation at Kiso. Establishing additional mid-latitude southern hemisphere green line stations would help clarify this issue.

Of course, the benefits of long term monitoring of airglow emission do not only apply to the green line. In fact, the amassing of a comparable climatology of the OH (8400 Å) hydroxyl emission (occurring near ~ 88 km) would also be useful for a more complete study of processes near the mesopause. Most of the attention until now has been given to the green line because it has been studied since the 1920s, but establishing a second baseline at a slightly lower altitude would provide for an interesting comparative study. This emission layer is closer to the mesopause and therefore may be more affected by dynamic processes occurring there than is the green line emission layer. This investigation would be subject to the same complicated interactions between chemistry and dynamics as green line studies but, if these interactions are understood, the differences in behavior between the green line and hydroxyl emissions have the potential to increase our understanding of the middle and upper atmosphere's response to processes in the mesopause and lower thermosphere regions.

BIBLIOGRAPHY

- Allen, M., Y. L. Yung, and J. W. Waters, Vertical transport and photochemistry in the terrestrial mesosphere and lower thermosphere (50 – 120 km), *J. Geophys. Res.*, *86*, 3617, 1981.
- Andrews, D. G., J. R. Holton, and C. B. Leovy, *Middle Atmosphere Dynamics*, Academic Press, 1987.
- Babcock, H. D., A study of the green auroral line by the interference method, *Astrophys. J.*, *57*, 209, 1923.
- Barbier, D., L'altitude des couches émettrices du ciel nocturne, *Mém. Soc. Roy. Sci. Liège*, *12*, 43, 1952.
- Barbier, D., Sur les variations systématiques des intensités des principales radiations de la lumière du ciel nocturne à l'Observatoire de Haute-Provence, *Ann. de Géoph.*, *15*, 412, 1959.
- Barbier, D., J. Dufay, and D. Williams, Recherches sur l'émission de la raie verte de la lumière du ciel nocturne, *Ann. Astrophys.*, *14*, 399, 1951.
- Barth, C. A., The 5577-angstrom airglow., *Science*, *134*, 1426, 1961.
- Barth, C. A., and A. F. Hildebrandt, The 5577 Å airglow emission mechanism, *J. Geophys. Res.*, *66*, 985, 1961.
- Bates, D. R., Forbidden oxygen and nitrogen lines in the nightglow, *Planet. Space Sci.*, *26*, 897, 1978.
- Blackman, R. B., and J. W. Tukey, *The Measurement of Power Spectra from the Point of View of Communications Engineering*, Dover Publications, New York, 1959.
- Bracewell, R., *The Fourier Transform and its Applications*, McGraw-Hill, New York, 1965.
- Brasseur, G., and S. Solomon, *Aeronomy of the Middle Atmosphere*, D. Reidel Publishing Company, Norwell, MA, 1986.
- Brenton, J. G., and S. M. Silverman, A study of the diurnal variations of the 5577 Å [OI] airglow emission at selected IGY stations, *Planet. Space Sci.*, *18*, 641, 1970.

- Broadfoot, A. L., and K. R. Kendall, The airglow spectrum, 3100 – 10000 Å, *J. Geophys. Res.*, 73, 426, 1968.
- Burnside, R. G., and C. A. Tepley, Airglow intensities observed in the southern and northern hemispheres, *Planet. Space Sci.*, 38, 1161, 1990.
- Campbell, W. W., Note on the spectrum of the aurora borealis, *Ap. J.*, 2, 162, 1895.
- Chamberlain, J. W., *Physics of the Aurora and Airglow*, American Geophysical Union, 1995.
- Chao, W. C., and M. R. Schoeberl, On the linear approximation of gravity wave saturation in the mesosphere, *J. Atmos. Sci.*, 41, 1893, 1984.
- Chapman, S., Some phenomena of the upper atmosphere, *Proc. Roy. Soc. (London)*, A132, 353, 1931.
- Christophe-Glaume, J., Étude de la raie 5577 Å de l'oxygène dans la luminescence atmosphérique nocturne, *Ann. de Géoph.*, 21, 1, 1965.
- Cogger, L. L., R. D. Elphinstone, and J. S. Murphree, Temporal and latitudinal 5577 Å airglow variations, *Can. J. Phys.*, 59, 1296, 1981.
- Colerico, M., et al., Coordinated measurements of F region dynamics related to the thermospheric midnight temperature maximum, *J. Geophys. Res.*, 101, 26783, 1996.
- COSPAR, *COSPAR International Reference Atmosphere CIRA*, Akademie-Verlag, Berlin, 1972.
- Coy, L., and D. C. Fritts, Gravity wave heat fluxes: a Lagrangian approach, *J. Atmos. Sci.*, 45, 1770, 1988.
- Dandekar, B. S., and S. M. Silverman, The effect of solar flares on the [OI] green line of the nightglow, *Planet. Space Sci.*, 12, 867, 1964.
- Dandekar, B. S., J. C. Pomalaza, and W. F. Bellew, Analytical study of the birefringent filter photometer used for airglow, *Appl. Opt.*, 4, 295, 1965.
- Davis, T. N., and L. L. Smith, Latitudinal and seasonal variations in the night airglow, *J. Geophys. Res.*, 70, 1127, 1965.
- Donahue, T. M., B. Guenther, and R. J. Thomas, Distribution of atomic oxygen in the upper atmosphere deduced from Ogo 6 airglow observations, *J. Geophys. Res.*, 78, 6662, 1973.

- Dufay, J., and M. Dufay, Excitation de la raie verte de l'oxygène au crépuscule, *Comptes rendus*, 226, 426, 1948.
- Dufay, J., and M.-L. Tchong, Recherches spectrophotométriques sur la lumière du ciel nocturne dans le région visible, *Ann. de Géoph.*, 3, 189, 1946.
- Dunn, R. B., and E. R. Manring, Recording night sky photometer of high spectral purity, *J. Opt. Soc. Am.*, 46, 572, 1956.
- Eastman Kodak Company, Kodak filters for scientific and technical uses, Kodak technical publication no. B-3H, ca. 1970.
- Elphinstone, R. D., J. S. Murphree, and L. L. Cogger, Dynamics of the lower thermosphere consistent with satellite observations of 5577 Å airglow, 2, Atomic oxygen, local turbulence, and global circulation results, *Can. J. Phys.*, 62, 382, 1984.
- Filosofo, I., J. A. Greenspan, and C. M. Groom, An automatic continuum compensating photometer for observations of aurora and airglow, *Appl. Opt.*, 4, 215, 1965.
- Fisher, R. A., Tests of significance in harmonic analysis, *Proc. Roy. Soc. (London)*, A125, 54, 1929.
- Frederick, J. E., D. W. Rusch, G. A. Victor, W. E. Sharp, P. B. Hays, and H. C. Brinton, The OI (λ 5577 Å) airglow: observations and excitation mechanisms, *J. Geophys. Res.*, 81, 3923, 1976.
- Fritts, D. C., Gravity wave saturation in the middle atmosphere: a review of theory and observations, *Reviews of Geophys. and Space Physics*, 22, 275, 1984.
- Fukuyama, K., Airglow variations and dynamics in the lower thermosphere and upper mesosphere – i. diurnal variation and its seasonal dependency, *J. Atmos. Terr. Phys.*, 38, 1279, 1976.
- Fukuyama, K., Airglow variations and dynamics in the lower thermosphere and upper mesosphere – II. seasonal and long-term variations, *J. Atmos. Terr. Phys.*, 39, 1, 1977.
- Gadsen, M., and E. Marovich, The nightglow continuum, *J. Atmos. Terr. Phys.*, 35, 1601, 1973.
- Garcia, R. R., and S. Solomon, A numerical model of the zonally averaged dynamical and chemical structure of the middle atmosphere, *J. Geophys. Res.*, 88, 1379, 1983.

- Garcia, R. R., and S. Solomon, The effect of breaking gravity waves on the dynamics and chemical composition of the mesosphere and lower thermosphere, *J. Geophys. Res.*, *90*, 3850, 1985.
- Garstang, R. H., Transition probabilities of auroral lines, in *The airglow and the aurorae; [papers presented at] a symposium held at Belfast in September 1955*, edited by E. B. Armstrong, and A. Dalgarno, 1956.
- Greenspan, J. A., Chapter III, in *Airglow calibrations symposium*, edited by G. J. Hernandez, and A. L. Carrigan, 1964.
- Greer, R. G. H., Oxygen aeronomy and the nightglow: a compact critique, in *Progress in atmospheric physics: proceedings of the 15th Annual Meeting on Atmospheric Studies by Optical Methods, held in Granada, Spain, 6 – 11 September 1987*, edited by R. Rodrigo, pp. 97 – 107, Kluwer Academic Publishers, 1988.
- Gulledge, I. S., D. M. Packer, S. G. Tilford, and J. T. Vanderslice, Intensity profiles of the 6300 Å and 5577 Å O I lines in the night airglow, *J. Geophys. Res.*, *73*, 5535, 1968.
- Hecht, E., and A. Zajac, *Optics*, Addison–Wesley, 1974.
- Hedin, A. E., MSIS–86 thermospheric model, *J. Geophys. Res.*, *92*, 4649, 1987.
- Hedin, A. E., Extension of the MSIS thermospheric model into the middle and lower atmosphere, *J. Geophys. Res.*, *96*, 1159, 1991.
- Hedin, A. E., et al., Revised global model of thermosphere winds using satellite and ground–based observations, *J. Geophys. Res.*, *96*, 7657, 1991.
- Hedin, A. E., et al., Empirical wind model for the upper, middle and lower atmosphere, *J. Atmos. Terr. Phys.*, *58*, 1421, 1996.
- Heppner, J. P., and L. H. Meredith, Nightglow emission altitudes from rocket experiments, *J. Geophys. Res.*, *63*, 51, 1958.
- Hernandez, G., The signature profiles of O¹S in the airglow, *Planet. Space Sci.*, *19*, 467, 1971.
- Hernandez, G., Lower–thermosphere temperatures determined from line profiles of the O I 17,924–K (5577 Å) emission in the night sky I. Long–term behavior, *J. Geophys. Res.*, *81*, 5165, 1976.

- Hernandez, G., Analytical description of a Fabry–Perot spectrometer. 4: Signal noise limitations in data retrieval; winds, temperature, and emission rate, *Appl. Opt.*, *17*, 2967, 1977.
- Hernandez, G., Mid-latitude thermospheric neutral kinetic temperatures, 1, Solar, geomagnetic, and long-term effects, *J. Geophys. Res.*, *87*, 1623, 1982.
- Hernandez, G., *Fabry-Perot Interferometers*, Cambridge University Press, 1986.
- Hernandez, G., Time series, periodograms, and significance, *J. Geophys. Res.*, *104*, 10355, 1999.
- Hernandez, G., and T. L. Killeen, Optical measurements of winds and kinetic temperatures in the upper atmosphere, *Adv. Space Res.*, *8*, 149, 1988.
- Hernandez, G., and O. A. Mills, Feedback stabilized Fabry–Perot interferometer, *Appl. Opt.*, *12*, 126, 1973.
- Hernandez, G., and R. G. Roble, Thermospheric dynamics investigations with very high resolution spectrometers, *Appl. Opt.*, *18*, 3376, 1979.
- Hernandez, G., and R. G. Roble, The geomagnetic quiet nighttime thermospheric wind pattern over Fritz Peak Observatory during solar cycle minimum and maximum, *J. Geophys. Res.*, *89*, 327, 1984.
- Hernandez, G., and R. G. Roble, Thermospheric nighttime neutral temperature and winds over Fritz Peak Observatory: Observed and calculated solar cycle variation, *J. Geophys. Res.*, *100*, 14647, 1995.
- Hernandez, G., and R. W. Smith, Winds and vertical wavelengths deduced from the ground-based measurement of the Doppler shifts of the $O_2(b\ ^1\Sigma_g^+ - X^3\Sigma_g^-)$, $OI(^1D_2 - ^1S_0)$, and the $X^2\Pi\ OH(6-2)$ band $P_1(2)_{c,d}$ line emissions in the midlatitude upper middle atmosphere, *Geophys. Res. Lett.*, *22*, 369, 1995.
- Hernandez, G., R. Weins, R. P. Lowe, G. G. Shepherd, G. J. Fraser, R. W. Smith, L. M. LeBlanc, and M. Clark, Optical determination of the vertical wavelength of propagating 12-hour period upper atmosphere oscillations, *Geophys. Res. Lett.*, *22*, 2389, 1995a.
- Hernandez, G., R. Wiens, R. P. Lowe, G. G. Shepherd, G. J. Fraser, R. W. Smith, L. M. LeBlanc, and M. Clark, Optical determination of the vertical wavelength of propagating 12-hour period upper atmosphere oscillations, *Geophys. Res. Lett.*, *22*, 2389, 1995b.

- Hernandez, G. J., and E. L. Layman, A direct calibration of a birefringent photometer, *Appl. Opt.*, *4*, 874, 1965.
- Hernandez, G. J., and S. M. Silverman, A re-examination of Lord Rayleigh's data on the airglow 5577 Å [O I] emission, *Planet. Space Sci.*, *12*, 97, 1964.
- Hines, C. O., Internal gravity waves at ionospheric heights, *Can. J. Phys.*, *38*, 1441, 1960.
- Hocking, W. K., Two years of continuous measurements of turbulence parameters in the upper mesosphere and lower thermosphere made with a 2-MHz radar, *J. Geophys. Res.*, *93*, 2475, 1988.
- Holton, J. R., and M. R. Schoeberl, The role of gravity wave generated advection and diffusion in transport of tracers in the mesosphere, *J. Geophys. Res.*, *93*, 11075, 1988.
- Hoya Corporation, *Hoya color filter glass*, ca. 1980.
- Hunten, D. M., Vertical transport in atmospheres, in *Atmospheres of Earth and the Planets*, edited by B. M. McCormac, pp. 59 – 72, D. Reidel, 1975.
- Hunten, D. M., F. E. Roach, and J. W. Chamberlain, A photometric unit for the airglow and aurora, *J. Atmos. Terr. Phys.*, *8*, 345, 1956.
- Jones, J. G., in *Airglow Calibrations Symposium*, edited by G. J. Hernandez, and A. L. Carrigan, AFCRL Rept. 65-114, 1965.
- Jordan, A. R., Atmospheric gravity waves from winds and storms, *J. Atmos. Sci.*, *29*, 445, 1972.
- Kleckner, E. W., J. J. Michalsky, L. L. Smith, J. R. Schmelzer, R. H. Severtsen, and J. L. Berndt, A multi-purpose computer-controlled scanning photometer, Tech. Rep. PNL-4081, Pacific Northwest Laboratory, Richland, Washington, 1981.
- Kleckner, E. W., D. W. Slater, and L. L. Smith, Photometric observations during the international magnetospheric study, Battelle Pacific Northwest Laboratories report, 1983.
- Koomen, M. J., D. M. Packer, and R. Tousey, The use of birefringent filters in measurements of the airglow, in *The airglow and the aurorae; [papers presented at] a symposium held at Belfast in September 1955*, edited by E. B. Armstrong, and A. Dalgarno, 1956.

- Krassovsky, V. I., N. N. Shefov, and V. I. Yarin, Atlas of the airglow spectrum 3000 – 12400 Å, *Planet. Space Sci.*, 9, 883, 1962.
- Levi, L., *Applied optics: a guide to optical system design*, vol. 1, Wiley & Sons, 1980.
- Lilly, D. K., and P. J. Kennedy, Observations of a stationary mountain wave and its associated momentum flux and energy dissipation, *J. Atmos. Sci.*, 30, 1135, 1973.
- Lincoln, J. V., Geomagnetic indices, in *Physics of geomagnetic phenomena*, edited by S. Matsushita, and W. H. Campbell, vol. 1, pp. 77, 86, Academic Press, 1967.
- Lindzen, R. S., Turbulence and stress owing to gravity wave and tidal breakdown, *J. Geophys. Res.*, 86, 9707, 1981.
- Lyot, B., Un monochromateur à grand champ utilisant les interférences en lumière polarisée. *Comptes Rendus*, 197, 1593, 1933.
- Manring, E. R., and H. B. Pettit, Observations of the [OI] 5577 nightglow at Sacramento Peak, New Mexico, February through June, 1955, in *The airglow and the aurorae: [papers presented at] a symposium held at Belfast in September 1955*, edited by E. B. Armstrong, and A. Dalgarno, 1955.
- Mayaud, P. N., *Derivation, Meaning, and Use of Geomagnetic Indices*, American Geophysical Union, 1980.
- McDade, I. C., D. P. Murtagh, R. G. H. Greer, P. H. G. Dickinson, G. Witt, J. Stegman, E. J. Llewellyn, L. Thomas, and D. B. Jenkins, ETON 2: Quenching parameters for the proposed precursors of $O_2(b\Sigma_g^+)$, *Planet. Space Sci.*, 34, 789, 1986.
- McLandress, C., On the importance of gravity waves in the middle atmosphere and their parameterization in general circulation models, *J. Atmos. Terr. Phys.*, 60, 1357, 1998.
- McLennan, J. C., and G. M. Shrum, On the luminescence of nitrogen, argon, and other condensed gases at very low temperatures, *Proc. Roy. Soc. (London)*, A106, 138, 1924.
- Megill, L. R., Photometric observations of the twilight glow [OI] 5577 and [OI] 6300, *J. Atmos. Terr. Phys.*, 17, 276, 1960.

- Menvielle, M., and A. Berthelier, The K-derived planetary indices: description and availability, *Reviews of Geophysics*, 29, 415, 1991.
- Nakamura, J., Latitude effect of night airglow, *Rep. Ionosph. Res. Japan*, 12, 419, 1958.
- Nastrom, G. D., and D. C. Fritts, Sources of mesoscale variability of gravity waves, I: Topographic excitation, *J. Atmos. Sci.*, 49, 3087, 1992.
- Neff, S. H., Observation of the O I 5577 Å nightglow at Christchurch, New Zealand, *J. Geophys. Res.*, 70, 1743, 1965.
- Noxon, J. F., Observation of daytime aurora, *J. Atmos. Terr. Phys.*, 25, 637, 1963.
- O'Brien, B. J., F. R. Allum, and H. C. Goldwire, Rocket measurement of midlatitude airglow and particle precipitation, *J. Geophys. Res.*, 70, 161, 1965.
- Offerman, D., V. Friedrick, P. Ross, and U. Von Zahn, Neutral gas composition measurements between 80 and 120 km, *Planet. Space Sci.*, 29, 747, 1981.
- Ogawa, T., and T. Shimakazi, Diurnal variations of odd nitrogen and ionic densities in the mesosphere and lower thermosphere: simultaneous solution of photochemical-diffusive equations, *J. Geophys. Res.*, 80, 3945, 1975.
- Ogawa, T., N. Iwagami, M. Nakamura, M. Takano, H. Tanabe, A. Takechi, A. Miyashita, and K. Suzuki, A simultaneous observation of the height profiles of the night airglow OI 5577 Å, O₂ Herzberg and atmospheric bands, *J. Geomag. and Geoelec.*, 39, 211, 1987.
- Öhman, Y., A new monochromator, *Nature*, 141, 157, 1938.
- Osterbrock, D. E., J. P. Fulbright, A. R. Martel, M. J. Keane, S. C. Trager, and G. Basri, Night-sky high-resolution spectral atlas of OH and O₂ emission lines for echelle spectrograph wavelength calibration, *Pub. Astron. Soc. Pac.*, 108, 277, 1996.
- Pasko, V. P., U. S. Inan, and T. F. Bell, Sprites as evidence of vertical gravity wave structures above mesoscale thunderstorms, *Geophys. Res. Lett.*, 24, 1735, 1997.

- Petitdidier, M., Étude de l'influence des phénomènes dynamiques au niveau de la mésopause sur l'intensité de l'émission de la raie verte, Ph.D. thesis, L'université Pierre et Marie Curie (Paris VI), 1978.
- Plagmann, M., et al., Annual variation of airglow heights derived from wind measurements, *Geophys. Res. Lett.*, 25, 4457, 1998.
- Purdy, C. M., L. R. Megill, and F. E. Roach, A new airglow photometer, *J. Res. Natl. Bur. Std.*, 65C, 213, 1961.
- Rayleigh, L., The light of the night sky: its intensity variations when analyzed by colour filters, *Proc. Roy. Soc. (London)*, A106, 117, 1924.
- Rayleigh, L., The light of the night sky: its intensity variations when analyzed by colour filters - III., *Proc. Roy. Soc. (London)*, A119, 11, 1928.
- Rayleigh, L., Absolute intensity of the aurora line in the night sky, and the number of atomic transitions required to maintain it, *Proc. Roy. Soc. (London)*, A129, 458, 1930.
- Rayleigh, L., and H. Spencer Jones, The light of the night-sky: analysis of the intensity variations at three stations, *Proc. Roy. Soc. (London)*, A151, 22, 1935.
- Rees, M. H., *Physics and chemistry of the upper atmosphere*, Cambridge University Press, Cambridge, 1989.
- Roach, F. E., A review of observational results in airglow photometry, *Ann. de Géoph.*, 11, 214, 1955.
- Roach, F. E., Manual for photometric observations of the airglow during the International Geophysical Year, Tech. Rep. 5006, National Bureau of Standards, 1956.
- Roach, F. E., Photometric observations of the airglow during the I QSY, *Ann. IQSY*, 1, 145, 1968.
- Roach, F. E., and H. B. Pettit, On the diurnal variation of OI 5577 in the nightglow, *J. Geophys. Res.*, 56, 325, 1951.
- Roach, F. E., D. R. Williams, and H. B. Pettit, The diurnal variation of OI 5577 in the nightglow, Geographical studies, *J. Geophys. Res.*, 58, 73, 1953.

- Rosenberg, N., and S. P. Zimmerman, Correlation between the 5577 Å [OI] night airglow intensity and solar activity, *Planet. Space Sci.*, 15, 863, 1967.
- Russell, C. T., and R. L. McPherron, Semiannual variation of geomagnetic activity, *J. Geophys. Res.*, 78, 92, 1973.
- Schaeffer, R. C., and W. G. Fastie, Tilting-filter measurements in dayglow rocket photometry, *Appl. Opt.*, 11, 2289, 1972.
- Schaeffer, R. C., P. D. Feldman, and E. C. Zipf, Dayglow (OI) λ 6300 and λ 5577 Å lines in the early morning ionosphere, *J. Geophys. Res.*, 77, 6828, 1972.
- Schoeberl, M. R., D. F. Strobel, and J. P. Apruzese, A numerical model of gravity wave breaking and stress in the mesosphere, *J. Geophys. Res.*, 88, 5249, 1983.
- Shepherd, G. G., N. J. Siddiqi, R. H. Wiens, and S. Zhang, Airglow measurements of possible changes in the ionosphere and middle atmosphere, *Adv. Space Res.*, 20, 2127, 1997.
- Shepherd, G. G., J. Stegman, P. Espy, C. C. McLandress, G. Thuillier, and R. H. Wiens, Springtime transition in lower thermospheric atomic oxygen, *J. Geophys. Res.*, 104, 213, 1999a.
- Shepherd, G. G., S. Zhang, and X. Wang, Variability in MLT dynamics and species concentrations as observed by WINDII, *Earth Planets Space*, 51, 845, 1999b.
- Silverman, S. M., Night airglow phenomenology, *Space Science Reviews*, 11, 341, 1970.
- Silverman, S. M., F. Ward, and R. Shapiro, The correlation between the 5577 Å night airglow intensity and geomagnetic activity, *J. Geophys. Res.*, 67, 2255, 1962.
- Singh, V., I. C. McDade, G. G. Shepherd, B. H. Solheim, and W. E. Ward, The O(¹S) dayglow emission as observed by the WIND imaging interferometer in UARS, *Ann. Géophys.*, 14, 637, 1996.
- Slipher, V. M., On the general auroral illumination of the sky and the wavelength of the chief auroral line, *Astrophys. J.*, 49, 266, 1919.
- Smith, L. L., and R. B. Alexander, Calibration of airglow photometers at Fritz Peak Observatory, *Ann. IQSY*, 1, 167, 1968.

- Smith, L. L., and R. W. Owen, The seasonal variation of nightglow NaI 5890 – 96 Å, [O I] 5577 Å and [O I] 6300 Å in the tropics, NBS Tech. Note 329, National Bureau of Standards, Boulder, Colorado, 1966.
- Smith, L. L., and W. R. Steiger, Night airglow intensity variations in the [O I] 5577 Å, [O I] 6300 Å, and NaI 5890 – 96 Å emission lines, *J. Geophys. Res.*, *73*, 2531, 1968.
- Smith, L. L., F. E. Roach, and J. M. McKennan, IQSY night airglow data, Tech. Rep. UAG-1, World Data Center A, 1968.
- Störmer, C., Photographies des aurores boréales et nouvelle méthode pour mesurer leur altitude, *Compt. Rend.*, *150*, 1631, 1910.
- Störmer, C., Résultats des mesures photogrammétriques de l'altitude de l'aurore boréale à Bossekop aux mois de février et mars 1910, *Compt. Rend.*, *152*, 1194, 1911.
- Swensen, G. R., S. B. Mende, and E. J. Llewellyn, Imaging observations of lower thermospheric O(¹S) and O₂ airglow from STS 9: Implications of height variations, *J. Geophys. Res.*, *94*, 1417, 1989.
- Taylor, M. J., and M. A. Hapgood, Identification of a thunderstorm as a source of short period gravity waves in the upper atmospheric nightglow emissions, *Planet. Space Sci.*, *36*, 975, 1988.
- Tohmatsu, T., *Compendium of Aeronomy*, Terra Scientific Publishing Company, Tokyo, 1990.
- Tousey, R., Rocket measurements of the night airglow, *Ann. Géophys.*, *14*, 186, 1958.
- Van Dijk, G., The magnetic character of the year 1931 and numerical magnetic characterization of days, *Terrestrial Magnetism*, *37*, 259, 1932.
- Van Rhijn, P. J., On the brightness of the sky at night and the total amount of starlight, *Pub. Ast. Lab. Groningen*, *31*, 1, 1921.
- Witt, G., J. Stegman, B. H. Solheim, and E. J. Llewellyn, A measurement of the O₂(b¹Σ_g⁺ – X³Σ_g⁻) atmospheric band and the OI(¹S) green line in the nightglow, *Planet. Space Sci.*, *27*, 341, 1979.
- Yano, K., A long-term aspect of the seasonal variation in the nightglow 5577 intensity at middle latitudes, *Planet. Space Sci.*, *15*, 1091, 1967.

Yao, I. G., Observations of the night airglow, 1 July 1957 - 31 December 1959, *Annals of the International Geophysical Year*, 24, 1962.

Yntema, L., On the brightness of the sky and total amount of starlight., *Publ. Ast. Groningen*, 22, 1, 1909.

VITA

Kerry Ann Deutsch was born on March 17, 1970 to Mary and Thomas McQuade in Pittsburgh, Pennsylvania. She graduated from Penn Hills High School in Penn Hills, Pennsylvania in 1988, and received a B.A. in physics from the Johns Hopkins University in 1992. Prior to beginning graduate school, she worked as a science data analyst at the Space Telescope Science Institute. From 1994 to 2000 she was a graduate student in the Geophysics Program at the University of Washington.